Analysis of Turbulent, Axisymmetric, Dense Jets Discharged to Quiescent, Uniform or Stratified Ambients

by

Syed Zafar Ahmad

A Thesis Presented to the

FACULTY OF THE COLLEGE OF GRADUATE STUDIES

KING FAHD UNIVERSITY OF PETROLEUM & MINERALS

DHAHRAN, SAUDI ARABIA

In Partial Fulfillment of the
Requirements for the Degree of

MASTER OF SCIENCE

In

MECHANICAL ENGINEERING

June, 1982

UNIVERSITY OF PETROLEUM & MINERALS
COLLEGE OF GRADUATE STUDIES

ANALYSIS OF TURBULENT, AXISYMMETRIC, DENSE JETS DISCHARGED TO QUIESCENT, UNIFORM OR STRATIFIED AMBIENTS

BY

SYED ZAFAR AHMAD

THESIS
PRESENTED TO THE FACULTY OF THE COLLEGE OF GRADUATE STUDIES
IN PARTIAL FULFILLMENT OF THE
REQUIREMENTS FOR THE DEGREE OF
MASTER OF SCIENCE IN MECHANICAL ENGINEERING

JUNE 1982

UNIVERSITY OF PETROLEUM & MINERALS
DHAHRAN, SAUDI ARABIA

COLLEGE OF GRADUATE STUDIES

This thesis, written by:

SYED ZAFAR AHMAD

under the direction of his Thesis Committee, and approved by all its members, has been presented to and accepted by the Dean of the College of Graduate Studies, in partial fulfilment of the requirements for the degree of

MASTER OF SCIENCE IN MECHANICAL ENGINEERING.

DEAN
College of Graduate Studies

Date ٢٥/٢/٨٣

Thesis Committee

Department Chairman

12/2/83
Chairman

W. Ahmed 10/1/83
Member

Member

Dedicated to

my parents, sisters and brother

ACKNOWLEDGEMENT

Praise and thanks be to Almighty Allah, first and last, who made every difficult thing easy for us.

Then, the author likes to offer his gratitude to the Univ. of Petroleum & Minerals for support of this research.

I would like to acknowledge my indebtedness to my major advisor, Dr. Imtiaz K. Madni who has been a constant source of help during this research. I sincerely appreciate the willing cooperation extended by Prof. Wolfgang Stahl who served as one of the members of the Thesis Committee. Thanks are also due to Dr. Zaki Ahmed who served as member of the Thesis Committee.

I have lot of good wishes for my father and sister's family, in Dammam, who were always a source of atonement and pleasure during the critical stages of this study. I wish to acknowledge the assistance given by a large number of sincere friends who helped me at different stages of this research and without their help and cooperation this thesis could never have been completed in time. They are Rehan, Hilal, Haneef, Khursheed, Imtaar, Tahir, Farrukh, Mohiuddin, Ikram, Israr and Inaam.

Lastly, I would like to thank Mr. Syed I. Jameel for his excellent typing of the manuscript.

TABLE OF CONTENTS

NOMENCLATURE

c	salinity
C	dimensionless salinity $(c - c_{\infty_o})/(c_o - c_{\infty_o})$
C_p	specific heat at constant pressure
D	diameter of jet or plume at discharge or mass diffusivity
D_{eff}	total or effective diffusivity for salinity
Fr_o	discharge Froude number, $u_o^2/[gD(\rho_{\infty_o} - \rho_o)/\rho_o]$, dimensionless
Fr	local Froude number $u^2/[2g\delta(\rho_\infty - \rho)/\rho_o]$, dimensionless
$f(y)$	initial velocity distribution
$F(Y)$	dimensionless initial velocity distribution
$g(y)$	initial temperature distribution
$G(Y)$	dimensionless initial temperature distribution
g	acceleration of gravity
$\vec{g}$	gravity vector, $-g\vec{k}$
G	density deficiency
$h(y)$	initial salinity distribution
$H(Y)$	dimensionless initial salinity distribution
H	discharge depth
$\vec{i}_s, \vec{i}_y, \vec{i}_\phi$	unit vectors parallel to the s,y,ϕ axes, respectively
J	flux of component of mass (salinity)
k	thermal conductivity
K_1, K_2, K_3	constants in models for turbulent viscosity
ℓ	mixing length
ℓ	unmodified mixing length in Monin-Oboukhov formula
ν_{eff}	total or effective kinematic viscosity
N	dimensionless total or effective kinematic viscosity, ν_{eff}/ν

α_{eff}	total or effective diffusivity for heat
N_H	dimensionless total or effective diffusivity for heat, α_{eff}/ν
N_M	dimensionless total or effective diffusivity for salinity, D_{eff}/ν
N_Y	transverse grid number at jet half-width
NYT	transverse grid number at jet thermal half-width
NYC	transverse grid number at jet concentration-half-width
NYJ	Max (NY, NYT, NYC)
Pr	Prandtl number, ν/α
q	heat flux due to molecular and turbulent transport
$\bar{R}$	radius of curvature, $(d\theta/ds)^{-1}$
Re_o	Reynolds number at discharge, $u_o D/\nu$, dimensionless
Re_{cr}	critical Reynolds number above which flow is always turbulent, dimensionless
Ri	gradient Richardson number, $\frac{-g}{\rho_a}\frac{\partial\rho}{\partial y}\Big/\left(\frac{\partial u}{\partial y}\right)^2$
s	distance along jet or plume axis
S	dimensionless axial distance, $s\, u_o/\nu$
ΔS	increment of S
s_ℓ	starting length
t	temperature
T	non-dimensional temperature, $(t - t_{\infty_o})/(t_o - t_{\infty_o})$
$\bar{T}$	stratification number, $(\rho_o - \rho_\infty)/[-\frac{D}{2}(d\rho_\infty/dz)]$
u	s-component of time mean velocity
U	dimensionless s-component of time mean velocity, u/u_o
v	y-component of time mean velocity
V	dimensionless y-component of time mean velocity, v/u_o
x	distance along x-axis.

X	dimensionless distance along x-axis, $x\ u_o/\nu$
y	Radial distance from jet centerline
Y	dimensionless radial distance from jet centerline, $y\ u_o/\nu$
$y_{\frac{1}{2}}$	radial distance from jet centerline to point at which $(u - u_\infty)/(u_c - u_\infty) = 0.5$
$y_{t_{\frac{1}{2}}}$	radial distance from jet centerline to point at which $(t - t_\infty)/(t_c - t_\infty) = 0.5$
$y_{c_{\frac{1}{2}}}$	radial distance from jet centerline to point at which $(c - c_\infty)/(c_c - c_\infty) = 0.5$
ΔY	increment of Y
z	vertical distance
Z	dimensionless vertical distance
Z_m	maximum height of rise.

Greek Symbols

α	thermal diffusivity, $k/\rho C_p$
β	thermal coefficient of expansion, $-(\partial\rho/\partial t)_p/\rho_{ref}$
β^*	concentration coefficient of expansion, $-\left(\frac{\partial\rho}{\partial c}\right)_t \Big/ \rho_{ref}$
γ	intermittency function
δ	mixing layer thickness
μ	viscosity
ν	kinematic viscosity, μ/ρ
ρ	density
τ	total or effective shear stress in s-momentum equation
θ	angle between i_s and the horizontal
ϕ	azimuthal angle
λ	degree of ambient stratification, dt_∞/dz

λ^*	degree of ambient stratification, dc_∞/dz
$\Delta( )$	for dependent variables, this means $( ) - ( )_\infty$

Subscripts

c	evaluated at edge of core or at jet centerline if no core exists
p	evaluated at constant pressure
e	evaluated at outer edge of jet
½	evaluated at velocity half-radius
o	value at jet discharge
ref	reference value
t	turbulent flow quantity
∞	free stream or ambient value
i,j	lattice or grid indices corresponding to S, Y directions, respectively
+,-	used in special notation, $\Delta Y_+ = (Y_{j+1} - Y_j)$, $\Delta Y_- = (Y_j - Y_{j-1})$, and similarly for ΔS
max	maximum
min	minimum

Superscripts

$( )'$	primes on dependent variables denote fluctuating quantities
$\overline{( )}$	bars on dependent variables denote time mean quantities
$(\rightarrow)$	denotes vector quantities.

LIST OF TABLES

LIST OF FIGURES

ABSTRACT

The explicit finite-difference scheme of DuFort-Frankel type which was successfully applied in buoyant jet analysis by previous investigators is now applied to solve partial differential equations of continuity, momentum, energy and salinity to simulate a warm, dense, highly salt-laden jet issuing from desalination plant outfall systems. Turbulent shear stress, heat flux, and component-of-mass flux term appearing in the governing equations are evaluated using an eddy viscosity model which includes effects such as intermittent turbulence near the edge of the jet and buoyancy on mixing. The turbulent Prandtl and Schmidt numbers used to relate the turbulent exchange of momentum and scalar constituents are kept constant at 0.7 for all calculations reported.

The following flow categories are considered: (1) The vertical dense jet discharging into quiescent, uniform or stratified ambient, and (2) the dense jet discharging horizontally or inclined to the horizontal into a uniform or stratified ambient.

The predictions of jet trajectory in the lower Froude number range agree favorably with the available experimental data. For higher densimetric Froude numbers, significant deviation between predictions and experiments is observed. However, the experimental data is very limited and additional data is needed before any conclusive remarks can be made.

ملخـــص

النهج الواضح للفرق المحدود من طراز (دوفورت ــ فرانكل) والذى طبقه المحققين القدامى بالنجاح فى تحليل التدفق العايم هو الذى يطبق لتحليل معادلات تفاضلية الجزئية للتسلسل والزفم والطاقه والملوحة لان تظاهر السير الحار والكثيف وذو ملوحة عالية الذى ناتج من مصب ومدة ازالة الملوحة . ويقدر ضغط قوة القص المضطرب والتدفق الحرارى ومركبة الثقل والمعادلات التى تتحكم التدفق قدرت باستخدام نموذج اللزوجة الدوامة الذى يحتوى على تأثير الاضطراب المتقطع عند ركن المنبثق وعيوبه عند التحضير .

واستخدمت ارقام (برانتل) و (شمت) لان يتعلق مع التبادل الاضطرابى للزخم وتبقى المحتويات المقشره ثابته على (٧ر٠) لجميع الحسابات المتوفره .

ولوحظ سيرين (١) السير العمودى الكثيف في المحيط الهادى أو منتظم أو مطبق و (٢) السير الافقى أو المائل الى الافق في المحيط الهادى أو منتظم أو مطبق . وسير المنبثق في حدود الرقم (فرود) الواطى يعطى النتائج الجيده مع معلومات التجربة الموجودة ولكن لرقم (فرود) العالى هناك اختلاف كبير بين النبؤة والتجربة . مع هذا ، المعلومات الموجودة تبدو قليلة وهناك احتياج للمعلومات الزائده قبل أى استنتاج من التجارب .

1. INTRODUCTION

1.1 STATEMENT OF THE PROBLEM

In the planning and design of plants for the desalination of seawater, a major consideration is to have environmentally acceptable disposal of the waste brine and cooling water. This is because a warm, dense, highly salt-laden effluent can severely damage the local biota. A schematic diagram of a dual purpose desalination plant which employs either a variation of the multiple effect falling film, or the multi-stage flash-distillation process in combination with the production of power, is shown in Fig. 1.1. The effluents from the desalination plant are the brine blow down and the cooling water used in the heat rejection section of a multi-effect falling film evaporator. If the total electric capacity of the power installation exceeds the net power produced by the back pressure turbine, there will be a cooling water effluent from the installed turbines as well.

If the plant in question is a distillation facility alone, the combined water and waste brine streams are likely to be 12-15°F warmer and a salinity 15% higher than the inlet saline water. They will also contain all of the dissolved materials removed from the product water plus any chemicals added to the brine during pretreatment or as corrosion products of the heating surfaces.

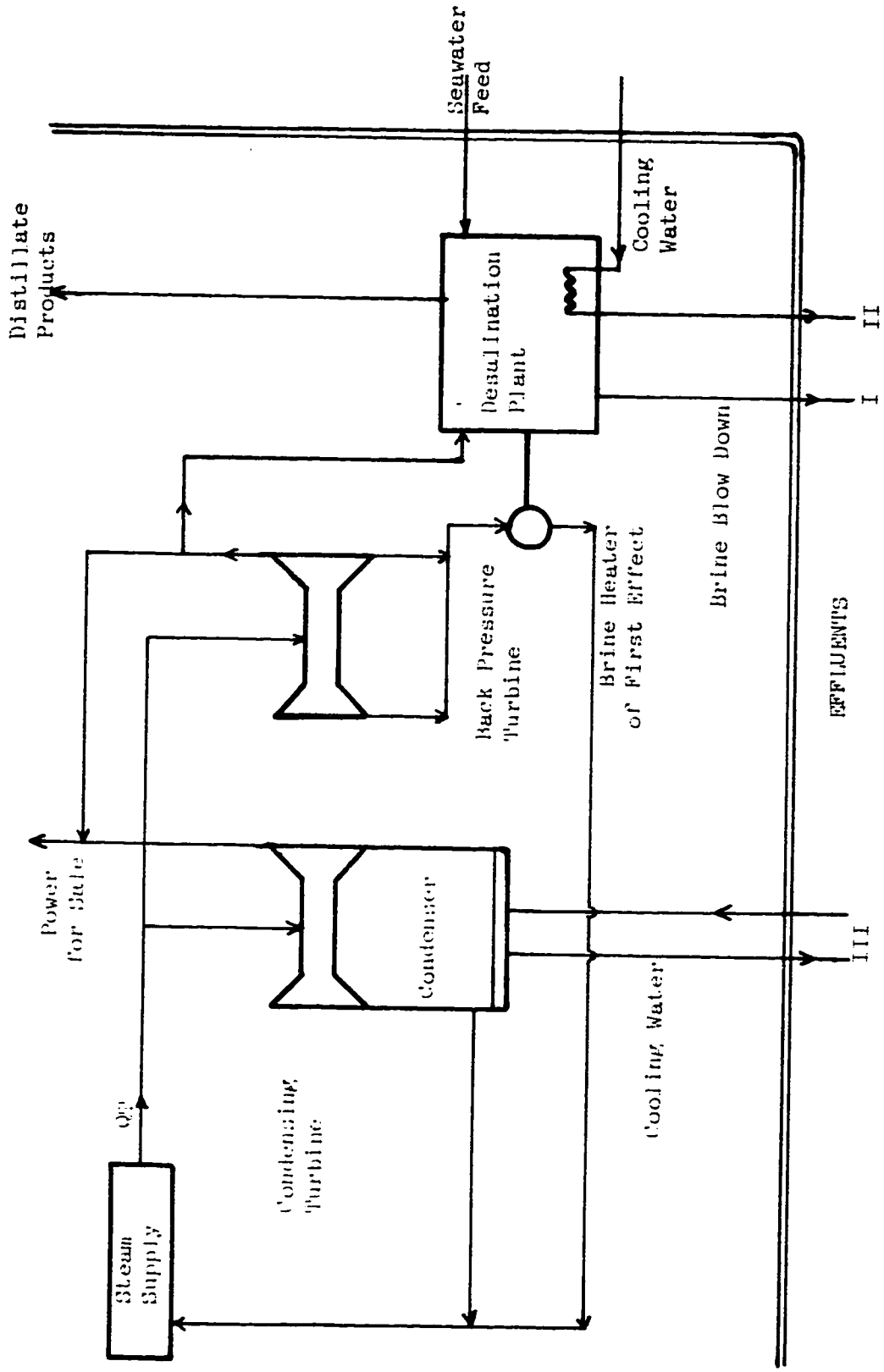

Fig. 1.1. Schematic of Dual Purpose Desalination Plant

Iron, copper, and zinc are the metallic elements that can be present in the effluents in measurable concentrations. Since cupro-nickel alloys are the most widely used materials of construction for heat exchanger tubings, copper will exist in higher concentrations than other metals in the effluent stream. The copper concentration in the mixed brine blow down and cooling water discharge will be a probable 0.15 ppm which is thirty to forty times the copper concentration in the receiving seawater and six to eight times the recommended water quality criteria of 0.02 mg/liter [1, 2]. It is feared that these wastes are unfavorable and even toxic to the marine organisms which constitute the basic food chain in the receiving waters. Copper concentrations of 0.05 mg/liter at 20°C were found to be toxic to the most important primary producers in the marine ecology—diatoms and dinoflagellates. Increased temperatures were found to have a synergistic action on the toxicity of the copper ion to marine phytoplanktons and many other varieties of algae which grow most favorably within a narrow range of temperature and salinity. Any major disturbance, such as that which would be produced by the discharge of warm salty water from a newly established desalination plant, would thus likely seriously interrupt or partially destroy the ecological food production in the receiving water.

Reduction of the copper content of any discharge may be accomplished by dilution, or by removal through ion ex-

change or some other chemical treatment. The latter have been proven to be economically prohibitive, hence dilution is resorted to as the most acceptable solution.

Dilution of the effluent streams by means of jets diffuses the streams of brine and cooling water, and thereby reduces the temperature, salinity, and copper concentration due to rapid mixing with the receiving water. Le Gros, et al. [30] showed that when dispersion was effective in reducing dissolved copper concentration to the desired 0.02 ppm, a satisfactory reduction of temperature and salinity was accomplished at the same time.

We, thus, understand that the disposal of waste heat and concentrated brine in a manner which does not alter organic life in the immediate surrounding is a major problem for the designer. The behavior of the effluents disposed into the marine environment must be studied to allow prediction of the maximum physical and chemical changes in the vicinity of the outfall that meets predetermined water quality criteria. An optimal discharge system requires knowledge of the velocity, temperature and concentration fields due to the discharge. The present study deals with the prediction of these quantities through mathematical modeling, in which the flow is modeled as a turbulent jet or plume issuing into an ambient of different density. The investigation concerns the 'near-field' problem describing the distribution of heat

and salinity in the immediate area of the discharge. This is really all that is required from the mixing-zone point of view.[15]

1.2 OBJECTIVES OF THE STUDY

With the background presented, the objectives of the present investigation can be summarized as follows:

1 Prediction of jet trajectory, centerline velocity, temperature and concentration decay for dense jets inclined at positive angles to the horizontal.

2 Prediction of centerline velocity, temperature, and concentration decay for a vertically discharged dense jet and its maximum height of rise for a range of discharge densimetric Froude numbers of practical interest.

3 Ocean, lakes and the atmosphere are frequently stratified in density. Stable stratification, where ambient density decreases with increasing height has the effect of reducing the turbulent mixing. It is intended to make predictions for vertical as well as inclined dense jets issuing into a stratified ambient.

1.3 APPROACH OF THE STUDY

The prediction of turbulent free shear flows of which jet flow is probably the most important part, was commonly done by integral methods. Integral methods employ integra-

tion of governing partial differential equations along the transverse direction of the flow, leading to ordinary differential equations with the main flow direction being the independent variable. This requires knowledge or assumption of velocity, temperature and/or concentration distributions so that integration could be performed over the cross-section. Extensive work has been done by Abraham [3, 4], Morton [5], Morton, et al. [6], Fan and Brooks [7], Hirst [8], Riester, et al. [9] and others.

With the advent of faster digital computers, however, direct numerical solutions of the partial differential equations has become more appealing. The direct solution of governing p.d.e's eliminates the need for assuming profile shapes and similarity, allows arbitrary initial and boundary conditions, and yields solutions for the local variables. This is especially true for other classes of turbulent flows. Examples of differential approaches in jet flows have, nevertheless, been few. Trent and Welty [10] were perhaps the first to apply finite difference method to solve partial differential equations in elliptic form (i.e., without employing boundary layer assumptions) to vertical plume flows. Later, Crew and Reid [11] solved the governing partial differential equations for the case of dense effluent discharged from a desalination plant. The method used was successive overrelaxation.

Madni [12], Madni and Pletcher [13, 14, 15, 16] reported numerical treatment of boundary layer type partial differential equations and developed turbulence models to predict the trajectory and decay of centerline temperature and velocity for a pure momentum jet in a coflowing ambient, forced plumes in stratified and unstratified ambients, and horizontal or inclined buoyant jets in unstratified ambients. The solution method utilized an explicit finite-difference scheme of the Du-Fort Frankel type.

The present work approaches the problem of dense jets in the same manner as was done by Madni [12], and Madni and Pletcher [14]. The same numerical scheme and assumptions have been used. The formulation has been extended to include a transport equation for salinity with the assumption that eddy diffusivities of heat and salinity are the same (i.e., turbulent Lewis number = 1). The turbulence modeling employs simple algebraic expressions for the eddy diffusivity of momentum — the so called zero-equation models.

1.4 SCOPE OF PRESENT INVESTIGATION

The current investigation was carried out in an attempt

to develop better methods for predicting the behavior of dense jets and plumes in response to current interest and the need for such prediction methods as, for example, in the design of desalination plants and ocean sewage outfalls.

The numerical model could be further extended to accommodate the effects of shallow water discharges and the influence of ambient turbulence. The results of jet trajectory and centerline temperature, velocity, and concentration decay for a variety of discharge parameters and ambient conditions can be useful in the conceptual design of outfall systems for a range of sizes of distillation plants to meet predetermined water quality criteria.

The computer program can be used to obtain results for coastal as well as atmospheric discharges, for ocean sewage outfalls, and discharges where both temperature and species concentrations are present (such as one from a desalination plant). Moreover, both positively and negatively buoyant jets can be handled and the turbulence model can be any of the so called simple algebraic (zero-equation) models.

The information obtained from the 'near field' study can be used as boundary conditions for the far field study.

2. PHYSICAL CONSIDERATIONS AND PREVIOUS STUDIES

2.1 BACKGROUND AND DEFINITIONS

A mixture of brine blow down and cooling water, under almost all combinations of temperature and salinity, will be negatively buoyant and will sink to the ocean floor. On being discharged, the dense effluent is immediately subjected to a negative buoyancy force proportional to the difference in density between the effluent and the lighter receiving water. The kinetic energy, due to the velocity through the port, is dissipated in the turbulent mixing of the jet while the negative force drives the effluent downward. This initial jet mixing causes a field of diluted effluent to be formed near the bottom of the receiving body which then moves with the ocean currents or is flushed away by tidal currents in the case of an enclosed bay or an estuary.

In general, a reservoir can be characterized by three regimes in which the effluent discharge may have an effect: the near field, a joining region, and the far field. In the near field region, which is the region surrounding the source, turbulent mixing occurs due to the shear between the jet and the ambient fluid. In the joining region, turbulent mixing diminishes and the discharge water begins to spread. In the far field region, which is a considerable distance from the

outlet, non-turbulent buoyancy-driven spreading of the water occurs. In the present analysis emphasis is placed on the 'near field' regime, since it is here that the temperature and salinity excesses are significant from the point of view of outfall design.

AMBIENT EFFECTS

The behavior of the jet is influenced by the initial conditions at diffuser exit, and by several ambient effects such as buoyancy, ambient density stratification, ambient currents, and turbulence levels. They are described briefly below.

Buoyancy:

When the jet is produced as a warm saline discharge, its density is greater than that of the ambient fluid due to its salinity. This negative buoyancy force has a pronounced effect on the jet behavior. For example, a saline jet discharging horizontally into a lighter ambient will be deflected downward, the amount of deflection depending on the degree of buoyancy under given flow conditions. Figure 2.1 shows a vertically discharged dense jet. We notice that a distinction must be made between the actual jet with upflow and a surrounding downflow region.

Near the ceiling level, i.e., the highest level reached by the jet, the jet fluid leaves the upflow region

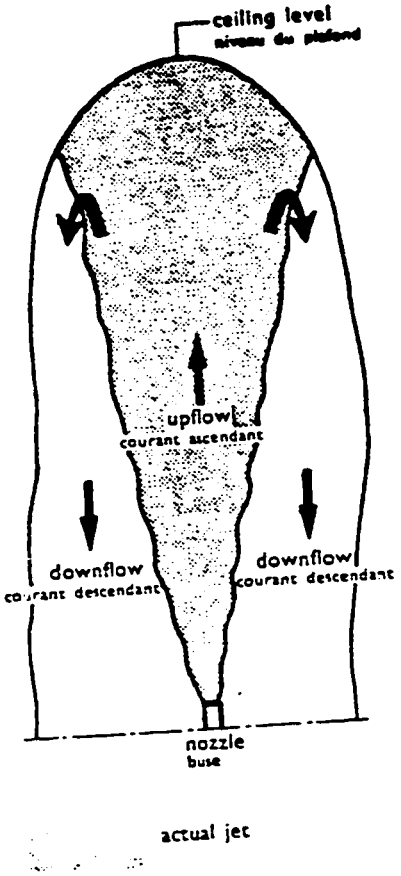

Fig. 2.1. Vertical dense jet.

and enters the downflow region. The zone of negative entrainment near the celing level has been verified by Zeitoun, et al. [2].

Ambient Density Stratification: If ambient density decreases with height, the stratification is referred to as stable stratification whereas the reverse is called unstable stratification. Stable stratification has the effect of gradually reducing the buoyancy force on a rising plume, until a region of zero buoyancy is reached where the plume motion upward will be only due to its vertical momentum. Finally, all upward motion is lost and the plume has reached its maximum height of rise.

Current Effect: The natural environment is seldom stagnant, and free stream velocity can affect the jet mixing, as also its trajectory in case of cross flow. This study has not considered such an effect.

Ambient Turbulence: The natural ambient is nearly always in a state of turbulence. This turbulence is not of significant importance as compared to plume generated turbulence, as long as the ambient velocity remains small relative to jet velocity.

2.2 PREVIOUS STUDIES

The majority of previous analytical models of horizontal buoyant jets employed the integral-type analysis which was first proposed by Morton, Taylor, and Turner [6]. This technique has been used by many investigators [3, 4, 7, 8, 9, 17, 18, 19, 20]. The main assumptions of the integral analysis are:

1. The rate of entrainment at the edge of the plume is proportional to some characteristic velocity at that location.

2. The profiles of velocity and scalar constituents are similar at all elevations within the plume.

3. The local variations in density are small in comparison to the density of the ambient fluid.

Most of the literature on the waste disposal in marine environments deals with effluents that are less dense than seawater, particularly sewage effluents. The mechanism of dilution for the discharge of a single jet into a homogeneous medium of higher density has been the subject of extensive theoretical and experimental studies.

Very little information is available in the literature on the analysis of the dispersion of an effluent with negative buoyancy. Turner [21] carried out experiments to observe the dynamic behavior of the tops of cumulus clouds, and, in particular, the effects that evaporation can have on the mixing and

the motion. When a cloud tower grows upwards into a dry environment, the evaporation of liquid water near the edge causes cooling, and hence a density change. Sometimes a thin layer of dense air produced in this way forms a strong downdraught, which is made visible by the motion of wisps of cloud.

The essential effect introduced by evaporation is that of the reversal of buoyancy. In the interior of the cloud, an upward motion is produced because the air there is lighter than the environment, while mixing near the edge can result in the formation of heavier fluid which drives the flow down again Turner attempted to compare the motion of turbulent jets of heavy salt solution injected upwards into a tank of fresh water with that of plumes which were initially buoyant but became heavy as they mixed with the environment. He found that salt jets reach a steady height about which only small fluctuations occur, while the plumes with reversing buoyancy exhibit violent regular oscillations.

Using dimensional arguments, Turner obtained an empirical correlation to fit his experimental data of time-mean value of the coordinates of the ceiling level. It was found that the following equation represents the data well:

$$\frac{Z_m}{D} = 1.74\ Fr_o' \qquad \textit{Turner}\ [21] \qquad (2.1)$$

where Z_m is the maximum height of rise, D the diameter of the orifice, and the Froude number, Fr_o' is defined as

$$Fr_o' = \frac{u_o}{\sqrt{gD \frac{\rho_\infty - \rho_{\infty o}}{\rho_o}}} \tag{2.2}$$

Here, u_o is the nozzle-discharge velocity, ρ_o is jet fluid density at discharge, and ρ_∞ is the ambient density. This definition of the Froude number is somewhat different from that used in the present study, viz:

$$Fr_o = \frac{u_o^2}{gD \frac{\rho_{\infty o} - \rho_o}{\rho_o}} = - \frac{\rho_o}{\rho_\infty} (Fr_o')^2 \tag{2.3}$$

so that $Fr_o' = |Fr_o|^{\frac{1}{2}}$

A positive value of the Froude number indicates a buoyant jet and negative Fr_o indicates a dense jet.

Abraham [22] analysed three-dimensional axisymmetric jets with negative buoyancy in homogeneous fluid. Some workers [5, 23] before Abraham, had assumed that the vertical flux of a tracer being contained in the jet is constant from the orifice to the ceiling level. This assumption leads to either an infinite concentration of the tracer or an infinite width of the jet at the ceiling level. As both these solutions are not realistic, Abraham took into consideration the decrease of the vertical flux of tracer near the ceiling level to determine the coordinate of the ceiling level. Making the usual assumption of Gaussian profiles for velocity and density, Abraham obtained for large values of Fr_o

$$\frac{Z_m}{D} = 1.94\left|Fr_o\right|^{\frac{1}{2}} \qquad \textit{Abraham [22]} \tag{2.4}$$

Although for a vertical dense jet, entrainment is negative near the ceiling level, Morton [5] and Priestley and Ball [23] assumed the vertical flows of a tracer contained within the jet to be constant from the orifice to the ceiling level. For large values of $|Fr_o|$, the following formulas were obtained:

$$\frac{Z_m}{D} = 1.86\left|Fr_o\right|^{\frac{1}{2}} \qquad \textit{Priestley and Ball [23]} \tag{2.5}$$

$$\frac{Z_m}{D} = 1.45\left|Fr_o\right|^{\frac{1}{2}} \qquad \textit{Morton [5]} \tag{2.6}$$

Zeitoun, et al. [2] conducted experiments on vertical and inclined dense jets [24] issuing into quiescent ambients. For a vertical dense jet, they also carried out an approximate analysis of steady flow regime and density structure assuming that rate of supply of dense fluid and the rate of transport of vertical momentum upwards from the source are constant in time, so that a steady regime was possible. Making use of eddy viscosity concept and Gaussian profiles, the governing partial differential equations of mass, momentum and density deficiency $\left(\frac{\rho - \rho_\infty}{\rho_\infty}\right)$ were converted to ordinary differential equations which were solved approximately by power series expansions. Finally, they arrived at the formula for maximum height of rise, viz:

$$\frac{Z_m}{D} = 2.09|Fr_o|^{\frac{1}{2}} \qquad \textit{Zeitoun, et al.} \text{ [2]} \tag{2.7}$$

which slightly exceeds the Turner's formula. However, their laboratory model with Froude number range of 34 to 2200 yielded following correlation of the average value of ceiling level of the jet:

$$Z_{avg} = 0.25 + 1.722|Fr_o|^{\frac{1}{2}}D \tag{2.8}$$
(inches)

Their experiments also revealed that lateral distribution of a dye tracer across the jet followed a normal distribution, with two distinctly different slopes identifying a middle zone of upward flow that entrained an outer zone of downward flow. The down flow, in turn, entrained the ambient water, see Fig. 2.1

A least square correlation for the two zones yielded expressions for concentration distribution at two different heights (Z/D = 2.44 and 34). Based on these results, a schematic of this jet was drawn, which is shown in Fig. 2.2. The turbulent Schmidt number was found to be 0.7 at $\frac{Z}{D} = 2.44$ inside the core of the jet (zone I) where the flow is directed upward. This means that a dissolved constituent spreads more rapidly in the lateral direction than does momentum. This may be explained by the entrainment of pollutant from the outside (zone II) where the flow is directed downward, inside the core of the jet. Thereby lateral spreading of momentum is retarded by the folding action of the jet.

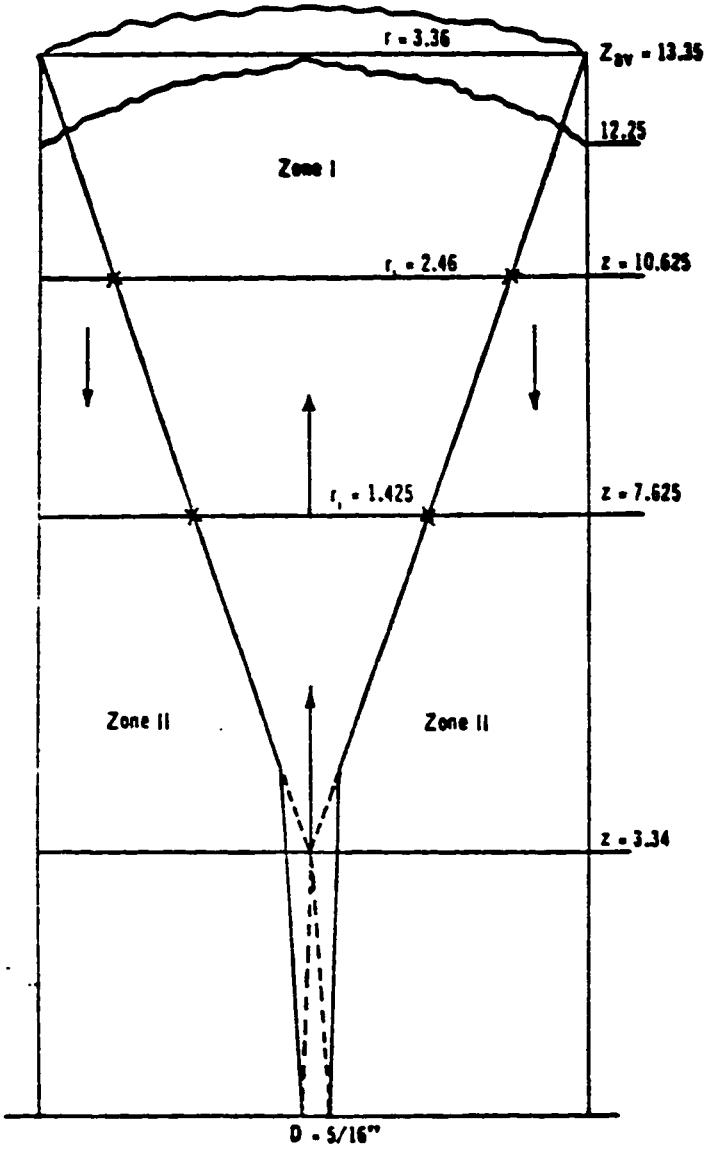

Fig. 2.2. Schematic of vertical dense jet, [2].

In region II, Sc_t is unity, which implies that the constituent is spreading out at the same rate as momentum. In this region, the jet fluid entrains the receiving water which does not contain any of the dissolved constituents. Zeitoun, et al., have mentioned that Sc_t varies with the height Z from the nozzle, because at higher levels momentum force becomes less important than the negative buoyancy force.

Zeitoun, et al., further extended their work to experimental and analytical investigation of inclined dense jets as well as vertical jets reaching the surface. They found that vertical submerged jets result in very limited dilution because the jets fold on themselves. However, vertical jets reaching the surface of the receiving water give more dilution than the submerged jets, but the surface spread is oscillatory in nature and mathematically indeterminable. A generalized form of the Taylor hypothesis was used in their integral analysis. For an inclined jet the maximum height of the jet was found to be proportional to $|Fr_o|^{\frac{1}{2}}$. Table 2.1 lists the correlations. The relative shapes of the trajectories for different initial angles of inclination were found to be in reasonable accord with their experimental data.

The work of Zeitoun, et al., was further extended by Holly and Grace [25]. They utilized a physical model to evaluate the degree of mixing attainable through use of a diffuser

TABLE 2.1

Properties of Inclined Jets [24]

θ_o	Z_m/D	X_m/D	$\frac{\rho_o - \rho_\infty}{\rho_{zm} - \rho_\infty}$
60°	$2.04\|Fr_o\|^{\frac{2}{3}}$	$3.28\|Fr_o\|^{\frac{1}{2}}$	$\|Fr_o\|^{\frac{1}{2}}/1.8$
45°	$1.43\|Fr_o\|^{\frac{2}{3}}$	$3.33\|Fr_o\|^{\frac{1}{2}}$	$\|Fr_o\|^{\frac{1}{2}}/2.4$
30°	$1.15\|Fr_o\|^{\frac{2}{3}}$	$3.48\|Fr_o\|^{\frac{1}{2}}$	$\|Fr_o\|^{\frac{1}{2}}/2.8$

located on the estuary floor or the ocean floor beyond the surf zone, from which the dense brine is discharged vertically through circular ports into a uniform and steady cross current. Correlations were developed to predict maximum height of the upper boundary of an arcing plume, the lateral spread of the plume, and the downstream density distribution.

Bosanquet, et al [20] used a slurry of crushed magnetite injected into a large mass of water to study the path taken by a jet of heavy fluid within a lighter one. They developed a method of predicting the coordinates of the heterogeneous jet systems in terms of the initial velocity, the density ratio, the nozzle diameter and the angle of inclination of the axis of projection. The theory gave trajectories favorably agreeing with their experiment. However, they had used very large density differences, from 20% to 100%. The present study assumes a Boussinesq fluid which does not allow such large density variation and hence the results of [20] will not be used for comparison.

Pena and Jain [26, 27] employing the integral approach and similarity conditions for velocity and temperature profiles, presented predictions for warm, submerged jets discharging into lakes during winter season when the ambient temperature of the lake is near the freezing mark. Figure 2.3 shows the density of water as a function of temperature. The density for a temperature less than 8.1°C is always greater than that of water at 0°C and is maximum at 4°C. If a

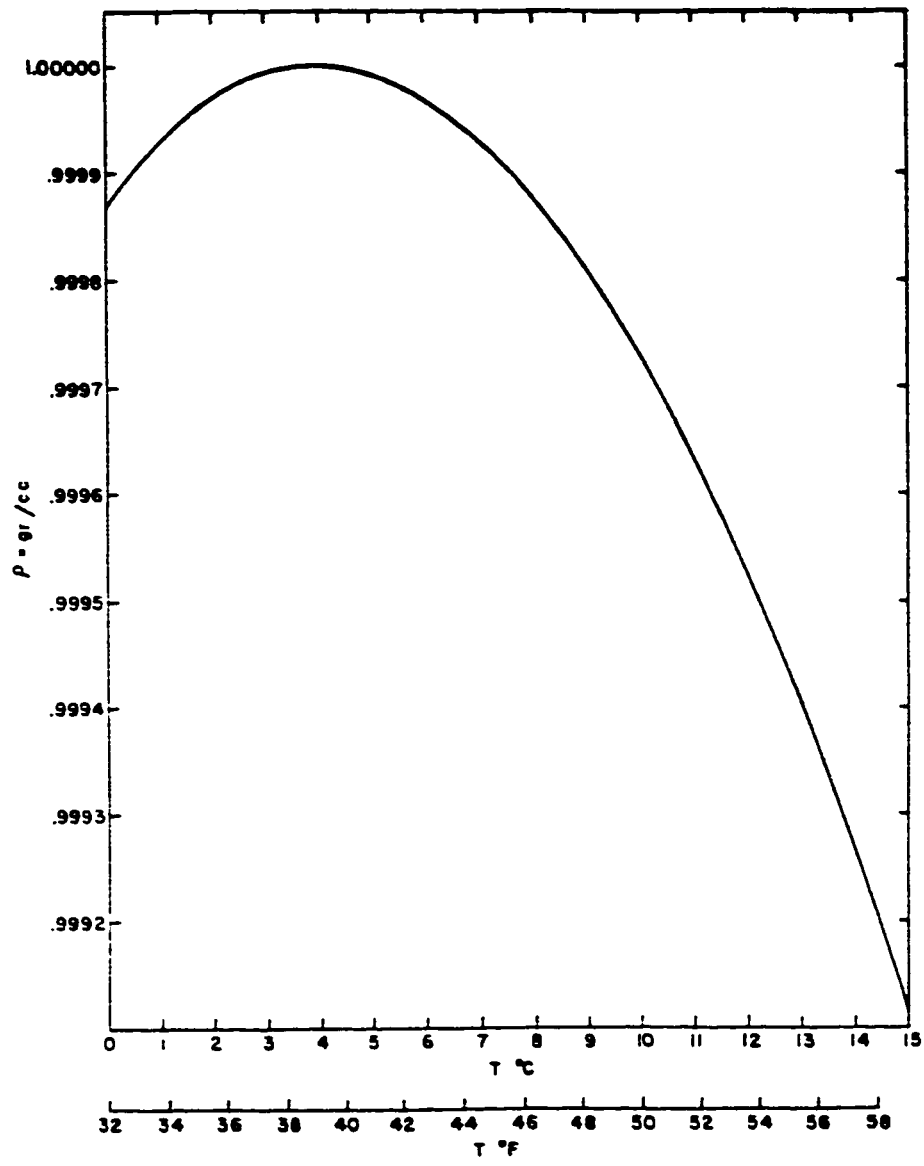

Fig. 2.3. Density of water as a function of temperature

discharge from a thermal power plant has a temperature above 8.1°C, the plume will rise to the point along its length where the plume temperature is reduced by entraining the surrounding colder water to 8.1°C. Thereafter, the density of the plume water is larger than that of the surrounding fluid and the plume sinks. Numerical results are presented for round as well as slot jets discharged at positive angles to the horizontal. The maximum rise of the jet was confirmed to be linearly proportional to the jet Froude number.

Crew and Reid [11] were perhaps the first to solve the dense jet problem by numerical integration of partial differential equations. The study was a part of the Office of Saline Water Research Program and basically dealt with the 'far field' region of the dense effluent. The dense effluent was continuously injected upwards through a circular port into a stream of uniform velocity and density. The equations were solved in a bounded region that means ellipticity of the equations was maintained, requiring an iterative method of solution. The results compared with an analytical solution for cases of low density-anomaly $\frac{\rho_\infty - \rho_o}{\rho_o}$ [28] agree closely. The analytical solutions of [28] which solved linearized equations in a bounded domain are not appropriate for an effluent of high density-anomaly. However, the numerical solution for cases of high density [28] do appear to be physically realistic extensions of the low density-anomaly solutions.

So far, the analysis of [11] seem to be the only study which attempts to solve the far field region using a differential approach.

Riester, et al [29, 31] carried an analytical/experimental study of submerged buoyant and dense fresh water and salt water jets injected horizontally into a quiescent unstratified reservoir. It was observed that dense jets did not penetrate as far into the reservoir as the corresponding positively buoyant jet. However, salt water (cold jets) buoyant and dense jets followed the same trajectory in contrast to the results for fresh water (hot jet). Thus, according to them, the practice of using buoyant fresh water jets to simulate the behavior of dense fresh water jets (or vice-versa) would yield misleading data.

The analytical model of Riester, et al., utilizes the integral approach of Morton, et al. [6]. The model successfully correlates data for both fresh and salt water jets. The essential feature of the model is that it uses a variable temperature density relationship. According to them, "The dependence of the flow characteristics on temperature and salt concentration is shown to be a significant factor contributing to the wide discrepancy in the data reported by previous investigators".

2.3 BASIC ASSUMPTIONS OF THE PRESENT STUDY

The general assumptions underlying the analysis of this investigation are the same as mentioned in [12] and are listed as follows:

1 The flow is steady,in the mean.

2 The fluid is assumed incompressible; density variations are included only in the buoyancy terms. This is commonly called the "Boussinesq approximation" [23].

3 The pressure variation is assumed to be purely hydrostatic.

4 Changes in density are assumed to be small enough so that a linear equation of state is valid.

5 The flow within the jet is assumed to be axisymmetric.

6 The governing equations can be reduced in accordance with boundary layer assumptions.

7 Viscous dissipation is neglected.

8 The ambient fluid is of infinite extent.

The flow was modeled as turbulent within the mixing

zone from the start, and even though the Reynolds number was included in the calculations wherever it appeared, it was not considered as a significant parameter in the jet problem being investigated. According to Ricou and Spalding [62], the critical Reynolds number for the flow to be turbulent, $Re_{cr} = 2.5 \times 10^4$; Rawn, Bowerman, and Brooks [32] mention that when discharge conditions corresponded to Re_o=5000 - 40,000, the jet dilution was not dependent on Re_o. Hinze [31], in reviewing several experiments with non-buoyant jets, observed a decreasing effect of Reynolds number, becoming negligible above 10^5; Cederwall [34] states that flow of an axisymmetric jet is instantaneously turbulent if $Re_o > 2 \times 10^3$, and according to the latest experimental work on buoyant vertical jets [35], by keeping $Re_o > 25000$, flow was always turbulent. In the present calculations Re_o was always greater than 10^6, even for the high buoyancy (low initial momentum) cases. Hence, the assumptions of turbulent mixing from the start and Re_o not being a significant parameter are justified.

However, in this investigation, like the work of Madni [12], laminar viscosity was not neglected. Many previous treatments for turbulent jets have neglected the laminar viscosity altogether. The effect of laminar viscosity is negligible in the main region, but not in the initial region [12].

2.4 SUMMARY OF PREVIOUS STUDIES

A summary of theoretical and experimental studies on dense jets revealed that experimental data are very scant for this class of jet flow and most of the analytical work has used the integral method. The presence of buoyancy introduces uncertainties in the mathematical modeling. No experimental data appears to be available in the literature for dense jets issuing into stratified ambients.

3. ANALYSIS

3.1 THE GOVERNING EQUATIONS

The governing equations for a steady incompressible turbulent flow with non-negligible body forces can be written as

Continuity:

$$\frac{\partial u_i}{\partial x_j} = 0. \tag{3.1}$$

Momentum:

$$\rho u_j \frac{\partial u_i}{\partial x_j} = - \frac{\partial p}{\partial x_i} + \frac{\partial}{\partial x_j}\left(\mu \frac{\partial u_i}{\partial x_j}\right) - \rho \frac{\partial}{\partial x_j} \overline{u_i' u_j'} + \rho g_i \tag{3.2}$$

Energy:

$$\rho C_p u_j \frac{\partial t}{\partial x_j} = \frac{\partial}{\partial x_j}\left(-k \frac{\partial t}{\partial x_j}\right) + \rho C_p \overline{u' t'} \tag{3.3}$$

Salinity:

$$\rho u_j \frac{\partial c}{\partial x_j} = \frac{\partial}{\partial x_j}\left(-\rho D \frac{\partial c}{\partial x_j}\right) + \rho \overline{u_i' c'} \tag{3.4}$$

The density ρ in the convective terms in Eqs.(3.2) and (3.4) can be taken equal to the reference density but in the body force term of Eq.(3.2), it is treated as a variable. This is the so-called Boussinesq assumption as listed under the assumptions in Chapter 2. We notice that temperature and salinity affect the flow field via the body force term in Eq.(3.2). Thus, the momentum equation cannot be solved

independently of the scalar transport equations. A linear equation of state for ρ can be derived by expanding $\rho(t, c)$ in a double Taylor series about the reference density ρ_o:

$$\rho = \rho_o[1 - \beta(t - t_o) - \beta^*(c - c_o)] \qquad (3.5)$$

where β and β^* are the expansivities of the fluid, given by

$$\beta = -\frac{1}{\rho_o}\left(\frac{\partial\rho}{\partial t}\right)_p$$

and

$$\beta^* = -\frac{1}{\rho_o}\left(\frac{\partial\rho}{\partial c}\right)_t$$

In the general formulation, consideration will be given to an axisymmetric dense jet discharging at an angle θ_o to the horizontal. A curvilinear co-ordinate system will be used for the analysis of the general problem. The coordinate system is shown in Fig. 3.1. The s-axis is located along the jet trajectory, while the y-axis is oriented normal to it. By trajectory here is meant a trace of the jet centerline. θ is the angle that the tangent to the trajectory at any point makes with the horizontal. Madni [12] was, perhaps the first to solve the partial differential equations for the jet flow in curvilinear co-ordinates using finite-differences. The present work extends the formulation of [12] to the case of dense jets.

The details of the derivation of the governing equa-

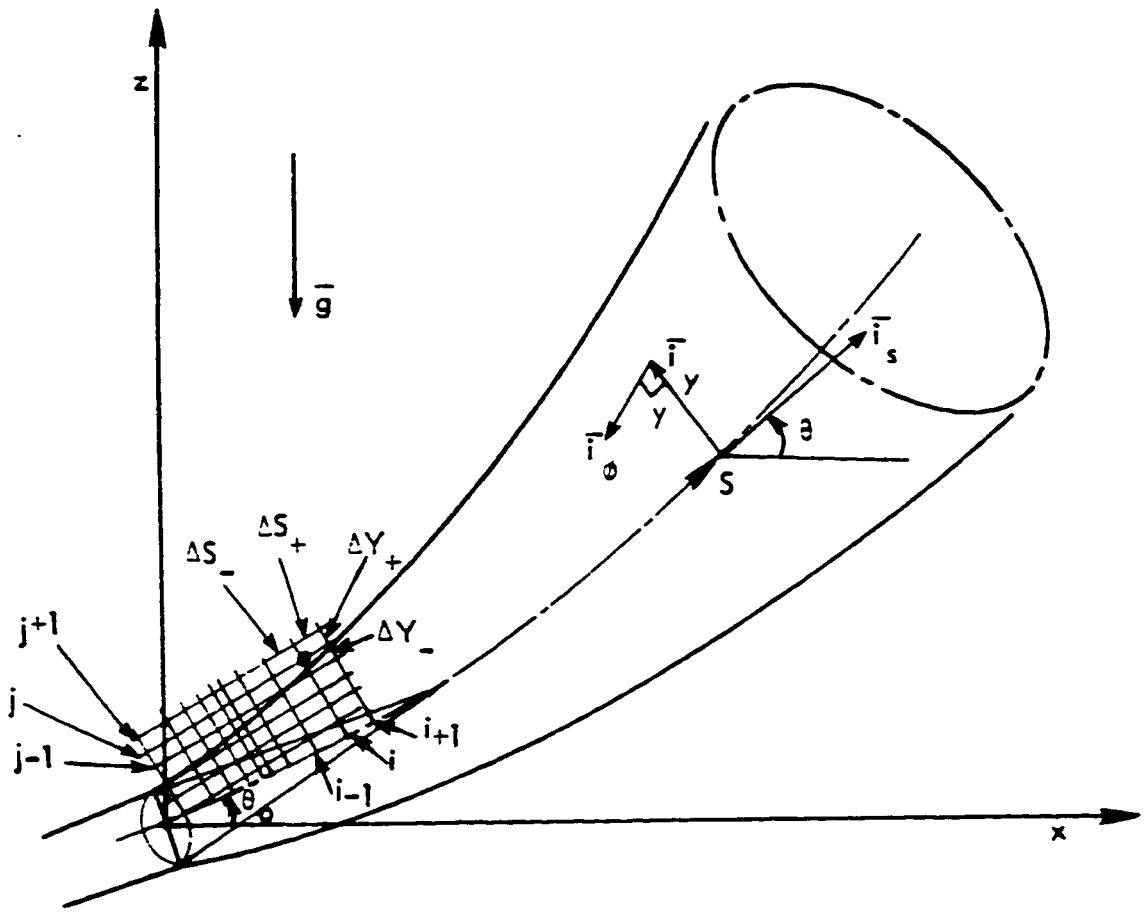

Fig. 3.1. Curvilinear coordinate system and finite-difference grid, [12].

tions, employing the assumptions listed in Chapter 2, are available in [12,16].The final form of the equations, in curvilinear co-ordinates, is as follows:

Continuity:

$$\frac{\partial}{\partial s}(uy) + \frac{\partial}{\partial y}(vy) = 0 \tag{3.6}$$

S-Momentum:

$$u\frac{\partial u}{\partial s} + v\frac{\partial u}{\partial y} = \frac{1}{\partial y}\ \frac{\partial}{\partial y}(y\tau) + \frac{\rho_\infty - \rho}{\rho_o} g \sin\theta \tag{3.7}$$

y-Momentum:

$$u^2\frac{d\theta}{ds} = \frac{\rho_\infty - \rho}{\rho_o} g \cos\theta \tag{3.8}$$

Energy:

$$u\frac{\partial t}{\partial s} + v\frac{\partial t}{\partial y} = \frac{1}{\rho\, Cp\, y}\ \frac{\partial}{\partial y}(-yq) \tag{3.9}$$

Salinity:

$$u\frac{\partial c}{\partial s} + v\frac{\partial c}{\partial y} = \frac{1}{\partial y}\ \frac{\partial}{\partial y}(-yJ) \tag{3.10}$$

Here τ, q, and J refer to momentum, heat and species fluxes respectively. These fluxes include both molecular and eddy counterparts, viz

$$\left.\begin{aligned} \tau &= \mu \frac{\partial u}{\partial y} - \rho \overline{u'v'} \\ q &= -k \frac{\partial t}{\partial y} + \rho\, Cp\, \overline{v't'} \\ \text{and} \quad J &= -\rho\, D \frac{\partial c}{\partial y} + \rho \overline{v'c'} \end{aligned}\right\} \qquad (3.11a)$$

Equations (3.5) to (3.10) form a set of non-linear coupled differential equations with two independent variables. This is an open set of equations for the number of unknowns exceeds the number of equations. In order to achieve closure, expressions for turbulent correlations $\overline{u'v'}$, $\overline{v't'}$, and $\overline{v'c'}$ have to be supplied. The process of replacing the exact but insoluble equations by approximate but soluble ones is referred to as 'modeling'. Boussinesq's concept [31] of modeling turbulent shear stresses relates these stresses to the rate of mean strain by use of an "apparent" or "turbulent" or "eddy" viscosity, as follows:

$$\tau = \mu \frac{\partial u}{\partial y} + \mu_t \frac{\partial u}{\partial y} = \rho(\nu + \nu_t) \frac{\partial u}{\partial y} = \rho\, \nu_{eff} \frac{\partial u}{\partial y} \qquad (3.11b)$$

where ν_t is called eddy diffusivity and ν_{eff} is the total or effective diffusivity.

Although the concept of eddy viscosity has received objections [31], it has enjoyed great success for many turbulent flows which are mainly thin shear flows, and gives a satisfactory description of the mean properties. The present work utilizes the eddy viscosity concept and does not neglect

the laminar counterpart of total viscosity which hitherto has been neglected in turbulent free shear flows except for a few exceptions [16, 32]. Laminar viscosity plays an important role in the initial region and cannot be neglected there [16].

In parallel with eddy viscosity, an eddy conductivity and eddy diffusivity for component of mass can be defined. The turbulent shear stresses are related to heat fluxes by a relation known as the Reynolds analogy between heat and momentum transfer. In the Reynolds analogy, it is assumed that the turbulent diffusivity for heat and momentum are related in a manner analogous to laminar flow according to

$$Pr_t = \frac{\nu_t}{\alpha_t} \tag{3.12}$$

where Pr_t is the turbulent Prandtl number and α_t, the turbulent diffusivity for heat. In a likewise manner, turbulent Schmidt number is defined as

$$Sc_t = \frac{\nu_t}{D_t} \tag{3.13}$$

where D_t is the turbulent mass diffusivity. This study assumes $Pr_t = Sc_t$, or a turbulent Lewis number Le_t equal to 1.

The eddy viscosity approach has worked well for wall boundary layers and tube flows [33], and has been successfully used in jet flows [16, 32]. Most models use a constant value

of Pr_t, a value of 0.5 has been used for a plane mixing layer, values closer to unity appear to be common in wall-bounded flows; for round jets, 0.7 has been extensively used [16, 32, 33]. The heat flux q is related to ν_t through Pr_t

$$\begin{aligned} q &= -\rho\, Cp \left(\alpha + \frac{\nu_t}{Pr_t}\right) \frac{\partial t}{\partial y} \\ &= -\rho\, Cp\, \alpha_{eff} \frac{\partial t}{\partial y} \end{aligned} \tag{3.14}$$

and

$$\begin{aligned} J &= -\rho \left(D + \frac{\nu_t}{Sc_t}\right) \frac{\partial c}{\partial y} \\ &= -\rho D_{eff} \frac{\partial c}{\partial y} \end{aligned} \tag{3.15}$$

Pr_t and Sc_t were kept equal to 0.7 in all calculations reported here.

3.2 INITIAL AND BOUNDARY CONDITIONS

Equations (3.6) to (3.9), being parabolic in character, possess an open boundary in the main flow direction. Thus the solution can be marched off in the downstream direction subject to the following boundary conditions

$$\left.\begin{array}{l} \lim_{y\to\infty} u(s,y) = u_\infty, \quad \lim_{y\to\infty} t(s,y) = t_\infty \\ \lim_{y\to\infty} c(s,y) = c_\infty \quad \text{and} \\ \frac{\partial u}{\partial y} = \frac{\partial t}{\partial y} = \frac{\partial c}{\partial y} = 0 \quad \text{and } v = 0 \quad \text{at } y = 0 \end{array}\right\} \tag{3.16}$$

The initial profiles are specified as

$$u(s_o,y) = f(y),\ t(s_o,y) = g(y)$$
$$c(s_o,y) = h(y),\ \theta(s_o) = \theta_o \qquad (3.17)$$

In most practical applications of the discharge problem, the initial profiles are nearly uniform [34, 35, 17]. Hence, uniform profiles of velocity, temperature and salinity were used as initial conditions in all calculations of the present work. The numerical scheme can easily accommodate any other profile should that become necessary. The transverse velocities at discharge have been set to zero following Madni's work [12]. Although not required from a mathematical point of view, they are needed for the numerical scheme.

3.3 NON-DIMENSIONAL FORMS

Non-dimensionalization is an extremely useful tool in that it renders solutions general and equations are reduced to a simpler form devoid of units.

The variables were non-dimensionalized as:

$$U = \frac{u}{u_o},\ V = \frac{v}{u_o},\ \bar{\rho} = \frac{\rho - \rho_{\infty o}}{\rho_o - \rho_{\infty o}},\ T = \frac{t - t_{\infty o}}{t_o - t_{\infty o}},\ C = \frac{c - c_{\infty o}}{c_o - c_{\infty o}}$$

$$S = \frac{su_o}{\nu},\ Y = \frac{yu_o}{\nu},\ N = \frac{\nu_{eff}}{\nu},\ N_H = \frac{\alpha_{eff}}{\nu} \qquad (3.18)$$

$$N_m = \frac{D_{eff}}{\nu}$$

In general $\rho_{\infty o} = \rho_\infty$ except when the ambient is stratified and ρ_∞ is a variable. The equations in non-dimensional form are given by

Continuity:

$$\frac{\partial}{\partial S}(U Y) + \frac{\partial}{\partial Y}(V Y) = 0 \tag{3.19}$$

S-Momentum:

$$U \frac{\partial U}{\partial S} + V \frac{\partial U}{\partial Y} = \frac{1}{Y}\left[Y N \frac{\partial U}{\partial Y}\right] + \frac{1}{Re_o Fr_o} \frac{G}{G_o} \sin\theta \tag{3.20}$$

y-Momentum:

$$U^2 \frac{d\theta}{dS} = \frac{\cos\theta}{Re_o Fr_o} \cdot \frac{G}{G_o} \tag{3.21}$$

Energy:

$$U \frac{\partial T}{\partial S} + V \frac{\partial T}{\partial Y} = \frac{1}{Y} \frac{\partial}{\partial Y}\left(Y N_H \frac{\partial T}{\partial Y}\right) \tag{3.22}$$

Salinity:

$$U \frac{\partial C}{\partial S} + V \frac{\partial C}{\partial Y} = \frac{1}{Y} \frac{\partial}{\partial Y}\left(Y N_M \frac{\partial C}{\partial Y}\right) \tag{3.23}$$

where

$$\frac{G}{G_o} = \frac{\rho_\infty - \rho}{\rho_{\infty o} - \rho_o}$$

$$= \frac{\beta(T - T_\infty)(t_o - t_{\infty o}) + \beta^*(C - C_\infty)(c_o - c_{\infty o})}{\beta(t_o - t_{\infty o}) + \beta^*(c_o - c_{\infty o})} \tag{3.24}$$

For an unstratified ambient $T_\infty = 0$.

In the above equations, Reynolds number Re_o and Froude number Fr_o appear in the buoyancy term of the momentum equation. They are defined as

$$Re_o = \frac{u_o \, D}{\nu}$$

and

$$Fr_o = \frac{u_o^2}{g \, D \, \frac{\rho_{\infty o} - \rho_o}{\rho_o}}$$

The initial and boundary conditions transform as

$$\left.\begin{aligned} &U(S_o,Y) = F(Y), \; T(S_o,Y) = G(Y) \\ &C(S_o,Y) = H(Y), \; \theta(S_o) = \theta_o \\ &\frac{\partial U}{\partial Y} = \frac{\partial T}{\partial Y} = \frac{\partial C}{\partial Y} = 0 \quad \text{and } V = 0 \quad \text{at} \quad Y = 0 \\ &\text{and} \\ &\lim_{Y \to \infty} U(S,Y) = U_\infty, \; \lim_{Y \to \infty} T(S,Y) = T_\infty, \; \lim_{Y \to \infty} C(S,Y) = C_\infty \end{aligned}\right\} \quad (3.25)$$

For uniform profiles, $F(Y) = G(Y) = H(Y) = 1.0$. For a quiescent ambient, which is the case here, $U_\infty = 0$, and when the ambient is unstratified $T_\infty = C_\infty = 0$. However, for a linearly stratified ambient

$$\left.\begin{aligned} &T_\infty = \frac{\lambda \, D}{Re_o(t_o - t_{\infty o})} Z \\ &\text{and} \\ &C_\infty = \frac{\lambda^* \, D}{Re_o(c_o - c_{\infty o})} Z \end{aligned}\right\} \quad (3.26)$$

where λ and λ^* are the ambient temperature and salinity stratification, defined as

$$\left.\begin{aligned} |\lambda| &= \frac{dt_\infty}{dz} \\ \text{and} \\ |\lambda^*| &= \frac{dc_\infty}{dz} \end{aligned}\right\} \qquad (3.27)$$

3.4 FINITE-DIFFERENCE FORMULATION

The set of equations (3.19) to (3.23) is to be solved over the region of interest, using a finite-difference method. The solution method employed an explicit formulation of the DuFort-Frankel type [36]. Figure 3.1 shows the details of the finite-difference grid used. The method is applicable for unequal grid spacings in both directions. However, for all computations in the present work, Δy spacings were kept equal, while Δs was varied.

Both mathematical and physical techniques for discretization abound in the literature. The physical technique of obtaining finite-difference approximation consists of setting up equations for the laws governing the physical system. This resistance network or cell control volume approach can be of great value in difficult cases which are immediately simplified by the examination of heat flows in a control volume. In the mathematical approach the continuous formulation of the problem is transformed into a discrete formulation by replacing

derivatives and other functions occuring by finite-difference approximations. The former is accomplished by expanding the variables in Taylor series about appropriate grid points, and then the resulting series is truncated to obtain difference approximation of the derivatives. The technique is simple, straightforward and flexible and one can assign an order of accuracy to each replacement.

The order of the terms neglected due to the truncation gives the order of the truncation error associated with the scheme. To illustrate how derivatives are approximated, an example of a simple, forward-difference approximation for $\left(\frac{\partial U}{\partial S}\right)_{i,j}$ will be developed.

Taylor series expansion for $U(S + \Delta S,Y)$ about (S,Y) gives

$$U(S + \Delta S,Y) = U(S,Y) + \Delta S \frac{\partial U}{\partial S}(S,Y) + \frac{(\Delta S)^2}{2!} \frac{\partial^2 U}{\partial S^2}(S,Y)$$

$$+ \frac{(\Delta S)^3}{3!} \frac{\partial^3 U}{\partial S^3}(S,Y) + O[(\Delta S)^4]$$

Simple algebra yields

$$\frac{\partial U}{\partial S}(S,Y) = \frac{U(S + \Delta S,Y) - U(S,Y)}{\Delta S} - \frac{(\Delta S)}{2!} \frac{\partial^2 U}{\partial Y^2}(S,Y)$$

$$+ \frac{(\Delta S)^2}{3!} \frac{\partial^3 U}{\partial S^3}(S,Y) + O[(\Delta S)^3]$$

or

$$\left(\frac{\partial U}{\partial S}\right)_{i,j} = \frac{U_{i+1,j} - U_{i,j}}{\Delta S} + O[\Delta S].$$

The truncation error is of the order of ΔS, hence this is a first-order approximation. The partial differential equations are thus transformed into a set of algebraic equations, which are then solved step by step to give a solution that exists at a finite number of discrete grid points. Both explicit and implicit methods can be developed by expanding the Taylor series about different grid points and using various combinations of these.

DUFORT-FRANKEL (D-F) SCHEME

Most finite-difference schemes applied to the jet flow problem have been implicit in nature [37]. The D-F formulation was successfully used for channel flows and wall-boundary layers [38, 39] and was applied to the turbulent jet problem by Madni [12]. In the texts on Numerical Analysis, the D-F scheme is listed under unconditionally stable explicit schemes. However, in application to plume predictions, instabilities were observed and a stability constraint was developed [16]. But still the scheme is attractive and allows greater streamwise stepsize than that is allowed by the implicit method of Patankar and Spalding [40].

The increased stability obtained by using the D-F formulation is because, instead of approximating the dependent variable at the junction points of the rectangular lattice $x = i\Delta x$, $t = j\Delta t$, it makes use of a diagonal lattice, obtained

by omitting those junction points for which i+j is, say odd. If ϕ is any dependent variable, then the term $\phi_t (= \partial\phi/\partial t)$ is represented by the difference of two ϕ_{ij} - values of the same i and j's differing by 2; i.e., $\phi_t(i\Delta x, j\Delta t) = (\phi_{i,j+1} - \phi_{i,j-1})/2\Delta t$; i+j odd. In the representation of ϕ_{xx} by a second difference with reference to i, the term $\phi_{i,j}$ corresponds to a point ommitted from the lattice. It is, therefore, replaced by the mean of the two terms of neighbouring j-values.

$$\phi_{xx}(i\Delta x, j\Delta t) = (\phi_{i-1,j} - \phi_{i,j-1} - \phi_{i,j+1} + \phi_{i+1,j})/(\Delta x)^2 \qquad \text{i+j odd}$$

Similarly, ϕ_x and ϕ_t may be represented by $(\phi_{i+1,j} - \phi_{i-1,j})/2\Delta x$ and $(\phi_{i,j+1} + \phi_{i,j-1})/2\Delta t$, respectively.

THE DIFFERENCE EQUATIONS

The DuFort-Frankel forms of Eqs.(3.19) to (3.23) are:

Continuity:

$$\frac{Y_{j+1} + Y_j}{4(\Delta S_+ + \Delta S_-)} [U_{i+1,j+1} + U_{i+1,j} - U_{i-1,j+1} - U_{i-1,j}]$$

$$+ \frac{(Y_{j+1} V_{i+1,j+1} - Y_j V_{i+1,j})}{\Delta Y_+} = 0 \qquad (3.28)$$

S-Momentum:

$$\frac{U_{i,j}}{(\Delta S_+ + \Delta S_-)} (U_{i+1,j} - U_{i-1,j}) + \frac{V_{i,j}}{(\Delta Y_+ + \Delta Y_-)} \times (U_{i,j+1} - U_{i,j-1})$$

$$= \frac{2}{Y_j(\Delta Y_+ + \Delta Y_-)} \times \left\{ \left[\frac{(Y_{j+1} + Y_j)(N_{i,j} + N_{i,j+1})}{4} \times \right. \right.$$

$$\times \frac{(U_{i,j+1} - 0.5[U_{i+1,j} + U_{i-1,j}])}{\Delta Y_+}\Bigg] - \Bigg[\frac{(Y_j + Y_{j-1})(N_{i,j} + N_{i,j-1})}{4}$$

$$\times \frac{(0.5[U_{i+1,j} + U_{i-1,j}] - U_{i,j-1})}{\Delta Y_-}\Bigg]\Bigg\} + \frac{G_{i,j}}{G_o} \frac{\sin\theta_i}{Re_o Fr_o} \qquad (3.29)$$

y-Momentum:

$$\frac{(U_{i,j})^2}{(\Delta S_+ + \Delta S_-)} (\theta_{i+1} - \theta_{i-1}) = \frac{G_{i,j}}{G_o} \frac{\cos\theta_i}{Re_o Fr_o} \qquad (3.30)$$

Energy:

$$\frac{U_{i,j}}{(\Delta S_+ + \Delta S_-)} (T_{i+1,j} - T_{i-1,j}) + \frac{V_{i,j}}{(\Delta Y_+ + \Delta Y_-)} (T_{i,j+1} - T_{i,j-1})$$

$$= \frac{2}{Y_j(\Delta Y_+ + \Delta Y_-)} \Bigg\{\Bigg[\frac{(Y_{j+1} + Y_j)(N_{Hi,j+1} + N_{Hi,j})}{4}$$

$$\times \frac{(T_{i,j+1} - 0.5[T_{i+1,j} + T_{i-1,j}])}{\Delta Y_+}\Bigg] - \Bigg[\frac{(Y_j + Y_{j-1})(N_{Hi,j} + N_{Hi,j-1})}{4}$$

$$\times \frac{(0.5[T_{i+1,j} + T_{i-1,j}] - T_{i,j-1})}{\Delta Y_-}\Bigg]\Bigg\} \qquad (3.31)$$

Salinity:

$$\frac{U_{i,j}}{(\Delta S_+ + \Delta S_-)} (C_{i+j,j} - C_{i-1,j}) + \frac{V_{i,j}}{(\Delta Y_+ + \Delta Y_-)} (C_{i,j+1} - C_{i,j-1})$$

$$= \frac{2}{Y_j(\Delta Y_+ + \Delta Y_-)} \Bigg\{\Bigg[\frac{(Y_{j+1} + Y_j)(N_{Mi,j+1} + N_{Mi,j})}{4}$$

$$\times \frac{(C_{i,j+1} - 0.5[C_{i+1,j} + C_{i-1,j}])}{\Delta Y_+}\Bigg] - \Bigg[\frac{(Y_j + Y_{j-1})(N_{Mi,j} + N_{Mi,j-1})}{4}$$

$$\times \frac{(0.5[C_{i+1,j} + C_{i-1,j}] - C_{i,j-1})}{\Delta Y_-}\Bigg]\Bigg\} \qquad (3.32)$$

where

$$\frac{G_{i,j}}{G_o} = \frac{\beta(t_o - t_{\infty o})(T_{i,j} - T_{\infty i}) + \beta^*(c_o - c_{\infty o})(C_{i,j} - C_{\infty i})}{\beta(t_o - t_{\infty o}) + \beta^*(c_o - c_{\infty o})} \qquad (3.33)$$

The finite-difference equations have been written in a form applicable for uneven grid spacing in both streamwise and cross-stream directions, even though ΔY, the cross-stream grid, was kept constant in the calculations.

The centerline derivative boundary condition, Eq.(3.17), was implemented using Taylor series expansions for the velocity and temperature about the centerline as follows:

$$U_{i+1,2} = U_{i+1,1} + \left(\frac{\partial U_{i+1}}{\partial Y}\right)_1 \Delta Y + \left(\frac{\partial^2 U}{\partial Y^2}\right)_1 \frac{(\Delta Y)^2}{2!} + O(\Delta Y)^3 \qquad (3.34)$$

$$U_{i+1,3} = U_{i+1,1} + \left(\frac{\partial U_{i+1}}{\partial Y}\right)_1 (2\Delta Y) + \left(\frac{\partial^2 U}{\partial Y^2}\right)_1 \frac{(2\Delta Y)^2}{2!} + O(\Delta Y)^3 \qquad (3.35)$$

Multiplying both sides of Eq.(3.34) by 4 and then subtracting Eq.(3.35) from it yields, after setting $\left(\frac{\partial U_{i+1}}{\partial Y}\right)_1 = 0$:

$$4U_{i+1,2} - U_{i+1,3} = 3U_{i+1,1} + O(\Delta Y)^3$$

Using a second order approximation to the zero derivative, therefore gives

$$U_{i+1,1} = \frac{4U_{i+1,2} - U_{i+1,3}}{3} \qquad (3.36)$$

Similarly,

$$T_{i+1,1} = \frac{4T_{i+1,2} - U_{i+1,3}}{3} \text{ and } C_{i+1,1} = \frac{4\,C_{i+1,2} - C_{i+1,3}}{3}$$

Another way of implementing the centerline boundary condition is to obtain a special form of Eqs.(3.20) and (3.21)

by letting $Y \to 0$ and then applying L'Hospital's rule to the right hand side of the equations. These equations are then differenced and the symmetry condition $U_{i+1,2} = U_{i+1,0}$ where the subscript 0 refers to the first grid on the other side of the centerline, is incorporated.

STABILITY, CONSISTENCY, AND CONVERGENCE

The concept of stability of a numerical solution is somewhat difficult to precisely define, although, as anyone experienced in obtaining numerical solution is well aware, instability usually manifests itself in a very obvious, usually catastrophic manner. Instability is generally considered to be the result of either the cumulative growth of round-off errors without bound as the solution is marched forward, or the growth of error due to the presence of an extraneous solution to the difference equations. Instability of either type will generally be seen as a strongly growing, oscillatory cumulative error which, in practice, rapidly causes a computer overflow.

A consistent finite-difference representation has an exact solution (assuming no round-off error) that approaches the solution of the differential equations which the difference equations replace as the mesh sizes approach zero. Consistency of a difference representation is dependent on the difference forms used to replace the various terms in

the differential equations and the boundary conditions. Sometimes the term convergence is synonymously used with consistency, but the former is in fact rather widely used to describe a characteristic of an iterative process [41].

Generally, the smaller the truncation error, the faster the convergence of the numerical solution to the true one [41]. Using derivatives of U in the Y direction as examples, the truncation errors can be examined.

In the standard explicit method,

$$\frac{\partial U}{\partial Y} = \frac{U_{i,j+1} - U_{i,j}}{\Delta Y} - \frac{\partial^2 U}{\partial Y^2}\,\frac{\Delta Y}{2!} - \frac{\partial^3 U}{\partial Y^3}\,\frac{(\Delta Y)^2}{3!}$$

The truncation error for this formulation is $O(\Delta Y)$.

In the D-F scheme,

$$\frac{\partial U}{\partial Y} = \frac{U_{i,j+1} - U_{i,j-1}}{\Delta Y} - \frac{\partial^3 U}{\partial Y^3}\,\frac{(\Delta Y)^2}{3!} - \frac{\partial^5 U}{\partial Y^5}\,\frac{(\Delta Y)^4}{5!}$$

and the truncation error is seen to be $O[(\Delta Y)^2]$ [16].

It is necessary that any truncation error be at most $O(\Delta Y)$, or $O(\Delta S)$ in case of streamwise differences, to satisfy consistency. This is true for all derivatives approximated by the present method, but one term deserves closer attention. The second-derivative term in the normal direction is written for constant mesh size, as:

$$\frac{\partial^2 U}{\partial Y^2} = \frac{U_{i,j+1} + U_{i,j-1} - U_{i+1,j} - U_{i-1,j}}{(\Delta Y)^2} + \frac{\partial^2 U}{\partial S^2}\left(\frac{\Delta S}{\Delta Y}\right)^2 - \frac{\partial^4 U}{\partial Y^4}\frac{(\Delta Y)^2}{12} \tag{3.37}$$

[It is worthy of note that for a standard explicit method, the numerator would be of the form $(U_{i,j+1} + U_{i,j-1} - 2U_{i,j})$. By comparing the two forms, the essential feature of the D-F scheme can be revealed.] The truncation error in Eq.(3.37) is:

$$O\left[\left(\frac{\Delta S}{\Delta Y}\right)^2\right] + O[(\Delta Y)^2]$$

Thus, the formulation is mathematically consistent only if ΔS goes to zero faster than ΔY, and this has been the main criticism levelled against the D-F formulation. Fortunately, the entire term consists of $\frac{\partial^2 U}{\partial S^2}\left(\frac{\Delta S}{\Delta Y}\right)^2$ and for boundary layer flows, $\frac{\partial^2 U}{\partial S^2}$ is negligibly small as compared to other terms in the equation. Thus, even for $\left(\frac{\Delta S}{\Delta Y}\right) \approx 1$, Eq.(3.37) would be expected to be a good approximation, even for finite ΔS and ΔY. A complete consistency analysis for the difference Eqs. (3.28) to (3.32) is carried out by Madni and Pletcher [16].

Stability is a very important consideration, since even the best finite-difference scheme in terms of truncation error can be unstable and hence gives a solution which is entirely different from that of the partial differential equations, rendering the results useless. A brief discussion

of the stability considerations for the present D-F formulation follows.

For the simple diffusion equation, this scheme is unrestrictedly stable [36], [41]. In its application to prediction of wall boundary layer flows and tube flows [38, 39], it was found to always be stable. Naturally, therefore, no stability constraint for the method was known or believed to exist. But when this method was applied to the jet calculations reported in Madni's work, constraints on the allowable streamwise stepsize were revealed. A careful application of the Von Neumann stability analysis by Madni [12] to eqs. (3.28), (3.29), and (3.31) resulted in the following stability constraint:

$$\Delta S_+ \leq \min_{j=2,NYJ} \left[\frac{U_{i,j}\ \Delta Y}{\left| V_{i,j} + \frac{FUNC}{2\Delta Y} \right|} \right]$$

where $NYJ = \max(NY, NYT, NYC)$, and

$$FUNC = \max\left[(N_{i,j-1} - N_{i,j+1}), (N_{Hi,j-1} - N_{Hi,j+1}), (N_{Mi,j-1} - N_{Mi,j+1})\right]$$

This is derived in [12]. No general theory is available for proving stability and convergence in the case of nonlinear equations with variable coefficients such as is the case here, and a common practice is to investigate the 'local' stability whereby the coefficients are considered constant or error-free in a small neighborhood of each grid point [16]. The stability criteria developed thereby is for 'local'

stability but if the requirement is checked at each grid point, then it is reasoned that an instability could not originate.

The analysis is thus a heuristic extension of the rather general theory of Von Neumann applicable to linear problems with constant coefficients. Even so, in the actual testing ground of numerical computations, the stability criterion obtained in this way proved to be the most effective in eliminating the stability problem.

This restriction is not severe, and except very close to nozzle exit it is really very generous as compared to that for the ordinary explit method (see Ref.[12]). A streamwise stepsize ΔS_+ of about 8-10% of the width of the mixing zone in the main region was found to give good results for the co-flowing stream calculations, and for quiescent ambient cases up to 6% of the mixing zone was used without stability problems. This is several times larger than would be possible using the ordinary explicit scheme where, in addition to the viscosity difference, the value of the viscosity itself appears in the denominator [16] (see also Ref.[12]). Following Madni, a small free-stream velocity, equal to 4% of jet velocity was specified for the quiescent ambient cases in order to increase allowable stepsize.

3.5 METHOD OF SOLUTION

A skeleton flow chart illustrating the order of calculation is shown in Fig. 3.2.

Equation (3.29) can be solved directly for $U_{i+1,j}$ if all the U's are known at the i and i-1 levels and the V's, T's and θ are known at the i level. As the D-F scheme requires information from two previous stream-wise stations, namely, i and i-1, a modification of the ordinary explicit method described in [65], which requires information from only one previous station, was used to start the solution. Details of this explicit scheme are given in Ref.[16]. Equation (3.29) is then solved for $U_{i+1,j}$ for all j values in the mixing zone, starting with the point adjacent to the jet centerline and working outward to the edge of the jet or plume, using the boundary conditions specified by Eq.(3.36) at the jet centerline. The outer boundary is located when $(U_{i+1,1} - U_{i+1,j})/(U_{i+1,1} - U_{\infty i+1})$ is not less than a specified value, in this case, 0.99. In section 3.2, the free stream boundary condition for U was applied at $y \to \infty$, but for practical purposes, the above criterion for locating the edge is sufficiently accurate. With the $U_{i+1,j}$'s determined, Eq.(3.28) can be solved for $V_{i+1,j+1}$, starting from the point adjacent to the jet centerline and working outward, using the specified boundary value of the normal component of velocity at the jet centerline. θ_{i+1} is then

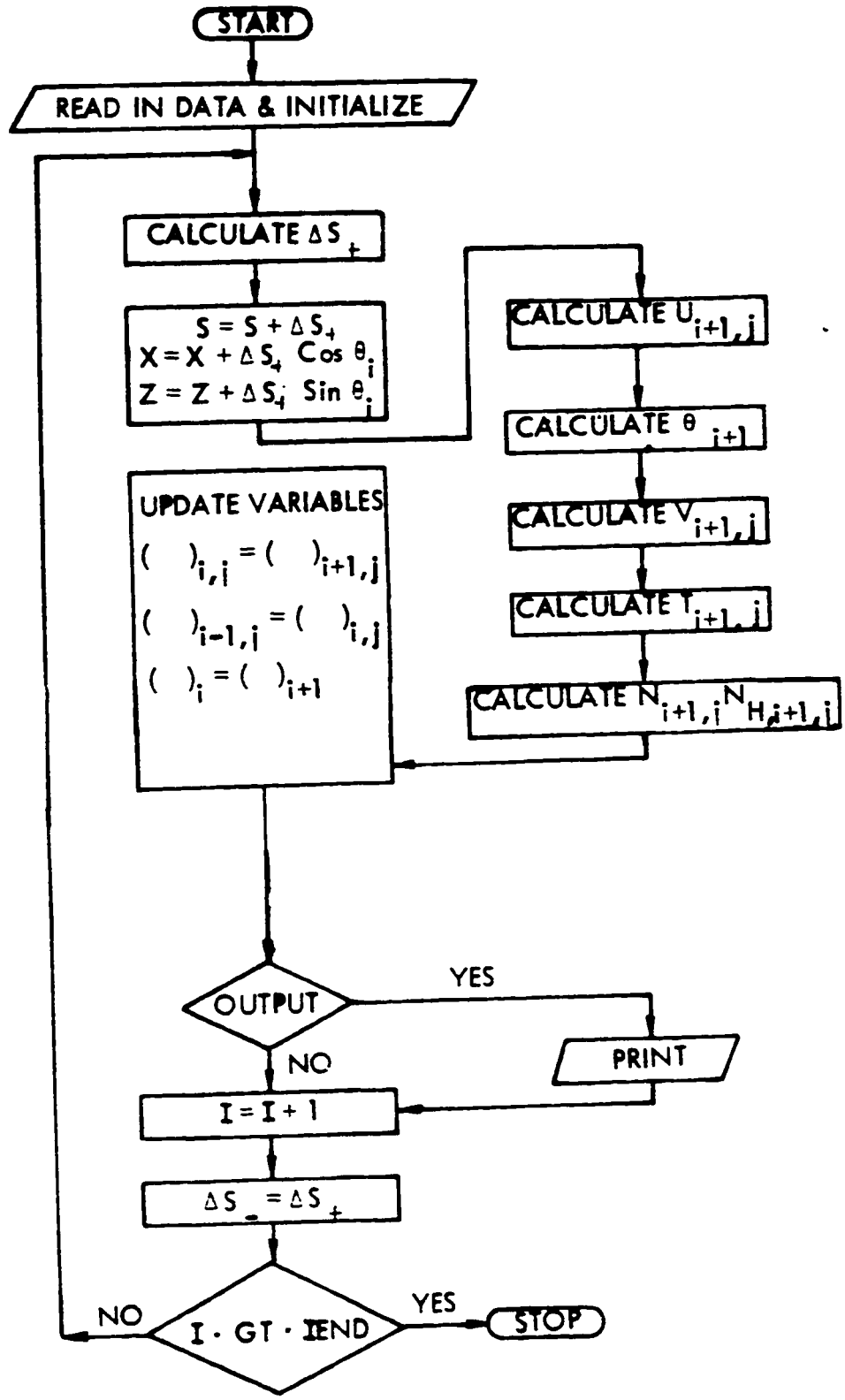

Fig. 3.2. Skeleton flow chart for the general calculation method, [12].

determined for the general problem of the buoyant curved jet by solving Eq.(3.30), and $T_{i+1,j}$'s are determined as explained earlier for U's, by solving Eq.(3.31), and $C_{i+1,j}$'s are determined by solving Eq.(3.32), i.e., the finite-difference form of the enery and salinity equations.

It is worth noting that the normal momentum equation appearing in the form shown as Eq.(3.30), shows a constant value of θ across the cross-section, hence evaluating it at the centerline would mean using $(U_{i,1})$ and $(T_{i,1})$. But a better and more realisitic estimate of θ at station i+1 can be made if Eq.(3.30) is representative of the entire flow cross-section at i [12]. Hence, Eq.(3.30) was integrated over the cross-section using the U and T values generated by the the S-momentum and energy equations. Thus, no profile assumptions were made as is the case with integral methods. This will be clarified further in the curved jet analysis in Chapter 5. In the first application of this analysis, as described in Chapter 4, the normal momentum equation did not appear, and was, therefore, not used.

According to Fig.3.2, the effective viscosity and conductivity are evaluated next. This is the place in the program where the different models for the turbulence are examined. More details on turbulence models will be presented in Chapters 4 and 5.

Finally, the variables are all updated to prepare for the next computational step, i.e., all variables at i+1 become quantities at i, and those at i become quantities at i-1. The solution is thus stepped off until all the desired flow region has been calculated.

An increasing streamwise step size was incorporated into the program. It should be emphasized that each variable is calculated explicitly at each location, no iterations or simultaneous solutions being required.

An interesting aspect of the solution procedure, namely, the generation of the plume trajectory, will be briefly described. Once the forward streamwise step ΔS_+ is calculated, its horizontal and vertical components, in order, are determined as follows:

$$\Delta X_+ = \Delta S_+ \cos \theta_i$$

$$\Delta Z_+ = \Delta S_+ \sin \theta_i$$

Then the cumulative distance travelled by the jet, and its coordinates, are generated by the summations:

$$\begin{aligned} S_{i+1} &= S_i + \Delta S_+ \\ X_{i+1} &= X_i + \Delta S_+ \cos \theta_i \\ Z_{i+1} &= Z_i + \Delta S_+ \sin \theta_i \end{aligned} \tag{3.38}$$

Although various numbers of radial grid points were used in

studying the convergence properties of the method, most calculations were made by dividing the discharge radius into 20 ΔY increments.

The method is fast and most of the computations reported here have required about 30 seconds of CPU time on the IBM system 3033.

4. VERTICAL DENSE JET IN UNIFORM OR STRATIFIED AMBIENT

4.1 INTRODUCTION

The experimental as well as theoretical analyses of vertical dense jet have been very scant. The experimental work is limited to those of Turner [21], and Zeitoun, et al. [2]. Theoretical analysis in terms of approximate methods for the prediction of vertical jets has been found only in [2]. Numerical treatment of the partial-differential equations governing the vertical plume flow in uniform ambient by finite-difference methods has been restricted to the work of Trent and Welty [10], Oosthuizen [42], and Madni and Pletcher [14]. But all these works have been limited to a positively buoyant jet discharged vertically to uniform or stratified ambients. The present work will apply the numerical scheme of [12] to the case of vertical dense jet.

For vertical, dense jets issuing into stratified ambients, there is a complete absence of experimental or theoretical work. However, due to the importance of this configuration for discharge into ocean and lakes which are frequently stratified in density, this study will include analysis of the stratified ambient case.

4.2 FLOW CONFIGURATION

Figure 4.1 shows the configuration of a vertical jet issuing into a uniform ambient. The jet is decelerated by buoyancy, causing the centerline velocity at discharge to start decreasing. The starting length, S_ℓ, defined as the axial distance to the point where mixing has reached the centerline, is based on density. A submerged jet will rise due to the initial momentum it possesses but the negative buoyant force will drive it downward. Thus, there are two regions of the jet, an upflow region and a downflow region. In case of a stably stratified ambient, the height of rise of the jet will be further suppressed.

The zero-momentum height is very important from the point of view of thermal and/or saline discharge design since it determines whether the plume will reach and spread out on the water surface or stay submerged and spread out below the water surface. The discharge system can be designed to achieve either of these conditions depending upon the requirements of the water quality standards.

4.3 GOVERNING EQUATIONS

The equations listed below are a degenerate form of those presented in Chapter 3 for $\theta_o = 90°$. Since the plume trajectory will follow a straight line, θ remains constant $= 90°$, and the y-momentum equation is absent. The resulting set of equations is the same as Eqs.(3.6) to (3.10).

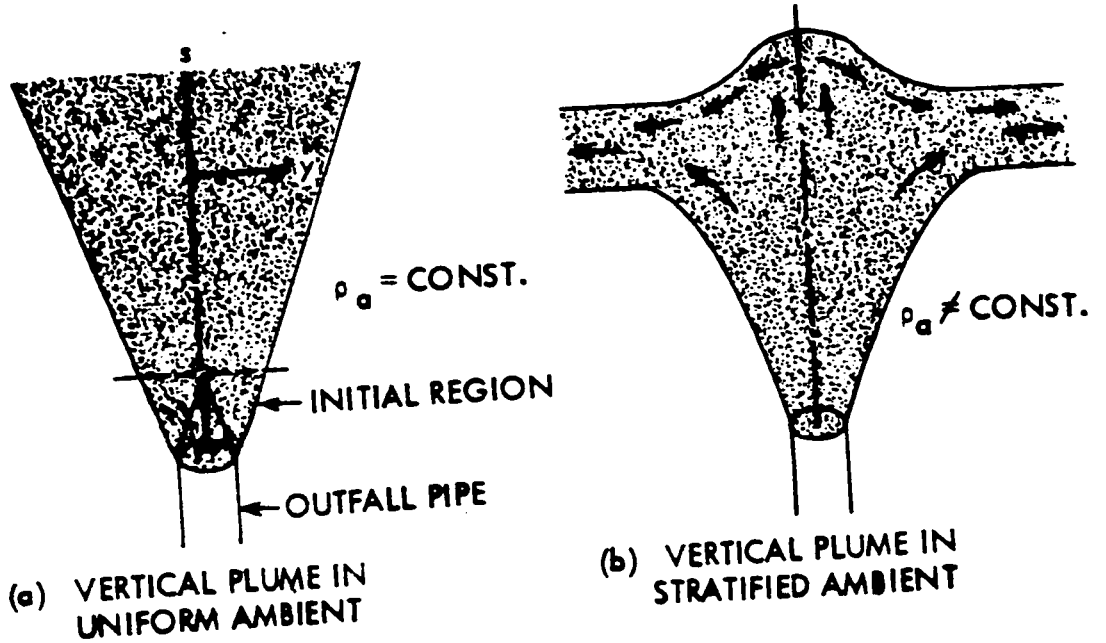

Fig. 4.1. Flow configurations for vertical jet

$$\frac{\partial}{\partial s}(uy) + \frac{\partial}{\partial y}(vy) = 0 \qquad (4.1)$$

$$u\frac{\partial u}{\partial s} + v\frac{\partial u}{\partial y} = \frac{1}{py}\frac{\partial}{\partial y}(y\tau) + \frac{(\rho_\infty - \rho)}{\rho_o} g \qquad (4.2)$$

$$u\frac{\partial t}{\partial s} + v\frac{\partial t}{\partial y} = \frac{1}{\rho\ Cp\ y}\ \frac{\partial}{\partial y}(-yq) \qquad (4.3)$$

$$u\frac{\partial c}{\partial s} + u\frac{\partial c}{\partial y} = \frac{1}{py}\ \frac{\partial}{\partial y}(-y\tau) \qquad (4.4)$$

the buoyancy term in the momentum equation is related to temperature and concentration via a linear equation of state, as shown in Chapter 3.

Here, s = z, since for a vertical configuration the streamwise coordinate coincides with the vertical.

The boundary conditions are given by Eq.(3.16) and the initial conditions by Eq.(3.17).

The variable boundary condition describing ambient stratification is explained in the next section.

4.4 NON-DIMENSIONALIZATION

The dimensionless variables are given by Eq.(3.18), and the normalized equations in terms of these variables can be written as:

$$\frac{\partial}{\partial S}(UY) + \frac{\partial}{\partial Y}(VY) = 0 \tag{4.5}$$

$$U\frac{\partial U}{\partial S} + V\frac{\partial U}{\partial Y} = \frac{1}{Y}\frac{\partial}{\partial Y}\left(YN\frac{\partial U}{\partial Y}\right) + \frac{G}{G_o}\frac{1}{Re_o\, Fr_o} \tag{4.6}$$

$$U\frac{\partial T}{\partial S} + V\frac{\partial T}{\partial Y} = \frac{1}{Y}\frac{\partial}{\partial Y}\left(YN_H\frac{\partial T}{\partial Y}\right) \tag{4.7}$$

$$U\frac{\partial C}{\partial S} + V\frac{\partial C}{\partial Y} = \frac{1}{Y}\frac{\partial}{\partial Y}\left(YN_M\frac{\partial C}{\partial Y}\right) . \tag{4.8}$$

where G/G_o is given by Eq.(3.24).

As mentioned earlier, the general behavior of the dense vertical jet in an ambient of variable density will depend on the initial relative buoyancy of the plume, and the degree of ambient stratification.

Buoyancy is represented by a non-dimensional parameter called the Froude number, Fr. It expresses the ratio of the inertia to buoyancy forces, so that a high Fr means that the effects of buoyancy will be small and vice versa.

Mathematically,

$$Fr = \frac{u^2}{2g\delta\,\dfrac{(\rho_\infty - \rho)}{\rho_o}} \tag{4.9}$$

The initial Froude number, therefore, would be represented by:

$$Fr_o = \frac{u_o^{\,2}}{gD\,\dfrac{(\rho_\infty - \rho_o)}{\rho_o}} \tag{4.10}$$

For a dense jet, Fr_o will always be negative.

The ambient stratification is generally linear. Thus, knowing $\lambda = \frac{dt_\infty}{dz}$ and $\lambda^* = \frac{dc_\infty}{dz}$, the ambient temperature and salinity can be evaluated from

$$t_\infty - t_{\infty_o} = \lambda z$$

$$c_\infty - c_{\infty_o} = \lambda^* z$$

Or, in terms of dimensionless variables, from Eq.(3.26).

Sometimes, a non-dimensional stratification number, $\bar{T}$, is defined

$$\bar{T} = \frac{\rho_o - \rho_{\infty_o}}{-\frac{D}{2}\frac{d\rho_\infty}{dz}} \qquad (4.11)$$

which can be expressed in terms of temperature and concentration.

4.5 THE DIFFERENCE FORMULATION

The difference forms of the continuity and energy equations are the same as Eqs. (3.28) and (3.31), while the momentum equation is written as follows:

$$\frac{U_{i,j}}{(\Delta S_+ + \Delta S_-)}(U_{i+1,j} - U_{i-1,j}) + \frac{V_{i,j}}{(\Delta Y_+ + \Delta Y_-)} \times (U_{i,j+1} - U_{i,j-1})$$

$$= \frac{2}{Y_j(\Delta Y_+ + \Delta Y_-)} \times \left\{\left[\frac{(Y_{j+1} + Y_j)(N_{i,j} + N_{i,j+1})}{4} \times \right.\right.$$

$$\left.\times \frac{(U_{i,j+1} - 0.5[U_{i+1,j} + U_{i-1,j}])}{\Delta Y_+}\right] - \left[\frac{(Y_j + Y_{j-1})(N_{i,j} + N_{i,j-1})}{4}\right.$$

$$\left.\left.\times \frac{(0.5[U_{i+1,j} + U_{i-1,j}] - U_{i,j-1})}{\Delta Y_-}\right]\right\} + \left[\frac{G_{i,j}}{G_o}\right] / (Re_o\, Fr_o) \qquad (4.12)$$

The initial and boundary conditions transform as explained in Chapter 3.

4.6 TRANSPORT MODELS AND RESULTS

1. UNIFORM AMBIENT

One of the most successful simple turbulence models was suggested by Ludwieg Prandtl in 1925 which has become known as the mixing-length hypothesis:

$$\mu_t = \rho \, \ell^2 \left| \frac{\partial u}{\partial y} \right| \tag{4.13}$$

where ℓ, a "mixing length", is the transverse distance over which particles maintain their original momentum.

Prandtl's Eq.(4.13) is unsatisfactory in that the apparent kinematic viscosity, ν_t, vanishes at points where $\frac{\partial u}{\partial y}$ is zero, i.e., at points of maximum and minimum velocity. This is certainly not the case because turbulent mixing does not vanish at points of maximum velocity. Prandtl later realised this difficulty and was able to set up a new hypothesis valid only for free turbulent flows. He assumed that the dimensions of the lumps of fluid which move in a transverse direction during turbulent mixing have the dimensions of the same order of magnitude as the width of mixing zone. It should be recalled that the previous hypothesis (Eq.4.13) implied that they were small compared with the transverse dimensions of the region of flow. The turbulent

kinematic viscosity, ν_t, is now formed by multiplying the maximum difference in the time-mean flow velocity with a length which is assumed to be propoportional to the width of the mixing zone. Thus,

$$\nu_t = K_1 \, y_{\frac{1}{2}} \, (u_{max} - u_{min}) \tag{4.14}$$

Here K_1 denotes a dimensionless number to be determined experimentally and $y_{\frac{1}{2}}$ denotes half the width of half depth. Based on H. Reichardt's extensive experimental data on free turbulent flow, K was found to be 0.0256 for a round turbulent jet [60]. However, for a buoyant jet 0.0246 was used successfully by Madni [12]. The same value of K_1 has been retained in the present analysis.

As in the outer part of the wall-boundary layer, mixing length is proportional to total boundary layer thickness rather than to distance from the wall [61], same is true for the initial region of the jet. The initial region is that region where mixing has not yet penetrated to the centerline of the jet and, as a result, a potential core exists in the middle of the jet. Therefore, considering mixing length ℓ to be proportional to the width, δ, of the mixing zone and, of course, constant over a cross section of the mixing zone:

$$\ell = K_2 \, \delta \tag{4.15}$$

A value of $K_2 = 0.0762$ was found to fit experimental data very well, [12, 61]. Thus Eq.(4.15) alongwith Eq.(4.13) was

used in the initial region of the jet and Eq.(4.14) was used in the main region.

It is well-known that in the central part of the jet, the turbulence is practically wholly continuous with respect to time, whereas, near the boundary of the jet, the turbulent flow becomes more and more intermittent. Oscillograms of the oscillating turbulent velocity components demonstrate that the position of the fairly sharp boundaries between the highly turbulent flow in the boundary-layer and the nearly turbulence-free external stream fluctuates strongly with time [31, 60]. Figure 4.2 shows the instantaneous picture of the wake flow behind a cylinder. To account for the intermittent character of the turbulence, Eq.(4.14) is modified such that

$$\nu_t = \gamma K_1 \, y_{\frac{1}{2}} \, (u_{max} - u_{min}) \tag{4.16}$$

where γ is an intermittancy factor defined as that fraction of time during which the flow at a given position remains turbulent. $\gamma = 1$ corresponds to continuous turbulent flow, and $\gamma = 0$ denotes continuous laminar flow. The following curve-fit expression of Madni [12] for γ was used in the present analysis:

$$\gamma = 1.0 \qquad 0 \leq \frac{y}{y_{\frac{1}{2}}} \leq 0.8$$

$$\gamma = (0.5)^q \qquad \frac{y}{y_{\frac{1}{2}}} > 0.8 \qquad \text{where}$$

$$q = \left[\frac{y}{y_{\frac{1}{2}}} - 0.8\right]^{2.5} \tag{4.17}$$

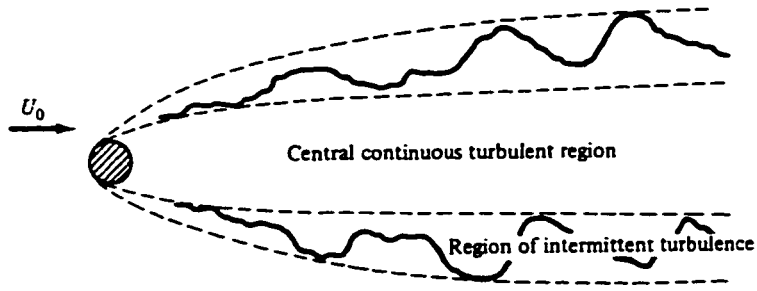

Fig. 4.2. Intermittent turbulence behind the wake of a cylinder, [31]

It may be interesting to note that introduction of intermittency function in the Prandtl's constant-viscosity model [Eq.(4.14)] did not make significant change in the vertical jet results. Whereas, as we shall see in the next chapter, intermittency function significantly changed the results for inclined jet. The reason for this may be that for vertical and horizontal, straight-line jets, constancy of turbulence quantities is not affected to a considerable extent by including an intermittency function. Hinze [31] has discussed such effect of intermittency in the turbulent region across the wake of a cylinder.

With the turbulence model of Eqs.(4.13), (4.15) and (4.16) the predicted centerline density variations for $Fr_o = -294$ are shown in Fig.4.3 along with the experimental measurements of Zeitoun, et al. [24]. The experiments show that concentration levels off to a constant value at a height of 18 diameters (about two-thirds the ceiling level of the jet). Above the zone of constant concentration the drop is rapid to a point of vanishing concentration and velocity, but it was found to be very difficult to reproduce the measurements near the top of the jet due to the fluctuations [24]. The constant concentration may be explained by a negative entrainment zone at which the inner core of the jet is entraining the outer ring of the jet of the same concentration, see Fig.2.1 [24]. It is noted that vertical submerged dense jets produce only a limited dilution of the effluent due to the negative entrainment resulting from the jet folding on itself.

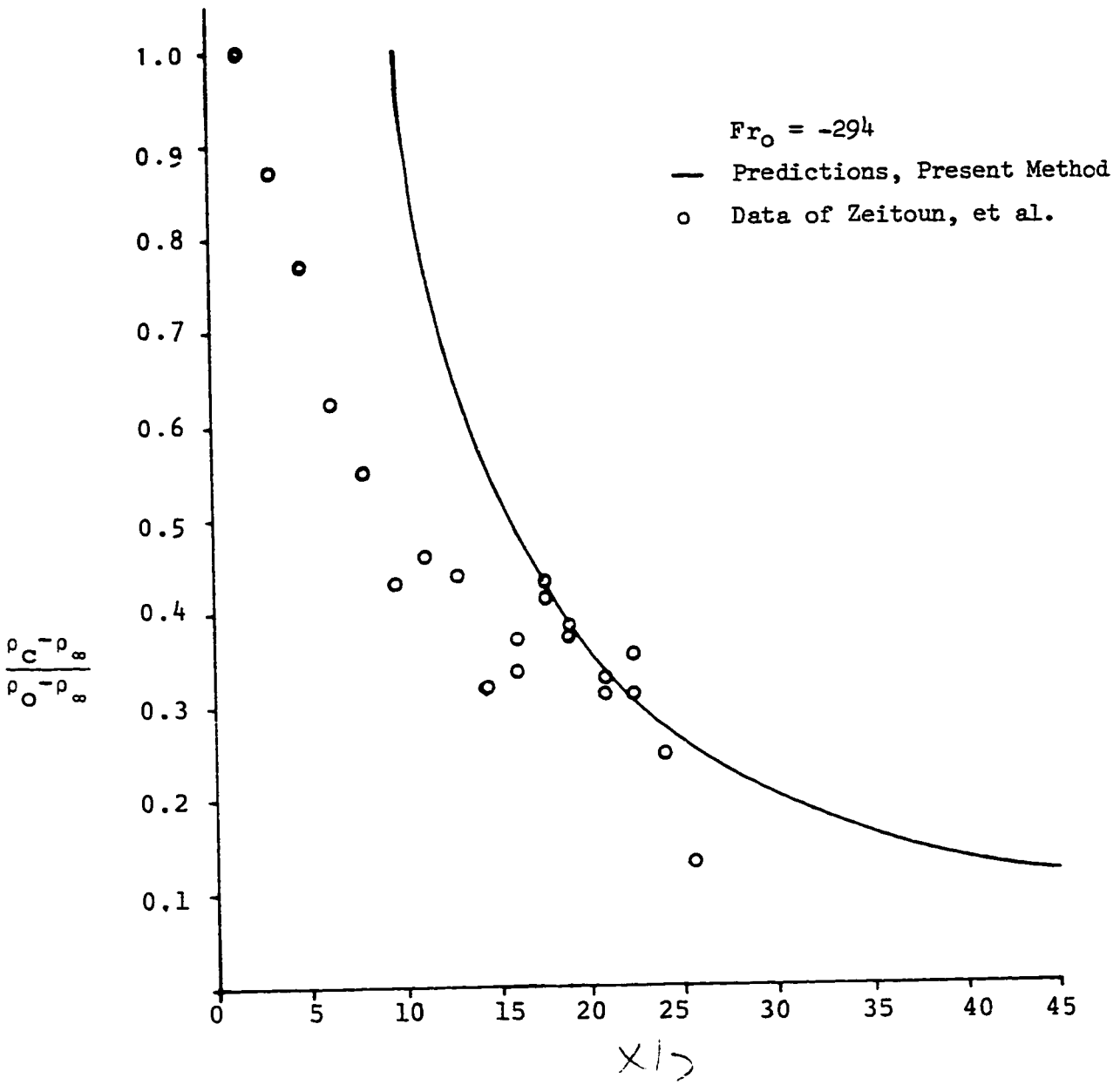

Fig. 4.3. Centerline density decay of a vertical submerged dense jet

The agreement between the centerline decay data of Zeiton, et al. and the predictions of the model is not very good. The cause for this discrepancy is not known. The only data available in the literature is that of Zeitoun, et al. [24] who have presented only one case of centerline decay, for one Froude number only. Just one experiment prevents one to conclude about the quality of the experiment and the method used as there is nothing to compare with. The validity of a model or problem formulation cannot be ascertained unless sufficient number of experiments are available so that quality of the experiment and the method used can be compared with other experiments. In fact we are in scarce need of more experimental research.

Figure 4.4 presents the maximum height of rise Zm/D against Froude number. The data shown are those of Turner [21] which cover the Froude number (Fr_o) range from -1 to -110. Also shown in the figure are Zeitoun, et al's [2] data for a higher Froude number range (-40 to -1000). The straight line in the figure is the correlation of Zeitoun, et al. There is considerable deviation between the predicted height of rise and the experimental data of Turner. However, in the Fr_o range -25 to -110, the agreement with Turner's data is very favorable. It is strange that Ref.[2] claimed to have checked Turner's correlation [Eq.(2.1)] whereas the Fig. 4.3 shows large deviations between the experimental data of Zeitoun, et al. [2] and Turner [21].

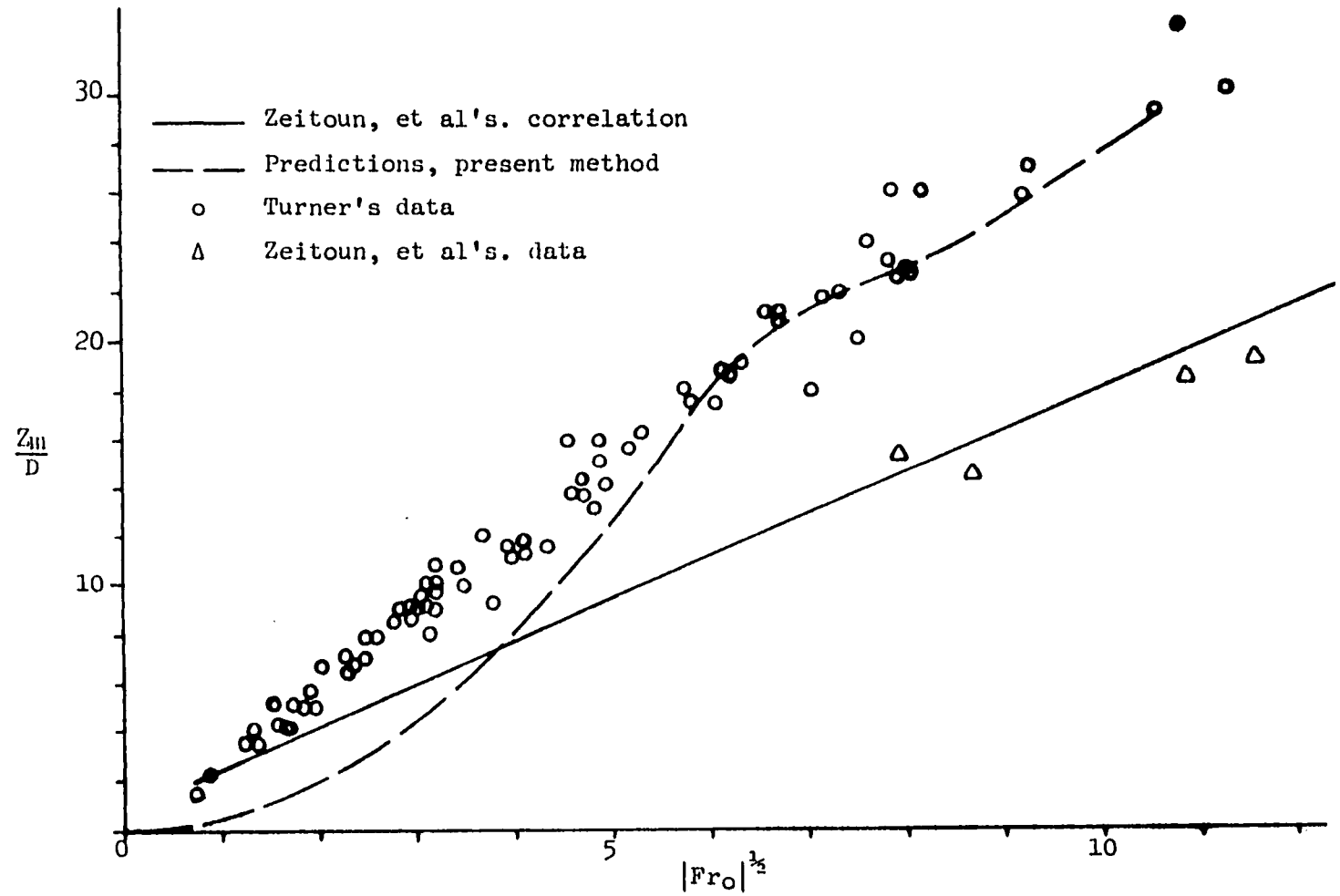

Fig. 4.4. Maximum height of rise for vertical dense jet in uniform ambient

As has been shown by previous investigators [15] that mixing length is affected by buoyancy forces, an effort was made in this study to apply a correction factor to the mixing-length for the vertical jet using an axial Richardson number. There was not any noticeable imporvement in the predictions. Including this effect in the model resulted in even worse agreement. Further light will be shed on this aspect of turbulence modeling in the next chapter.

It appears that additional experimental data is needed before the discrepancy between prediction and experiment is attributed solely to the effects of buoyancy on the turbulent viscosity for this configuration.

2. STRATIFIED AMBIENT

The same turbulence modeling was employed for the stratified ambient analysis as well. To the author's knowledge, there are no experimental data available in the literature for this case. The results for maximum height of rise for various values of the stratification number $\bar{T}$ were calculated and are shown in Fig. 4.5.

4.7 SUMMARY

Prandtl's mixing-length model, Eqs.(4.13) to (4.16)

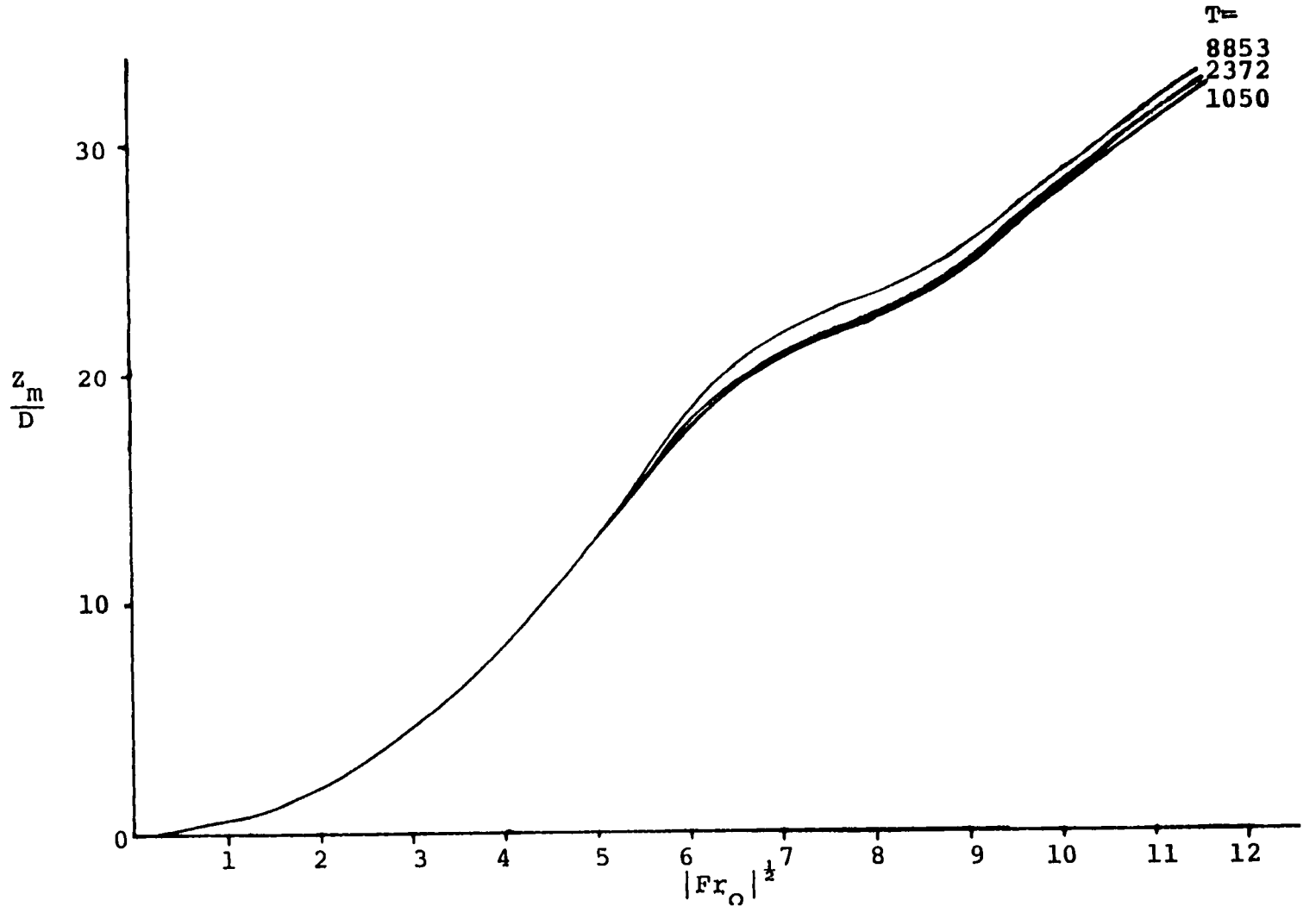

Fig. 4.5. Effect of stratification on maximum height of rise of vertical dense jet

was applied to a vertical dense jet configuration. The use of an intermittency function in the model did not change the results. At this moment no comment could be made about the validity of the model and/or theoretical formulation unless sufficient experimental measurements are available. However, in the event, experimental data used in this study prove to be reliable an important avenue to be explored is to include a y-momentum equation in the analysis. This might help in modeling the downward outer core of the jet. The effect of stratification on the maximum height of rise is seen to be nominal.

5. THE INCLINED DENSE JET IN UNIFORM OR STRATIFIED AMBIENT

Attention is now directed to the configuration in which the jet or plume follows a curved path. The aim and main challenge of a curved jet calculation is to predict the jet trajectory along with estimates of the flow parameters. Cases investigated were the dense jet discharging horizontally and at 30°, 45°, and 60° to the horizontal into quiescent, uniform or stratified ambient.

5.1 INTRODUCTION

The most obvious practical application of this configuration is in the submerged offshore outfalls from desalination plants. Compared with a vertical dense jet, a horizontal dense jet should undergo greater dilution. It was observed by Riester, et al. [9] that the horizontal dense jet will not be a mirror image of the horizontal buoyant jet. For most rapid mixing and dispersion of the effluent, an inclined discharge to the horizontal might be preferred because inclined jet does not fold on itself, [24]. In more recent outfall construction it has been the practice to orient the ports so that the effluent is issued at a positive angle into the receiving water [24]. Choice of the discharge configuration would also depend on the exact requirements of the

water quality standards at the proposed site of the desalination plant.

The characteristic of jets that issue at a positive angle to the horizontal into a lighter ambient fluid is that they follow a curved trajectory as they rise upward due to initial momentum and then fall due to the negative buoyancy forces. They have been experimentally studied by Zeitoun, et al [24], Bosanquet, et al. [20], and Riester, et al. [9]. Zeitoun, et al. measured the trajectory of the outer boundary of the jet discharged at angles 30°, 45°, and 60° to the horizontal and Bosanquet, et al. studied horizontal and 45° angled dense jets and measured centerline trajectories at different discharge Froude numbers. Riester, et al. conducted experiments for horizontally discharged dense jets for different Froude numbers.

Theoretical analyses for the prediction of dense jets discharged to a quiescent medium have been reported by Zeitoun, et al. [24], Bosanquet, et al. [20], Jain and Pena [26], and Crew and Reid [11]. With the exception of [11] which dealt with the far field region of a dense jet issued to a flowing ambient, all have used the integral approach. In this chapter, the same explicit scheme that was applied to vertical dense jet is employed for differential analysis of the configuration. An additional equation, the conservation of transverse momentum, is solved.

5.2 FLOW CONFIGURATION

Figure 5.1 shows the flow configuration for a dense jet discharging at angle θ_o to the horizontal. The environment is initially homogeneous and is at rest. Here $\bar{x}$ and z are horizontal and vertical coordinates, respectively. L is a scale factor, normally taken as the diameter of the nozzle.

One of the assumptions listed in Chapter 2 that underlies the present analysis, is that the jet cross-section remains axisymmetric. For horizontal non-buoyant jets and vertical jets, this assumption is justified by experimental observation. For a buoyant or dense, curved jet, however, the cross-section is probably never really axisymmetric and it is assumed as such only to simplify the analysis. It was shown by Madni and Pletcher [15] and later by Hwang and Pletcher [49] that within limits this assumption works and proves useful for predictions.

5.3 THE GOVERNING EQUATIONS

The differential equations governing the motion and dilution of the dense jet were presented as Eqs. (3.6) to (3.10)in the general formulation of Chapter 3. They are repeated here for convenience.

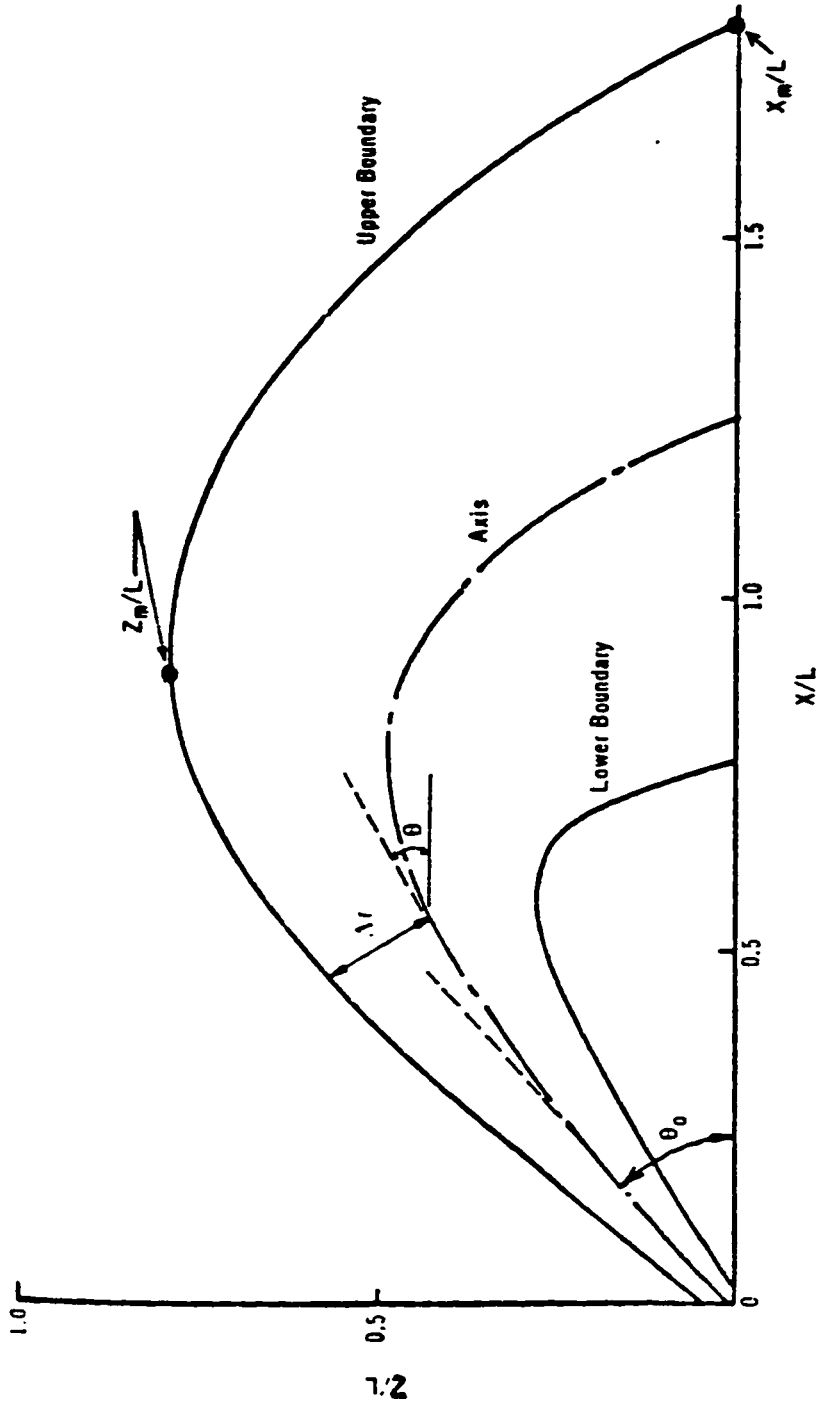

Fig. 5.1. Flow configuration for an inclined, dense jet

Continuity:

$$\frac{\partial}{\partial s}(uy) + \frac{\partial}{\partial y}(vy) = 0 \tag{5.1}$$

s-Momentum:

$$u\frac{\partial u}{\partial s} + v\frac{\partial u}{\partial y} = \frac{1}{\rho y}\frac{\partial}{\partial y}(y\tau) + \frac{(\rho_\infty - \rho)}{\rho_o} g \sin\theta \tag{5.2}$$

y-Momentum:

$$u^2\frac{d\theta}{ds} = \frac{(\rho_\infty - \rho)}{\rho_o} g \cos\theta \tag{5.3}$$

Energy:

$$u\frac{\partial t}{\partial s} + v\frac{\partial t}{\partial y} = \frac{1}{\rho\, y\, Cp}\frac{\partial}{\partial y}(-yq) \tag{5.4}$$

Salinity:

$$u\frac{\partial c}{\partial s} + v\frac{\partial c}{\partial y} = \frac{1}{\rho y}\frac{\partial}{\partial y}(-yJ) \tag{5.5}$$

where $\frac{\rho_\infty - \rho}{\rho_o}$ is given by Eq.(4.6).

As before:

$$\left.\begin{aligned} \tau &= \rho\, \nu_{eff} \quad , \nu_{eff} = \nu + \nu_t \\ q &= -\rho\, Cp\, \alpha_{eff}\frac{\partial t}{\partial y} \quad , \alpha_{eff} = \alpha + \alpha_t \\ J &= -\rho\, D_{eff}\frac{\partial c}{\partial y} \quad , D_{eff} = D + D_t \end{aligned}\right\} \tag{5.6}$$

and

$$Pr_t = \frac{\nu_t}{\alpha_t} \quad , Sc_t = \frac{\nu_t}{D_t}$$

Comparing this formulation with that of the vertical plume, one additional unknown, θ, is observed to be present, along with one additional equation, the conservation of transverse momentum. The y-momentum equation written in the form shown in Eq. (5.3) is simply a balance between the centrifugal force due to the jet turning, acting in the direction of the radius of curvature, and the component of buoyancy in the direction opposite to that of the centrifugal force.

$$\text{Centrifugal force} = \frac{u^2}{|\bar{R}|} = u^2 \frac{d\theta}{ds}$$

where

$\bar{R}$ is the radius of curvature of the trajectory.

The initial and boundary conditions, being the same as Eqs. (3.16) and (3.17), are listed here for the reader's convenience.

Initial Conditions:

$$u(s_o,y) = f(y),\ t(s_o,y) = g(y),\ \theta(s_o) = \theta_o \qquad (5.7)$$

θ_o for the cases investigated in this chapter is 0°, 30°, 45°, and 60°.

Boundary Conditions:

$$\left.\begin{aligned} &\frac{\partial u}{\partial y}(s,0) = \frac{\partial t}{\partial y}(s,0) = 0,\ v(s,0) = 0 \\ &\lim_{y\to\infty} u(s,y) = u_\infty, \quad \lim_{y\to\infty} t(s,y) = t_\infty \end{aligned}\right\} \qquad (5.8)$$

The non-dimensional forms and finite-difference equations have been presented in Chapter 3, and will not be repeated here.

5.4 SOLUTION METHOD - SOME ASPECTS

It is a novelty of Madni and Pletcher's work that the transverse momentum equation, Eq. (5.3) was integrated in such a way that while curvature effects over the cross-section were neglected, a better and more realistic estimate of θ at station i+1 was obtained by making Eq. (5.3) representative of the entire flow cross-section at i. Hence, the equation was integrated as follows:

$$\int_0^\delta u^2 \frac{d\theta}{ds} y dy = \int_0^\delta \frac{\cos\theta}{Re_o Fr_o} \frac{\rho_\infty - \rho}{\rho_{\infty o} - \rho_o} y dy$$

or since θ = constant over the cross-section

$$\frac{d\theta}{ds} \int_0^\delta u^2 y dy = \frac{\cos\theta}{Re_o} \int_0^\delta \left(\frac{\rho_\infty - \rho}{\rho_{\infty o} - \rho_o}\right) \frac{1}{Fr_o} y dy \qquad (5.9)$$

The integration was performed by using Simpson's rule [12]. The velocity and density profiles were obtained from the s-momentum, energy, and concentration equations respectively.

With reference to Fig. 3.2 , θ_{i+1} is determined from the transverse momentum equation as explained above and then the coordinates of the trajectory are generated according to

Eq. (3.38). This procedure is illustrated in Fig. 5.2 . The typical forward streamwise step shown is greatly exaggerated for clarity.

5.5 TRANSPORT MODELS AND RESULTS

Once again the simple mixing length model was retained in the initial region with $\ell = 0.0762\,\delta$ as before. In the case of positive buoyant jets, predictions of starting length and deflection using this formulation were found to be consistent with Abraham's calculations [12].

In the main region of flow, first, calculations were made assuming that buoyancy had no effect on the effective viscosity. Prandtl's constant viscosity model that was used for vertical jet analysis, was employed here as well, with constant kept the same, i.e.,

$$\nu_t = K_1\, y_{\frac{1}{2}}\, (u_{max} - u_{min}) \qquad (5.10)$$

where

$$K_1 = 0.0246.$$

However, the predictions were not good. Several references [50, 51, 52, 60] have discussed the influence of buoyancy on the structure of turbulence. Buoyancy-induced turbulent shear flows are still a challenging task for mathematical modelers [52]. Whereas an eddy-viscosity model based on pure-forced

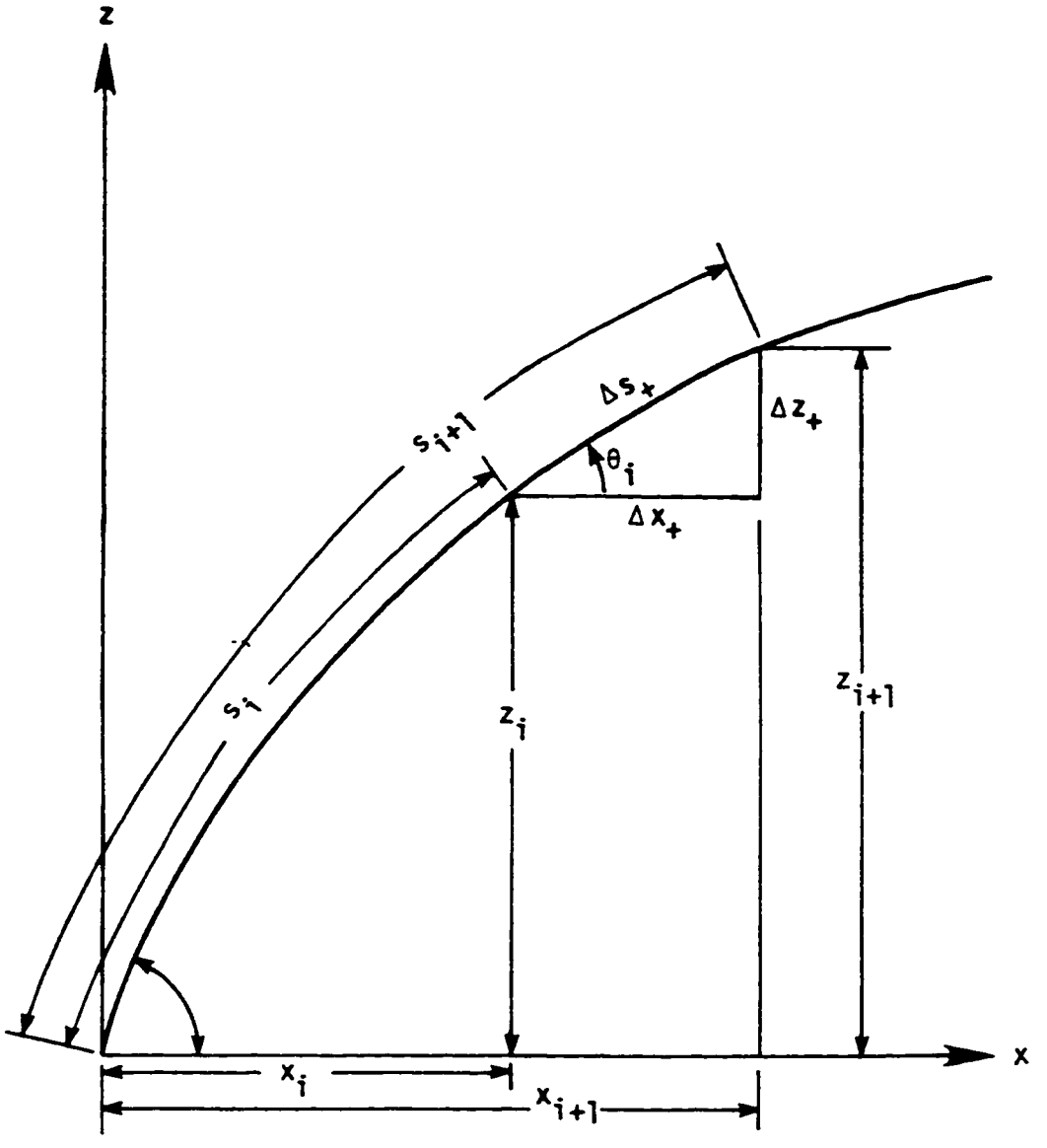

Fig.5.2. Generation of jet trajectory.

convection did not work well for a downward heated flow in a vertical pipe [53], a pure-forced-convection model (Eq. 5.10) was found to give good predictions for a vertical buoyant jet [12]. However, the same model failed to give good predictions for an inclined buoyant jet. It was reported by Madni [15] that modification of the apparent mixing-length to account for buoyancy effects via a Richardson number resulted in startling improvements in the agreement between predictions and experiment.

The stratification parameter, $-\frac{g}{\rho}\frac{\partial \rho}{\partial y} \Big/ \left(\frac{\partial u}{\partial y}\right)^2$, is known as the Richardson number, Ri. It is an additional criterion of stability (and hence turbulence). According to Richardson [43], Ri = 0 corresponds to a homogeneous fluid, Ri > 0 denotes stable, and Ri < 0 unstable stratification. Richardson showed that turbulent mixing may be expected to disappear for Ri > 2. Taylor [54] refined the reasoning and obtained Ri ≥ 1 as the limit of stability. However, for a horizontal heated surface jet, Hossain and Rodi [55] showed that mixing collapses at Ri = 0.6.

A global representation of Ri is used in the model, viz.,

$$Ri = g \frac{\left(\beta \frac{\partial t}{\partial y} + \beta^* \frac{\partial c}{\partial y}\right)}{\left(\frac{\partial u}{\partial y}\right)^2}$$

$$= g \frac{\left(\beta \frac{(t_\infty - t_c)}{\delta_t} + \beta^* \frac{(c_\infty - c_c)}{\delta_c}\right)}{\left(\frac{u_\infty - u_c}{\delta}\right)^2} =$$

$$= \frac{g\nu}{u_o^3} \frac{\left[\beta \frac{(t_o - t_{\infty o})(T_\infty - T_c)}{\delta_t} + \beta^* \frac{(c_o - c_{\infty o})(C_\infty - C_c)}{\delta_c}\right]}{\left(\frac{u_\infty - u_c}{\delta}\right)^2} \qquad (5.11)$$

where δ, δ_t, and δ_c are velocity, temperature, and concentration half-widths of the jet respectively.

The Monin-Oboukhov formula for modification of the apparent mixing-length due to small buoyancy effects, one of the earliest of such formulae, is given in [51] as

$$\frac{\ell}{\ell_o} = 1 - K_3 \, Ri \qquad (5.12)$$

where ℓ_o is the mixing length without buoyancy and ℓ is the modified mixing length. In the present work the value of $K_3 = 3.0$ proved to be the most suitable. Moreover, for stable conditions ($Ri > 0$), Giles, et al. [56] had used $K_3 = 3.0$ successfully for a wall jet.

It is important to note that the effective viscosity appears to be mainly influenced by the components of the density gradient involved in Eq.(5.11) which are in the direction of the earth's gravity. This was seen to be approximately true from the vertical plume results of [14], in which the deviation of predicted centerline decay values from experiment was not significant enough to suggest modifying the mixing-length to include a Richardson number effect. However,

this relative independence of Ri cannot be true for an inclined jet. Hence, to give Eq. (5.12) more meaning, a cos θ term was introduced as follows [12]:

$$\frac{\ell}{\ell_o} = 1 - K_3 \, Ri \cos \theta \qquad (5.13)$$

Here, θ is the local angle, so that, as the jet turns upward (or downward), θ will increase (or decrease) altering the effect of Ri on the mixing length.

Equation (5.13) was implemented in the model of Eq. (5.10) as follows:

$$\nu t_o = \ell_o^2 \left|\frac{\partial u}{\partial y}\right| \simeq K_1 \left(y_{\frac{1}{2}}\right)^2 \frac{\Delta u_c}{y_{\frac{1}{2}}}$$

$$= K_1 \, y_{\frac{1}{2}} \, (u_{max} - u_{min})$$

So that

$$\nu t = \ell^2 \left|\frac{\partial u}{\partial y}\right| = \frac{\ell^2}{\ell_o^2} \times \ell_o^2 \left|\frac{\partial u}{\partial y}\right|$$

i.e.,

$$\nu t = K_1 \, y_{\frac{1}{2}} \, (u_{max} - u_{min})(1 - K_3 \, Ri \cos \theta)^2 \qquad (5.14)$$

where $K_1 = 0.0246$, $K_3 = 3.0$.

The model of Eq. (5.14) assumes a constant value for the turbulent viscosity across the mixing layer, but measurements [31] indicate that it in fact varies and has an intermittent character near the outer edge of the mixing layer (see

Fig. 4.2). To account for this effect, Eq.(5.14) was modified such that

$$\nu_t = \gamma K_1 y_{\frac{1}{2}} (u_{max} - u_{min})(1 - K_3 Ri \cos\theta) \qquad (5.15)$$

where γ is equal to an intermittency function given by Eq. (4.17), [12].

RESULTS OF UNIFORM AMBIENT

Figure 5.3 shows results using the model of Eq.(5.14) and (5.15) for a 60° angled dense jet issuing at a discharge Froude number $Fr_o = 1081$. It is noted that intermittency markedly affects the jet trajectory. Runs were made for other configurations as well, and it was found that introduction of intermittency function significantly improved the predictions. The predictions for the vertical dense jet were found to be unchanged with the introduction of intermittency in the formulation.

Figures 5.4 to 5.6 show trajectories for inclined jets discharged at 30°, 45°, and 60° to the horizontal for different Froude numbers. Along with the predicted trajectories are shown the experimental results of Zeitoun, et al. [24]. It is seen that for lower Froude numbers the agreement is very good for all configurations. However, as the Froude number increases the predictions tend to underpredict the experiments.

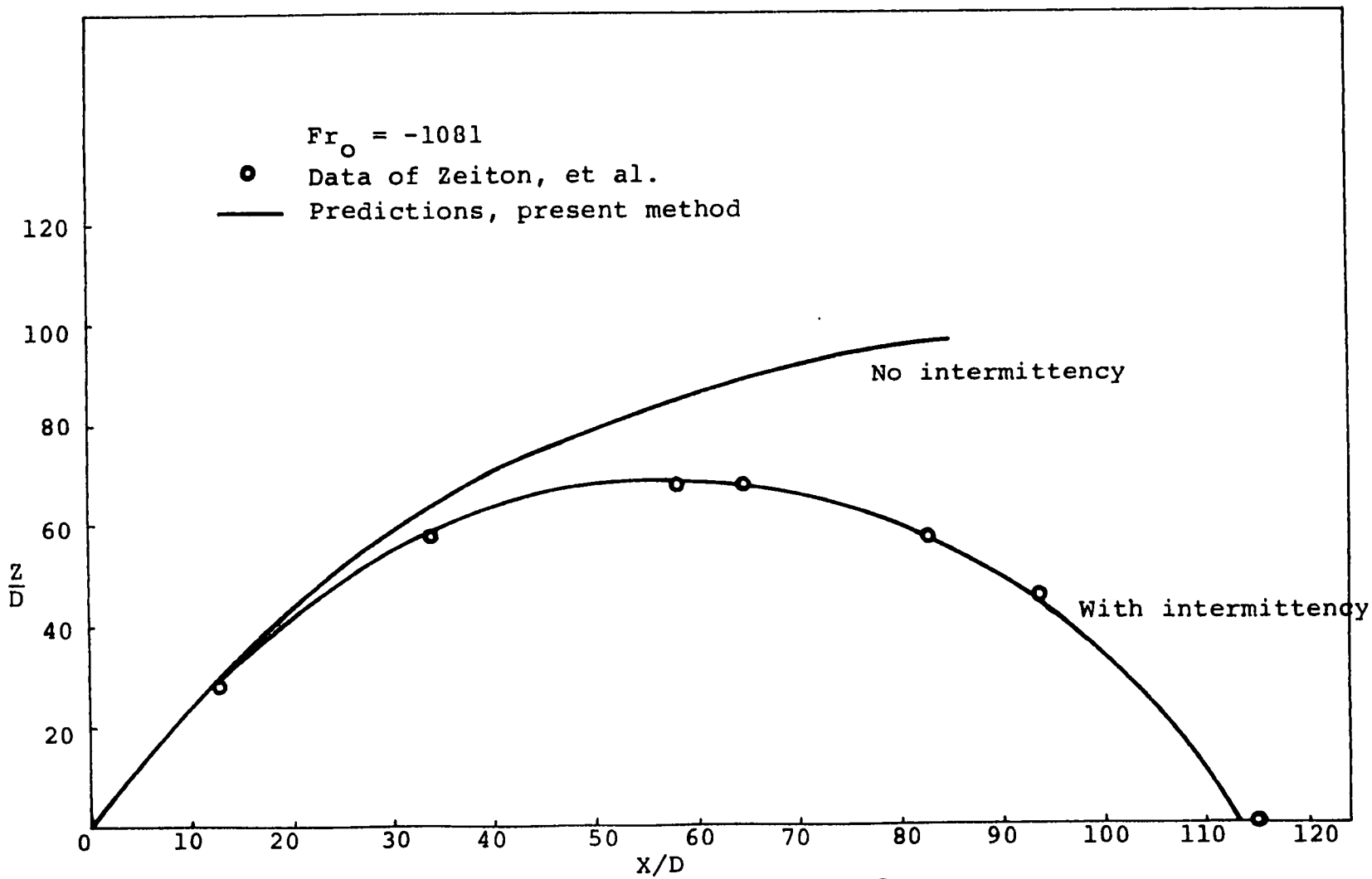

Figure 5.3. Effect of intermittency function on a 60^{o} angle dense jet (Top Boundary).

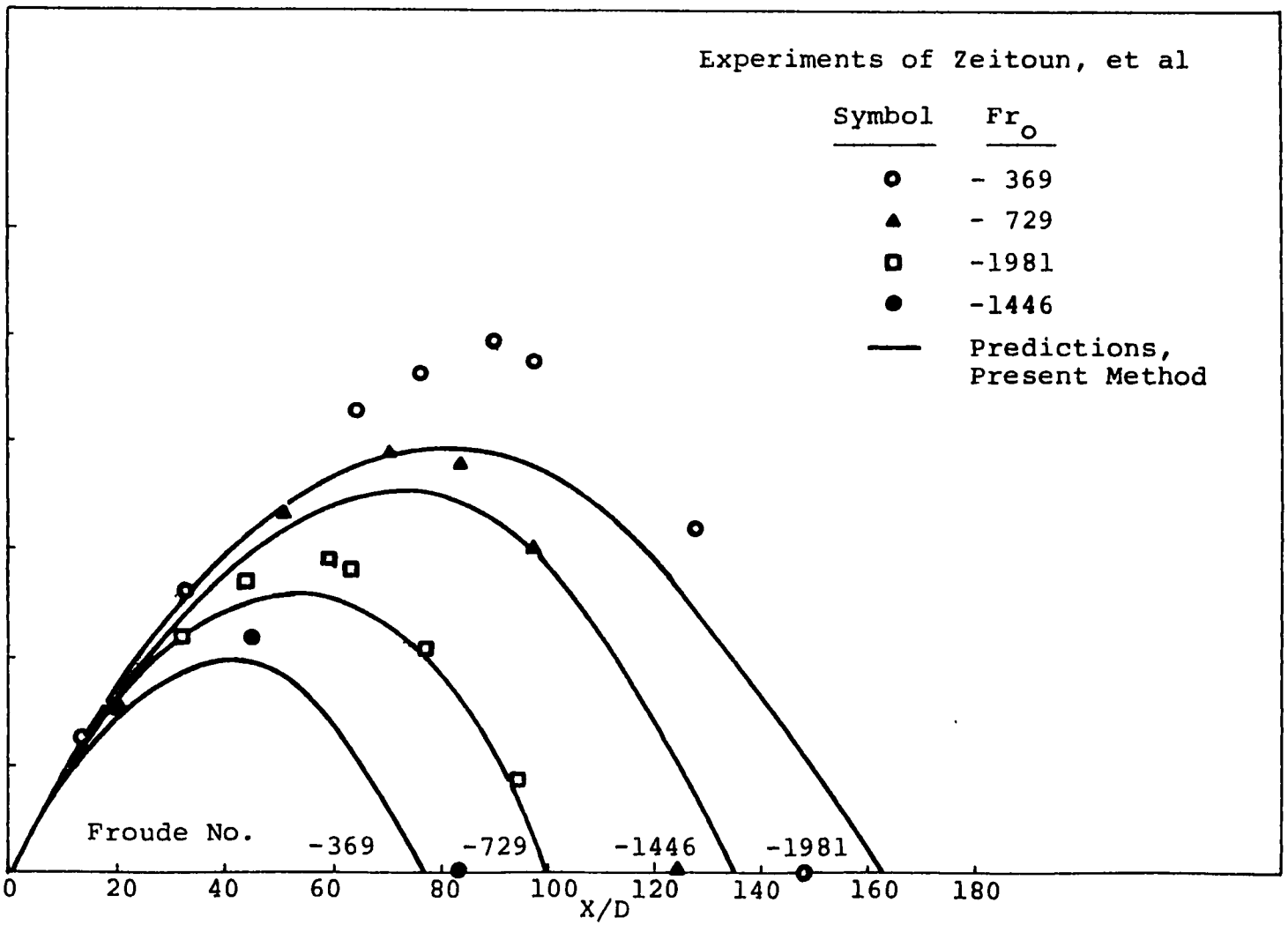

Figure 5.4. Path of top boundary of 30° angle dense jets.

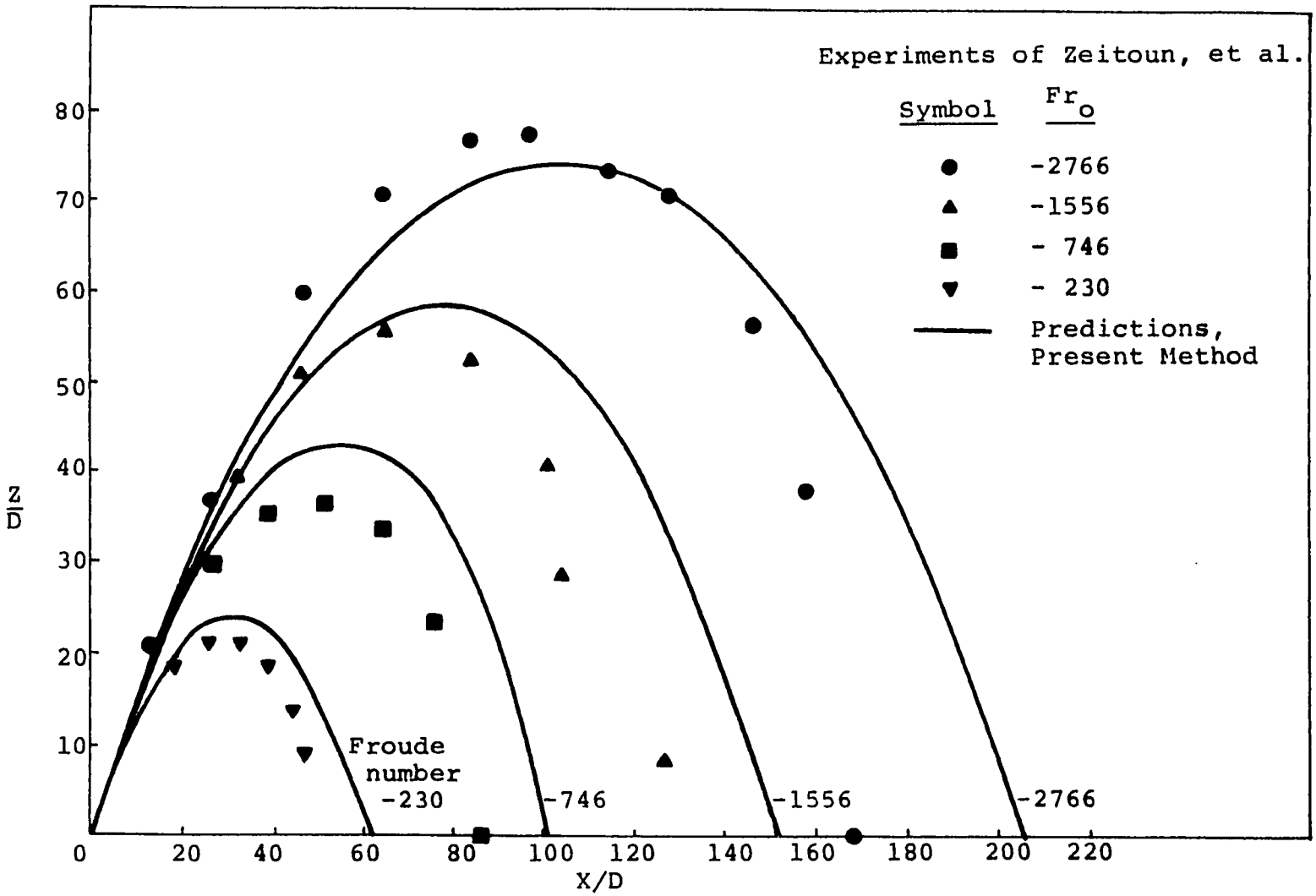

Figure 5.5. Path of top boundary of 45° angle dense jets.

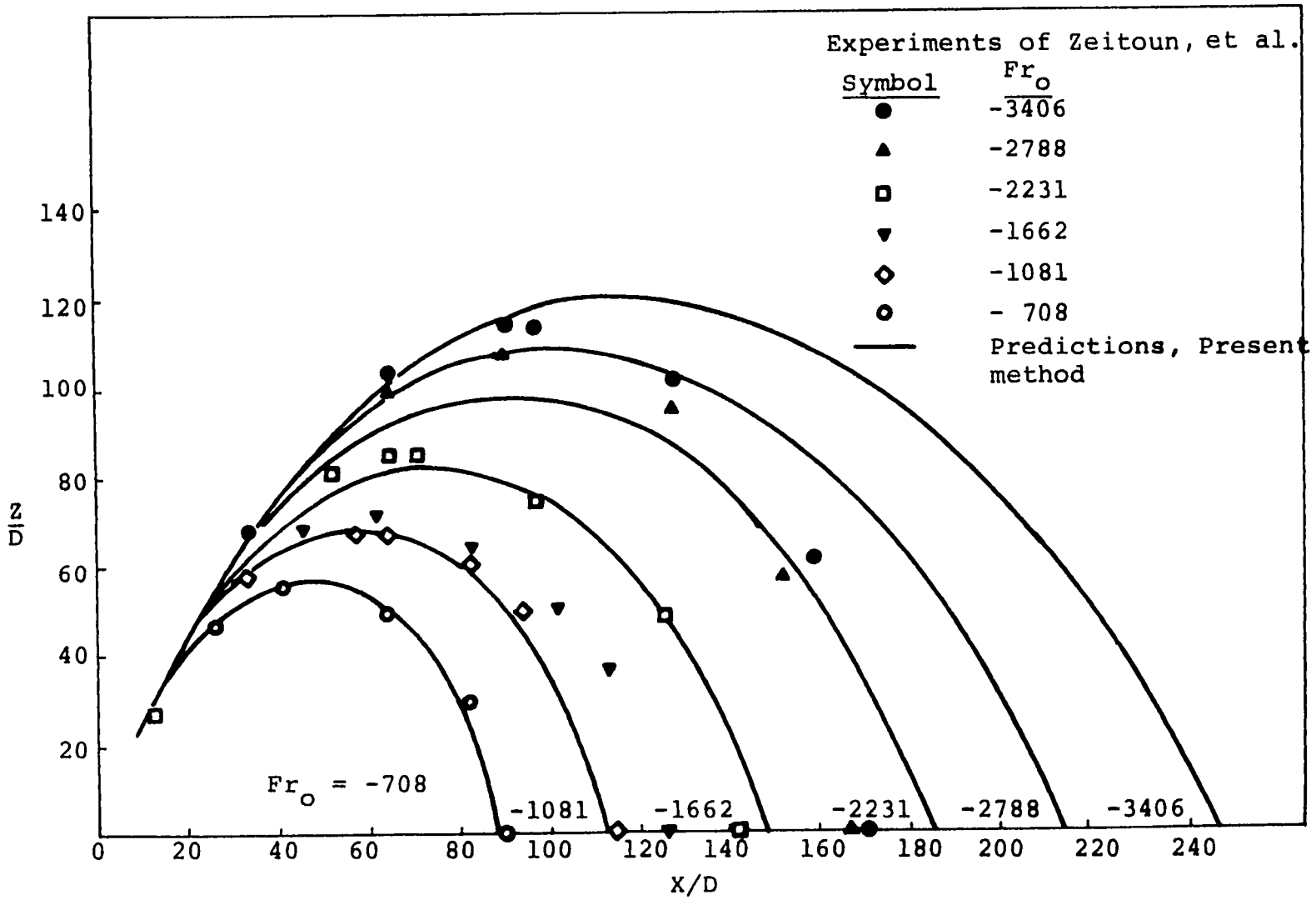

Figure 5.6. Path of top boundary of 60^{o} angle dense jets.

Efforts were made to introduce buoyancy-correction factors other than that of Eq.(5.12)(see for example references [58],[59]) but none came up better than that of Eq. (5.12). It was observed by many workers [44, 45, 46] that eddy diffusivities for momentum as well as for heat change with Richardson number, both α_t and ν_t decreasing at different rates with increasing values of Ri. Under unstable conditions, both α_t and ν_t increase with increasing negative Ri and after reaching a maximum both decrease. It was, therefore, decided to try a variable $Pr_t = f(Ri)$ according to available models (see for example reference [44]) but that worsened the predictions.

A possibility might be to modify mixing-length to take into account curvature effects. The following function was found to work well for jets discharging into flowing ambients [49]

$$C.F. = 1 - \beta_c \, Ri_c$$

here C.F. is the correction factor due to curvature and Ri_c is gradient curvature Richardson number defined as

$$Ri_c = 2 \frac{u / \bar{R}}{\frac{\partial u}{\partial y}}$$

where $\bar{R}$ is radius of curvature. On a global basis, we have

$$Ri_c = 2 \, u_c \, \delta \cdot \frac{d\theta}{ds} \quad (u_c - u_\infty)$$

Here $\left(\frac{d\theta}{ds}\right)^{-1}$ can be recognized as the radius of curvature of the jet centerline.

The present study did not consider curvature correction factor in the mixing-length model.

When the trajectory data for each configuration are normalized with respect to X_m, the maximum horizontal spread, they tend to cluster around a single curve. Figures 5.7, 5.8 and 5.9 represent $Z/\bar{X}_m$ versus X/X_m for 30°, 45°, and 60° configuration respectively. The figures show prediction of Zeitoun, et al. [24] which are superimposed for different Fr_o. The predictions of the present method show a dependence on Fr_o. The agreement of the present model with experimental data is very good. It is strange that Zeitoun, et al. did not present results of their integral analysis in the form of Figures 5.4 to 5.6.

Figures 5.10 and 5.11 show the straight line correlations of Zeitoun, et al. alongwith their experimental points for the maximum height of the jet Z_m/D and the maximum horizontal spread X_m/D with Froude number for the 45° and 60° jets. The figure also shows the predicted curves obtained from the present method. Figure 5.12 presents similar relationship for a 30° angled jet. For the first two cases the predictions and experiment closely match for Z_m/D versus $|Fr_o|^{\frac{1}{2}}$ curve whereas X_m/D curves tend to deviate from each other in a linear fashion as $|Fr_o|^{\frac{1}{2}}$ increases. The last case is strange in the sense that predictions of the present analysis and the correlations of Zeitoun, et al. intersect each other and the former have

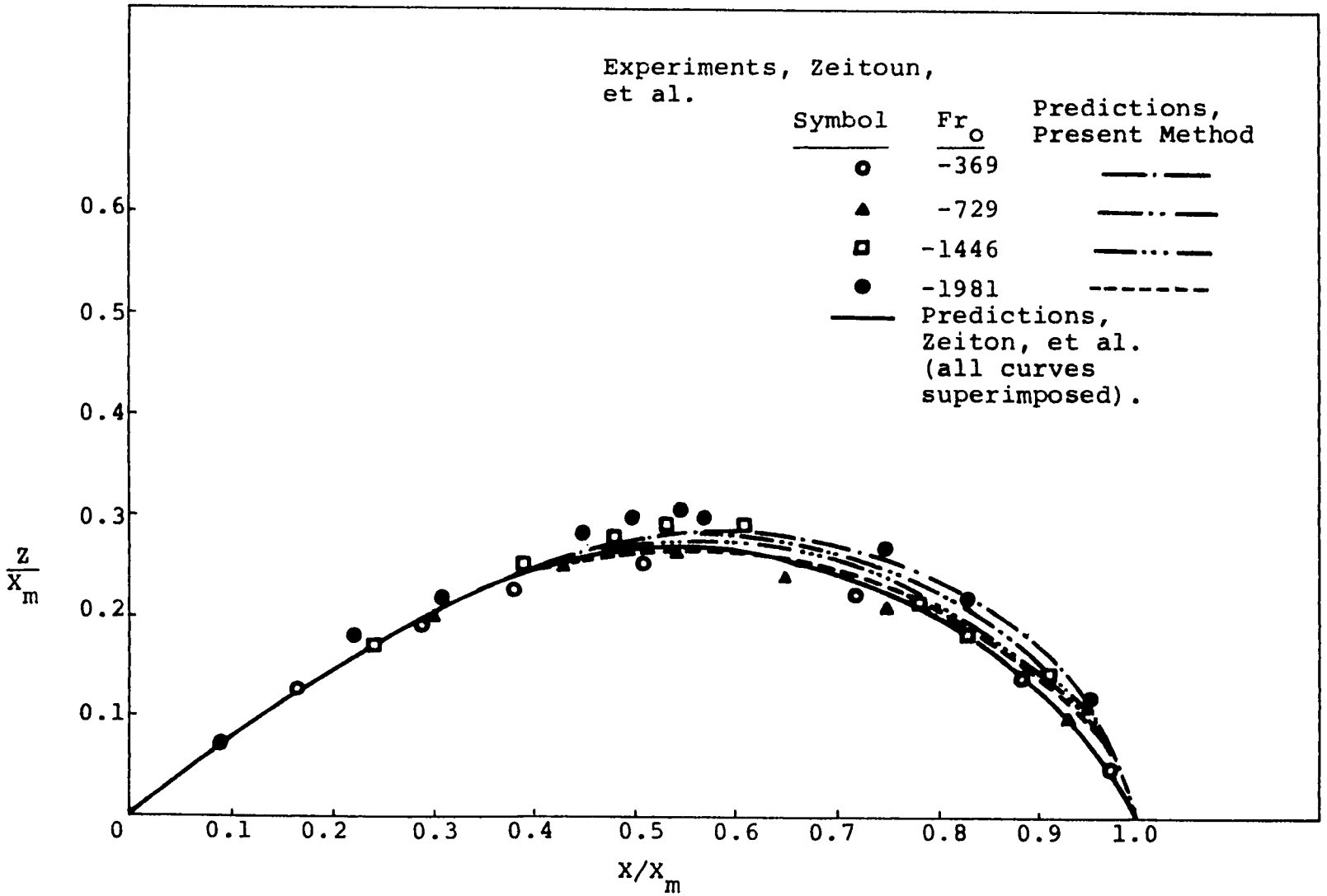

Figure 5.7. Normalized profile of upper boundary of dense jet for $\theta_o = 30^o$.

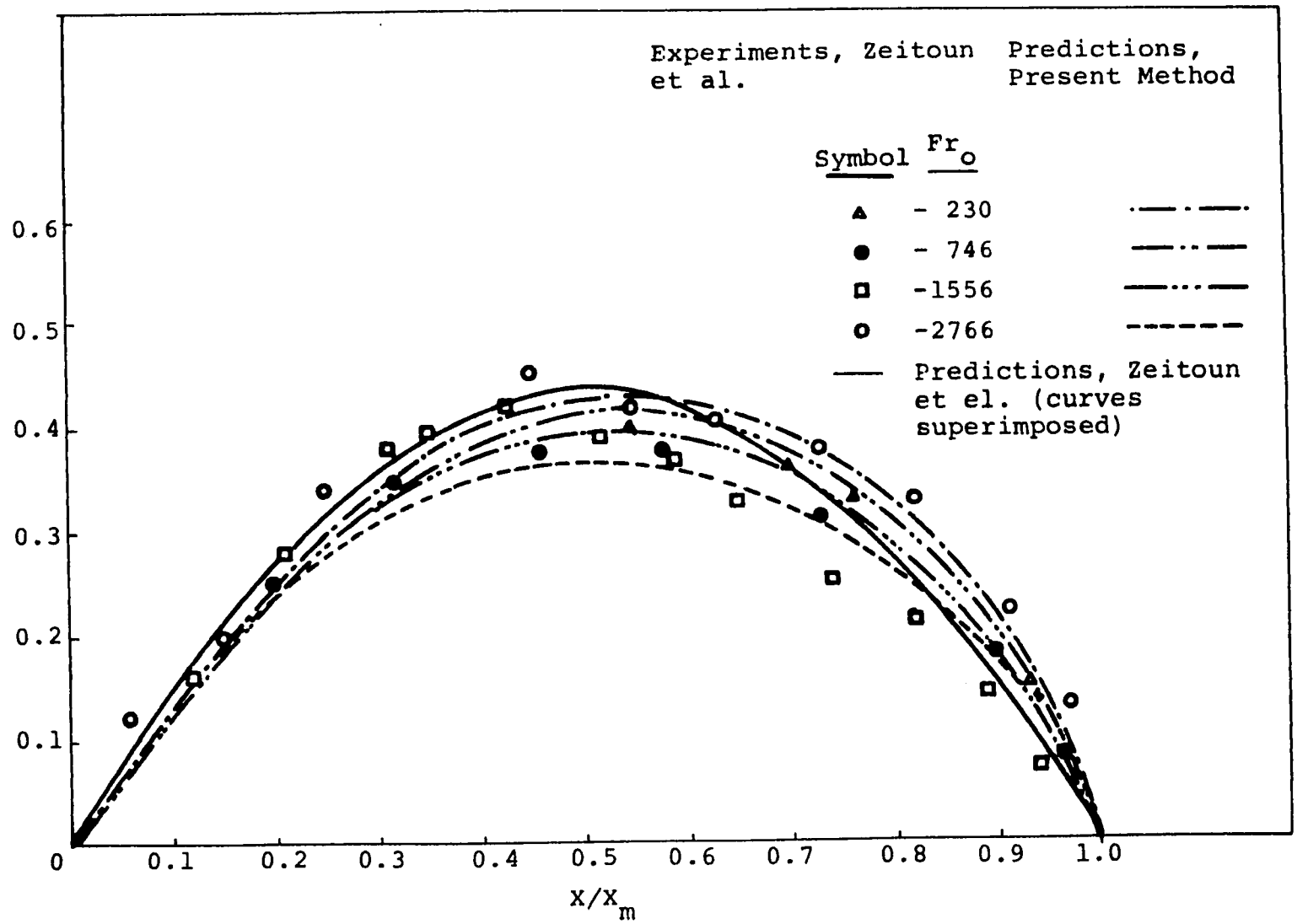

Figure 5.8. Normalized profile of upper boundary of dense jet for $\theta_o = 45^o$.

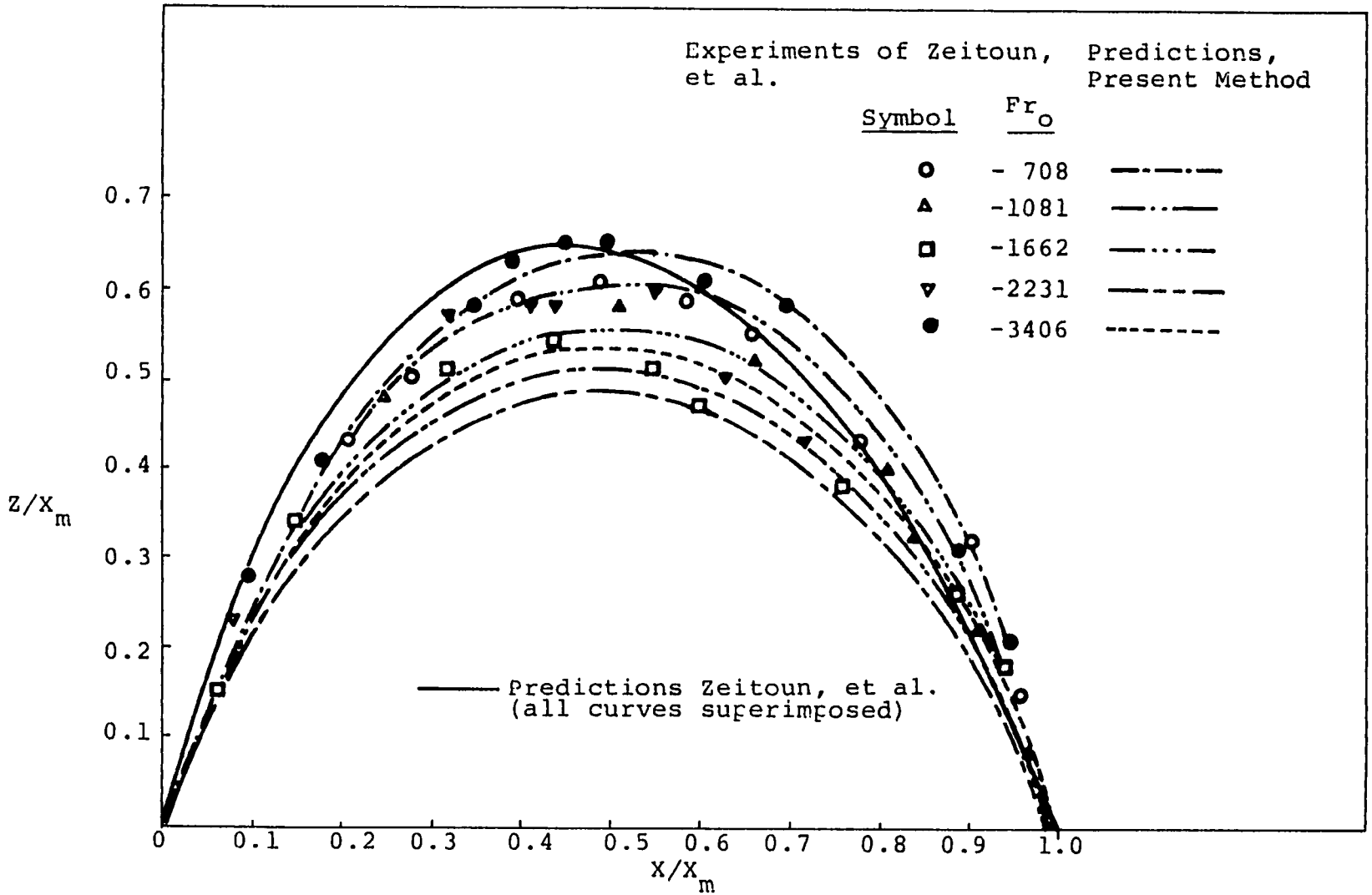

Figure 5.9. Normalized profile of upper boundary of dense jet for $\theta_o = 60^o$.

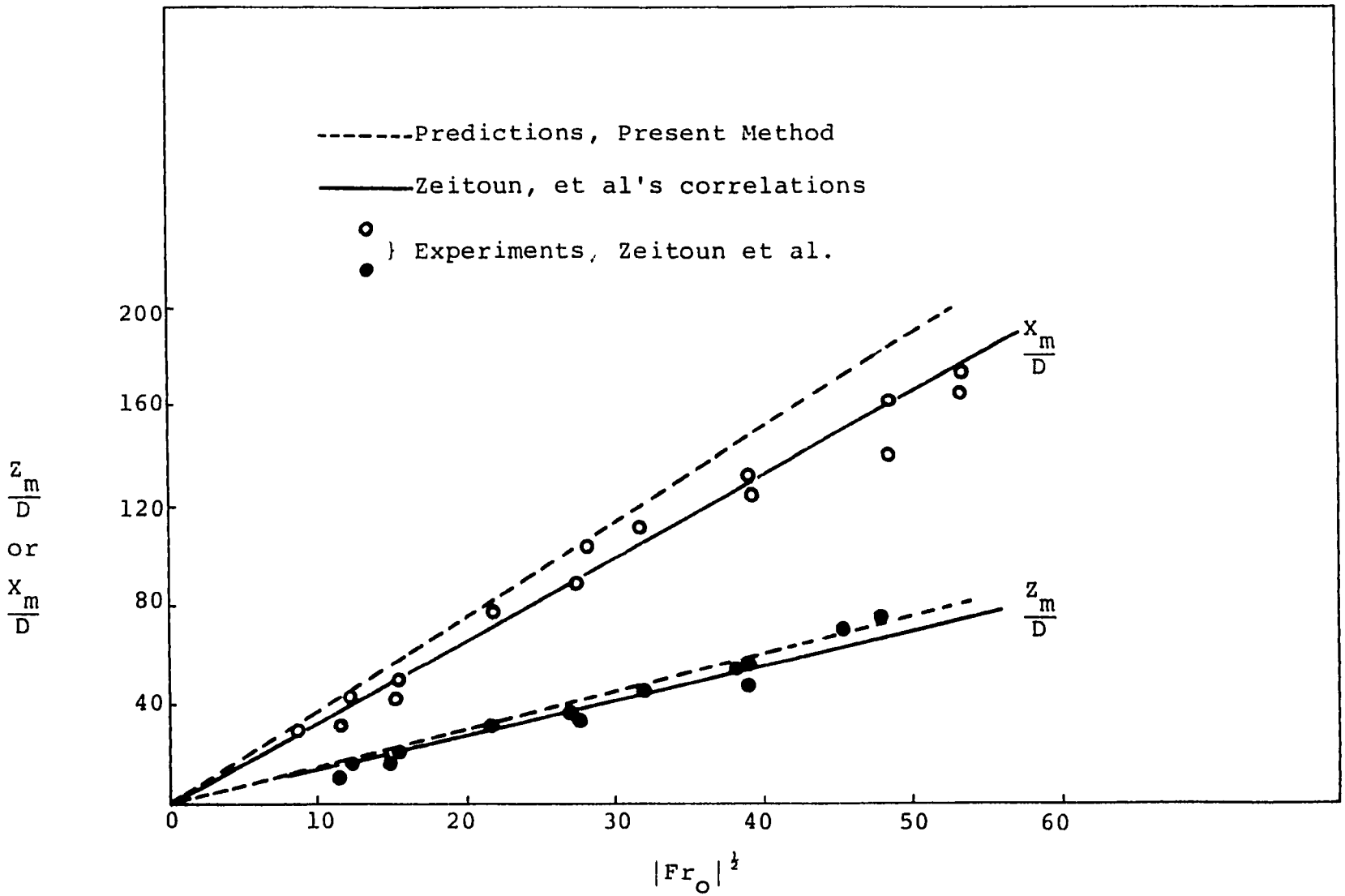

Figure 5.10. Dimensions of 45° angle dense jets.

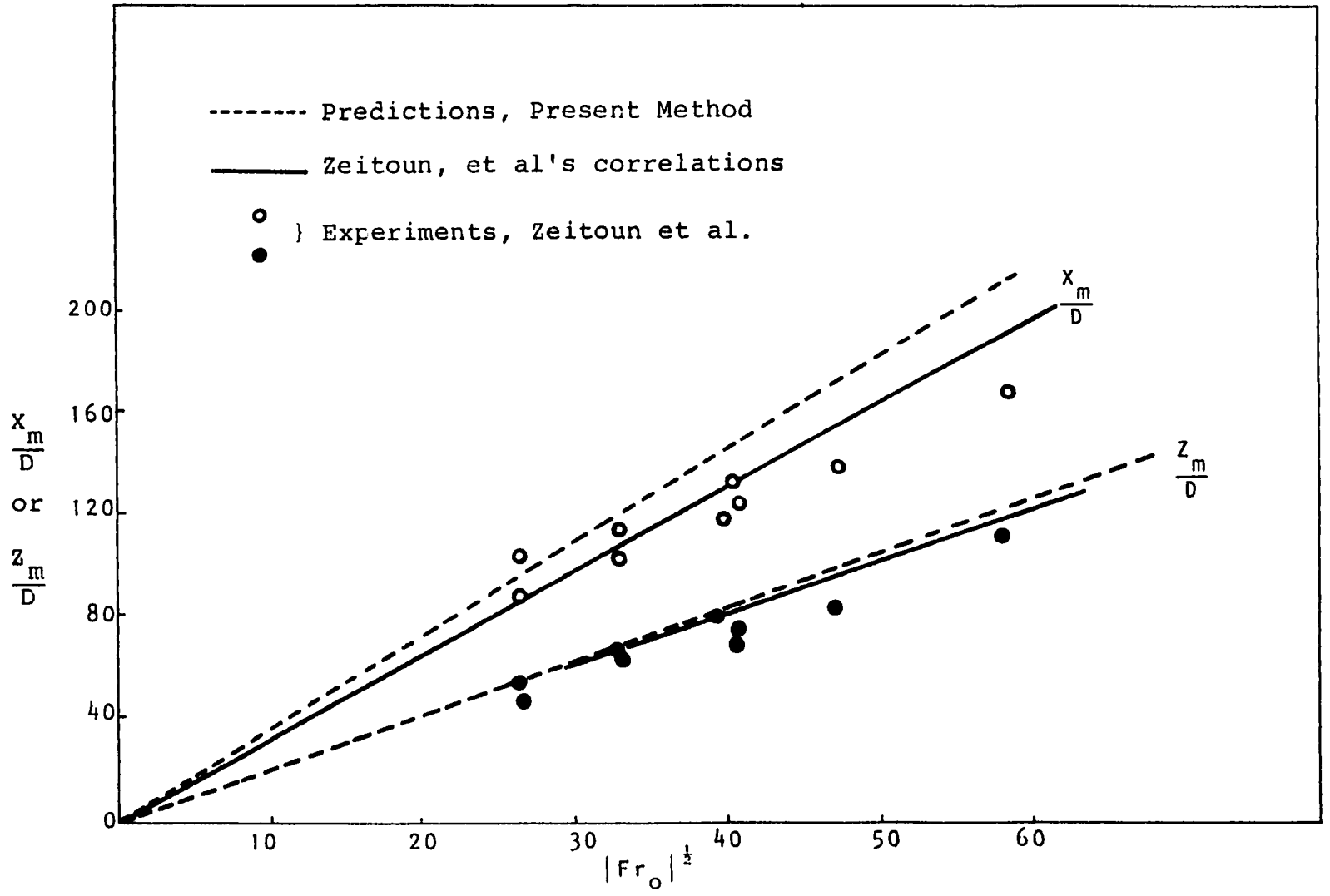

Figure 5.11. Dimensions of 60° angle dense jets.

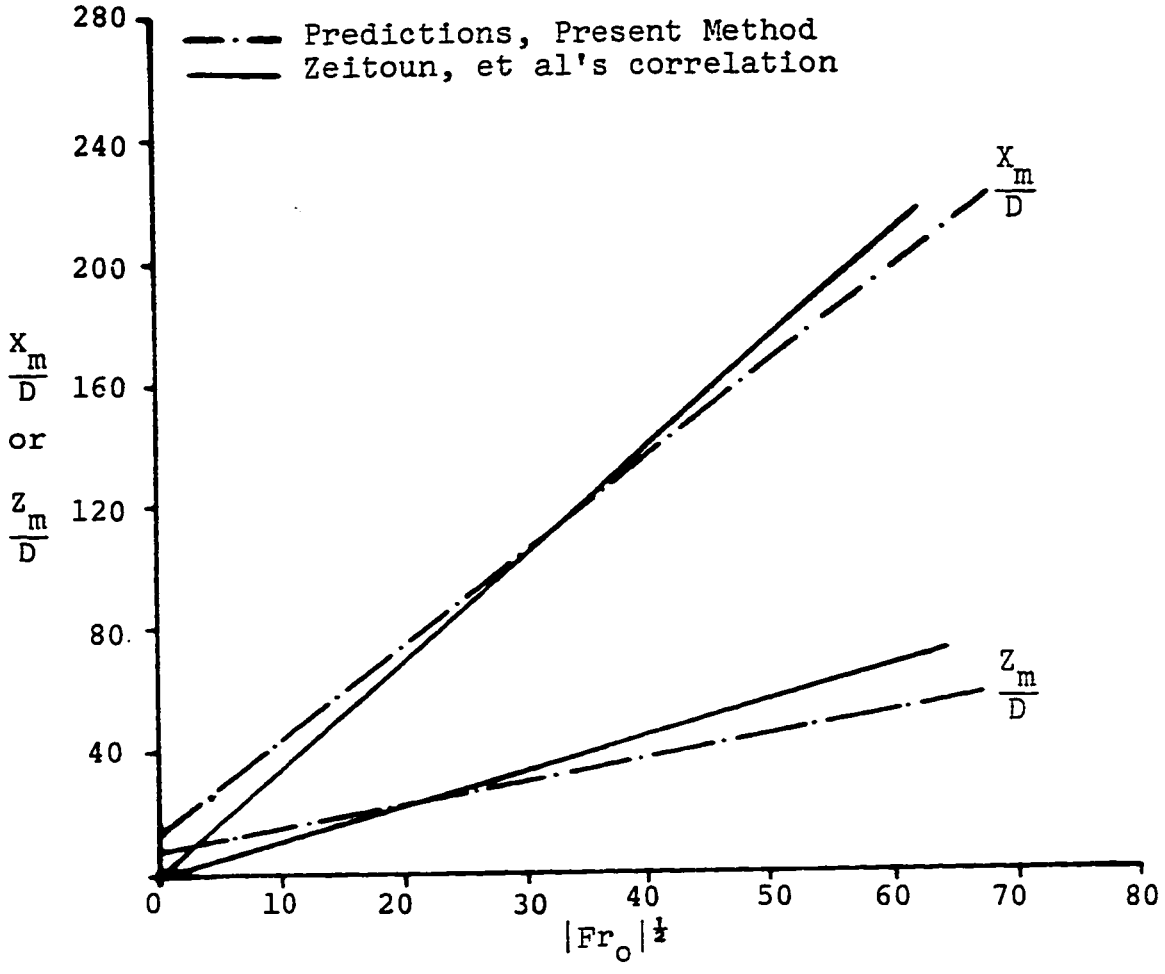

Fig. 5.12. Dimensions of 30° angle dense jets

a non-zero y-intercept for both Z_m/D and X_m/D. Table 5.1 presents a summary of the correlations of the jet dimensions with Froude numbers.

In Figure 3.13 the ratio of the product of the maximum height and maximum horizontal spread to the height of a vertical jet squared, $\frac{X_m Z_m}{H_m^2}$, is plotted for different angles of injection for $Fr_o = -708$. The maximum ratio is found to be at an angle of 72^o, which is different from 63° obtained by Zeitoun, et al. It is concluded, based on this study, that a 72° angled nozzle will produce a maximum path and therefore maximum dilution of the effluent under the same conditions of initial flow.

Figures 5.14 and 5.15 present predicted trajectories for horizontally discharged negatively buoyant jets. Also shown are the experimental data of Riester, et al. [9]. The data in Fig. 5.14 is for a cold fresh water jet ($T_o = 20.56°C$) issued to a hot fresh water ambient ($T_\infty = 43.33°C$). Figure 5.15 presents a cold salt jet ($T_o = 15.56°C$) issued to a cold fresh water ambient ($T_\infty = 15.56°C$) for different Froude numbers. The agreement with experiment is much better in the fresh water jets than in the saline water jets although in an absolute sense predictions are not good. The level of agreement worsens as the Froude number is increased. This was the case in inclined jets as well. It was shown in Ref. [9] that a horizontal dense jet will not be the mirror image of a corresponding horizontal buoyant jet. In order to

TABLE 5.1

Dimensions of Inclined Dense Jets

Initial Angle of Jet	Z_m/D		X_m/D	
	Zeitoun, et al.	*Present Method*	*Zeitoun, et al.*	*Present Method*
60°	$2.04\ \lvert Fr_o\rvert^{\frac{1}{2}}$	$2.1\lvert Fr_o\rvert^{\frac{1}{2}}$	$3.28\ \lvert Fr_o\rvert^{\frac{1}{2}}$	$3.7\lvert Fr_o\rvert^{\frac{1}{2}}$
45°	$1.43\ \lvert Fr_o\rvert^{\frac{1}{2}}$	$1.5\lvert Fr_o\rvert^{\frac{1}{2}}$	$3.33\ \lvert Fr_o\rvert^{\frac{1}{2}}$	$3.9\lvert Fr_o\rvert^{\frac{1}{2}}$
30°	$1.15\ \lvert Fr_o\rvert^{\frac{1}{2}}$	$0.73\lvert Fr_o\rvert^{\frac{1}{2}}+8$	$3.48\ \lvert Fr_o\rvert^{\frac{1}{2}}$	$3.04\lvert Fr_o\rvert^{\frac{1}{2}}+14$

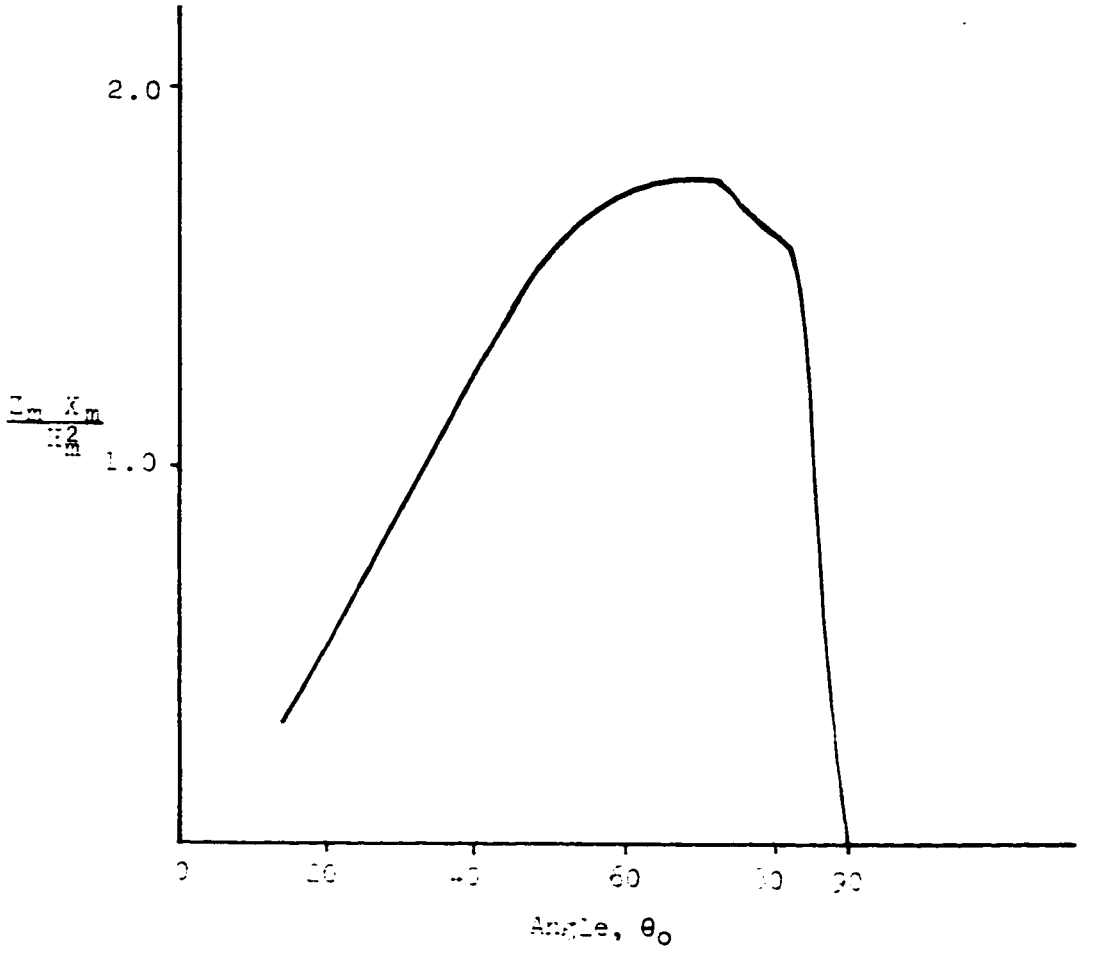

Figure 5.13. Variation of jet dimensions with angle of injection.

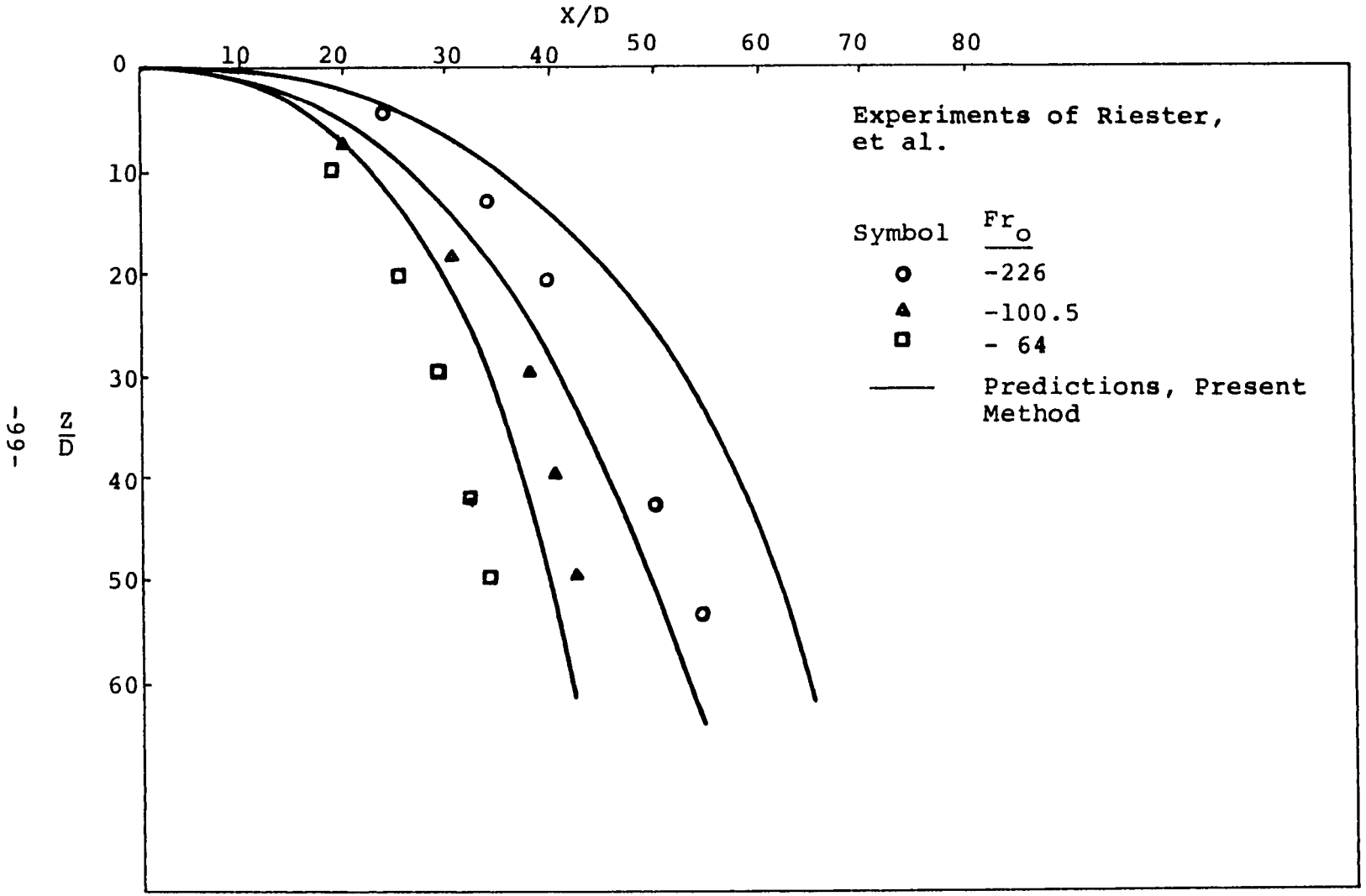

Figure 5.14. Centerline trajectory of a horizontal jet, cold fresh water jet issued to hot fresh water ambient.

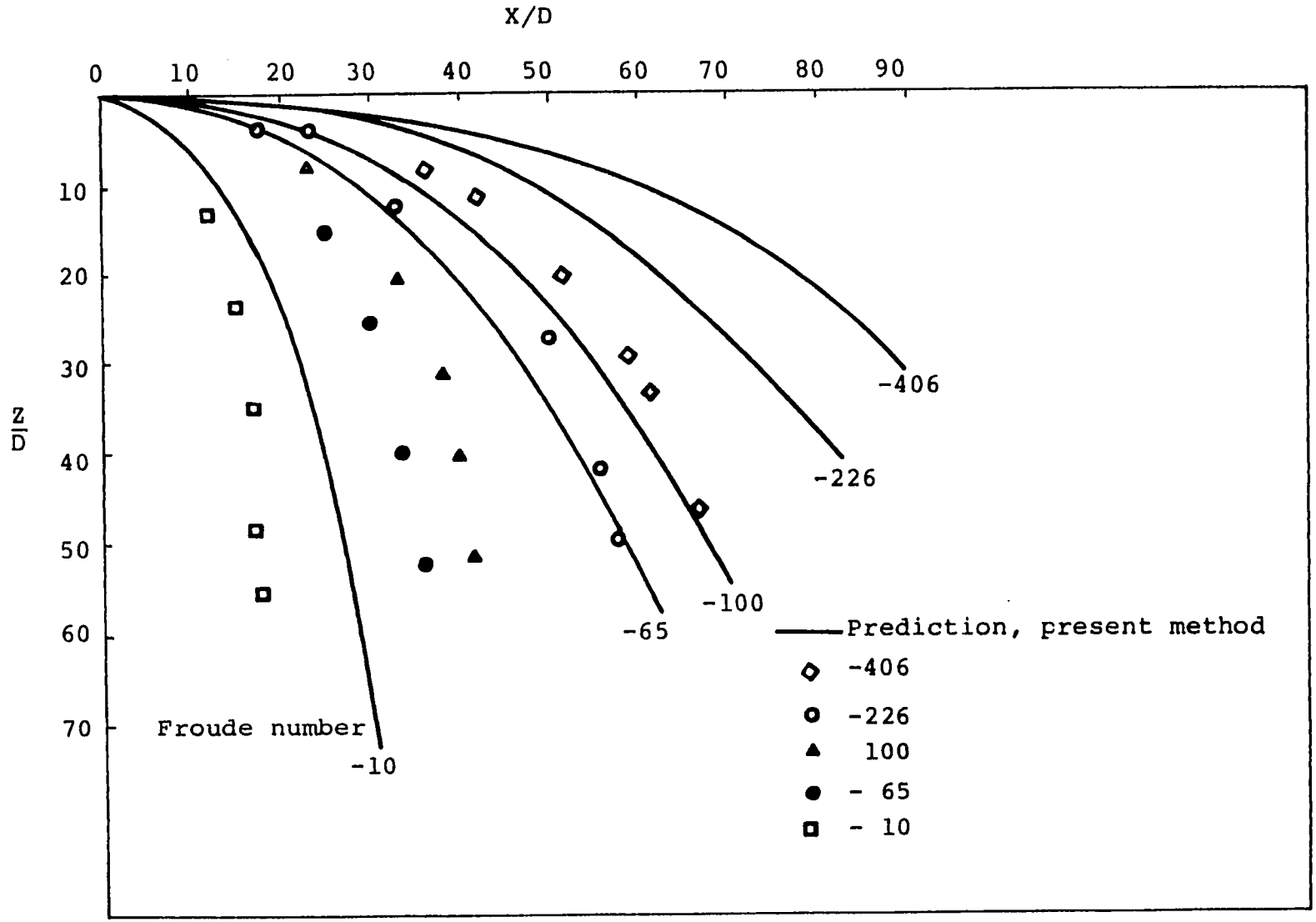

Figure 5.15. Centerline trajectory of horizontal dense jets (salt water).

experimentally model a reservoir under the influence of a negatively buoyant jet, one must, therefore, test with a negatively buoyant jet and not a positively buoyant jet. But in case of a salt water jet the buoyant and dense jets appear to be mirror image of each other for the same Froude number [9].

Figure 5.16 shows the predicted centerline temperature decay $\frac{T_c-T_\infty}{T_o-T_\infty}$ versus $\frac{S}{D}$ for $Fr_o = -65$, and -226. Figure 5.17 shows centerline concentration decay $\frac{C_c - C_\infty}{C_o - C_\infty}$ versus $\frac{S}{D}$ for $Fr_o = -65$, -406 and -10 for a salt water jet. Figure 5.18 shows jet spread $\frac{\Delta r}{D}$ as a function of $\frac{S}{D}$ for $Fr_o = -10$, and -406 for a horizontally discharged dense jet. Unfortunately, there is no experimental data available for such parameters.

STRATIFIED AMBIENTS

Figures 5.19 and 5.20 show the trajectory and centerline temperature decay, respectively, for a dense jet ($Fr_o = -746$) discharged at 45° into uniform and stratified ambients. As the stratification number, $\bar{T}$, decreases the maximum height Z_m/D and horizontal spread X_m/D decrease, showing that stratification hinders dilution. However, normally, density stratification in oceans is small ($\bar{T} \simeq 8000$),[8], so that the dilution is almost unaffected by this stratification.

5.6 SUMMARY

Results have been obtained for inclined dense jets issued to uniform or stratified ambients. The introduction of intermittency function and buoyancy correction factors

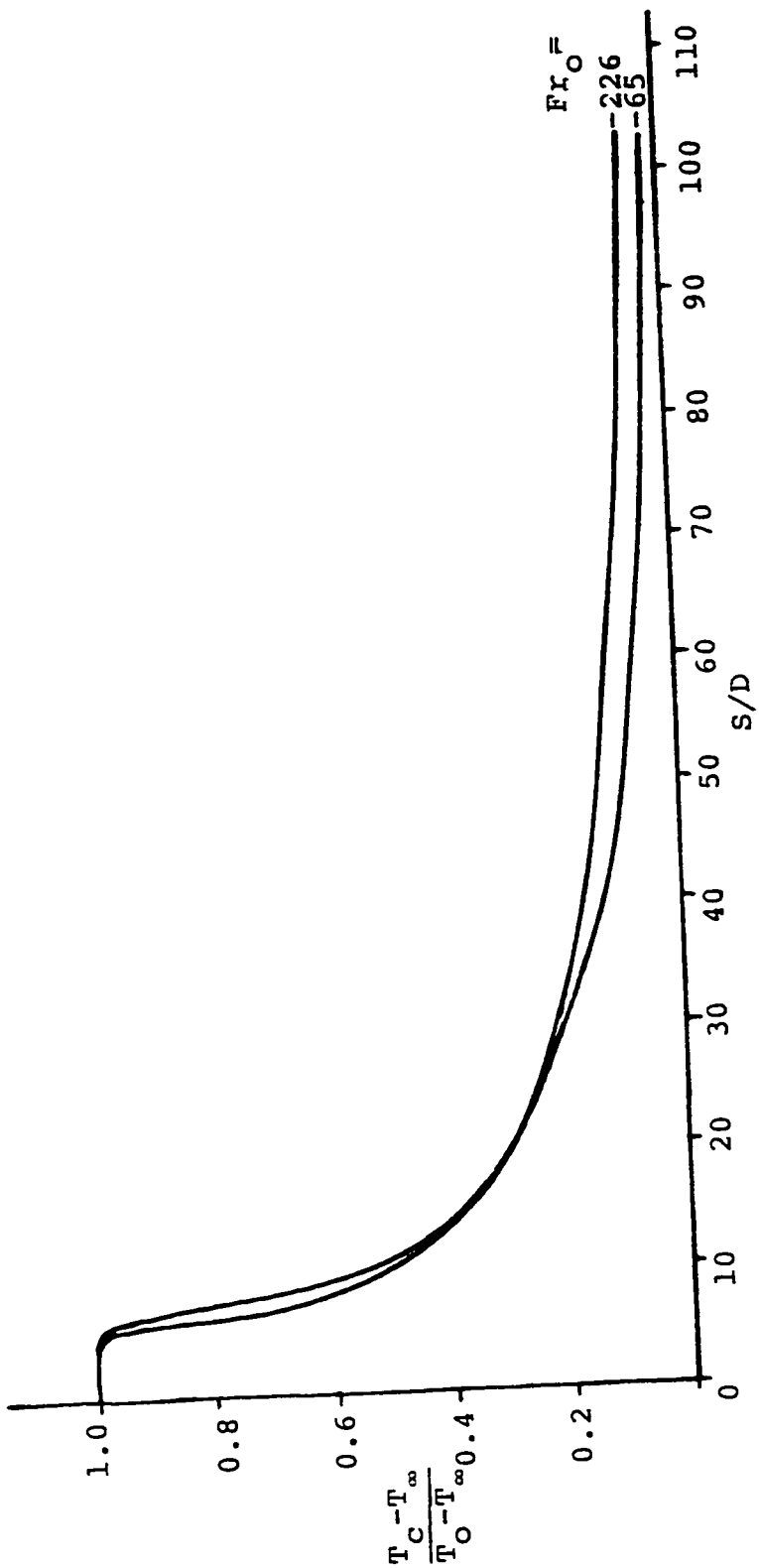

Fig. 5.16. Centerline temperature decay for horizontal dense jet

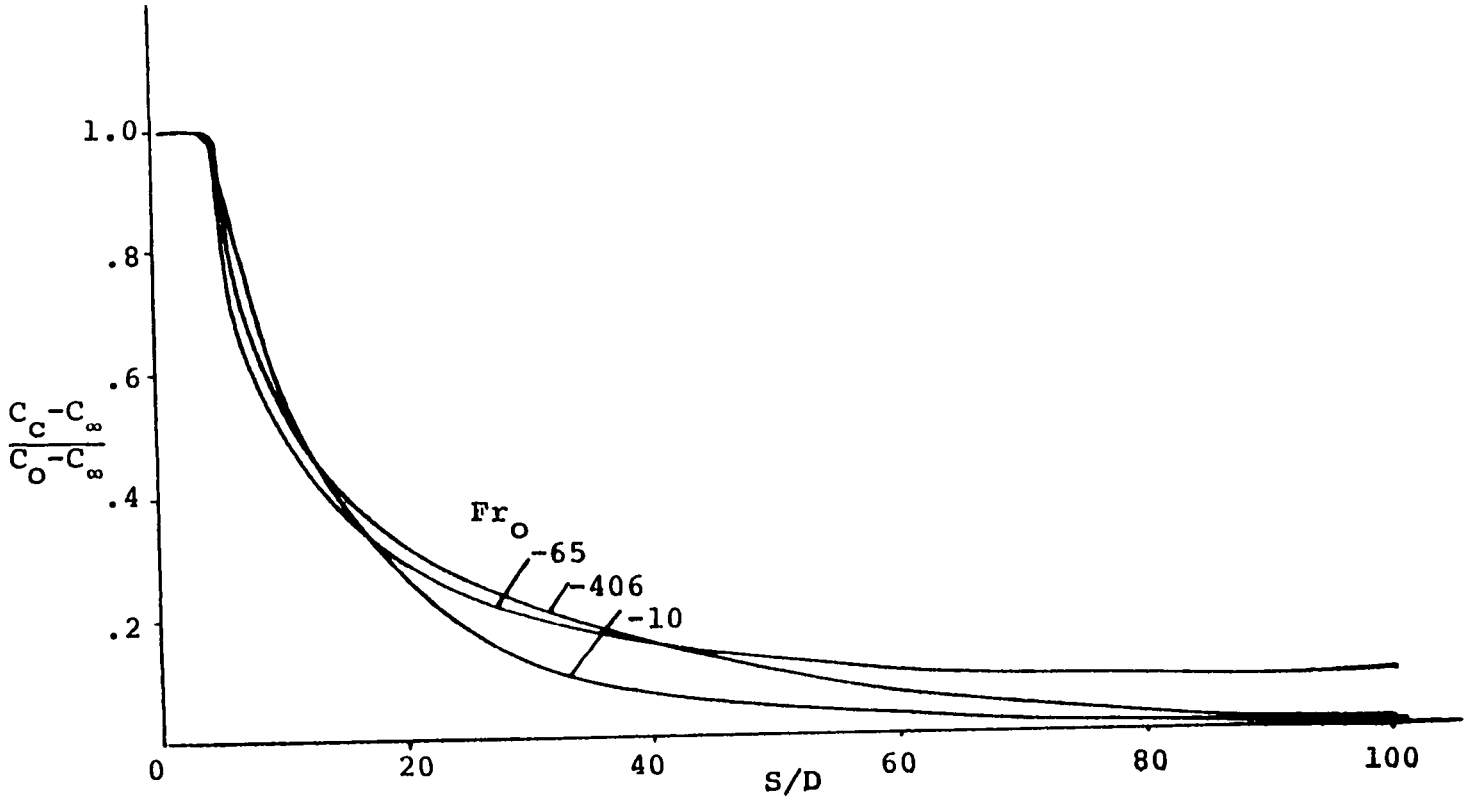

Figure 5.17. Centerline concentration decay for horizontal jet (salt water jet).

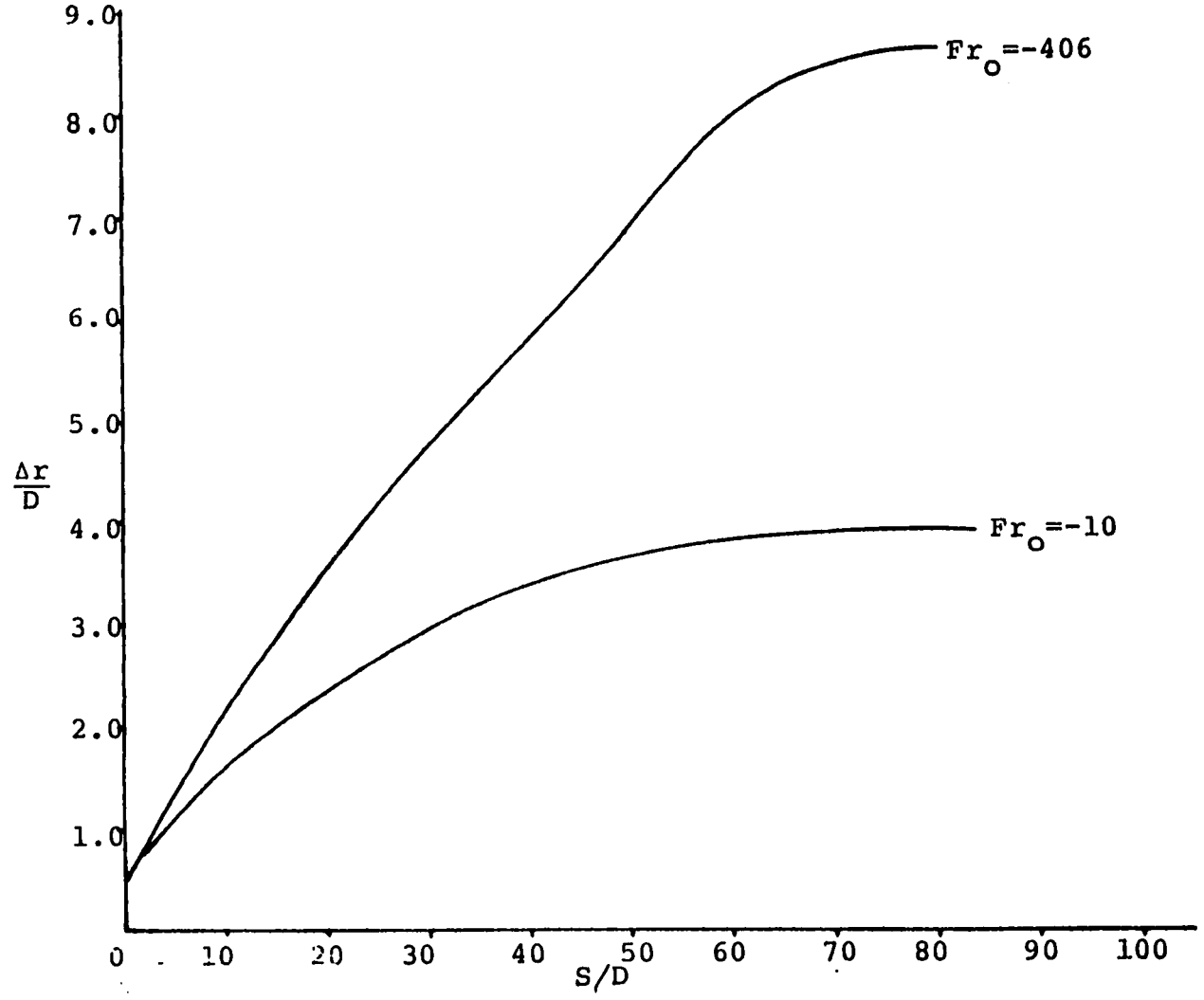

Fig. 5.18. Relative spreading versus arc length for horizontal jets

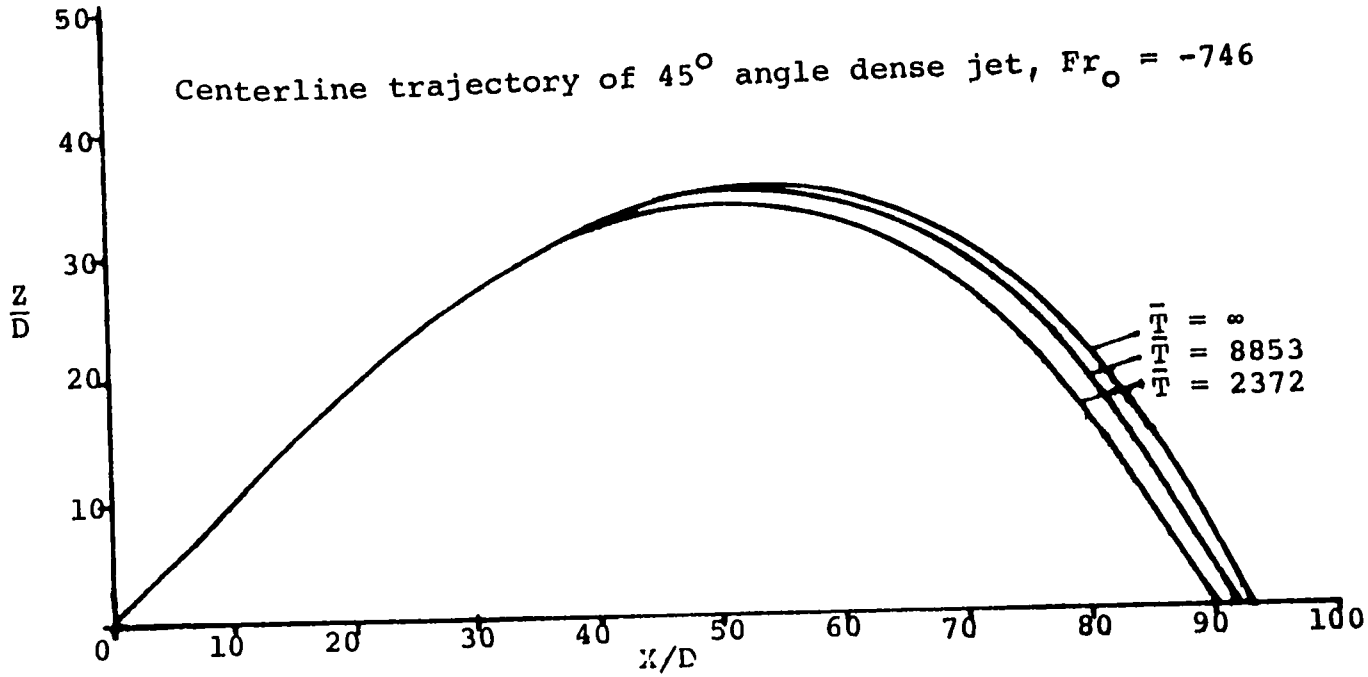

Figure 5.19. Effect of stable stratification on jet trajectory.

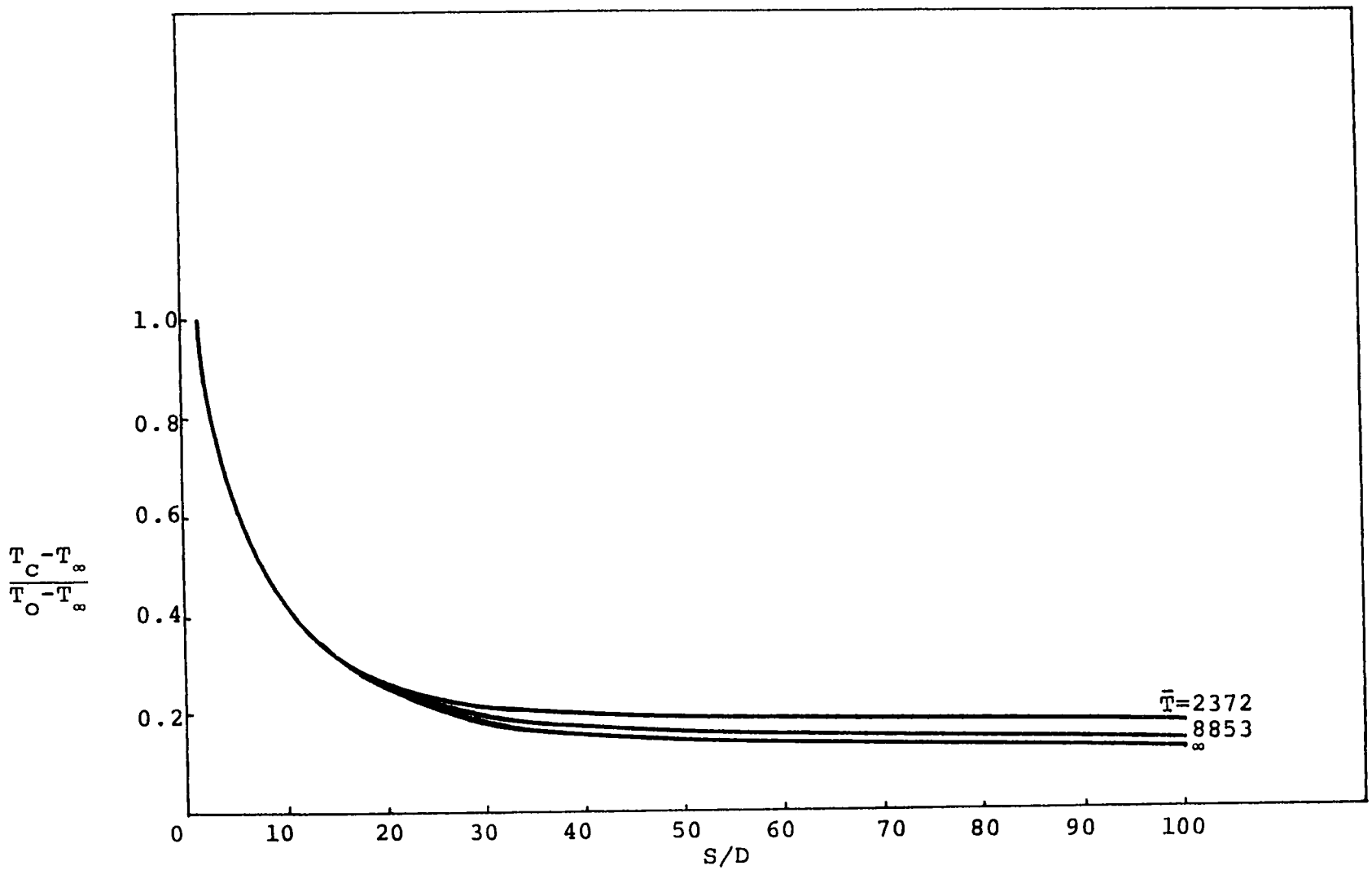

Figure 5.20. Effect of stratification on centerline temperature decay Fr_o=-746, θ_o=450.

in the effective viscosity appear to significantly improve the predictions. The transverse momentum equation has been solved neglecting curvature affects on the cross-section. By plotting $\frac{Z_m X_m}{H_m^2}$ versus angle θ_o, it seems that an angle of 72° from the horizontal will produce a jet of maximum path and hence greatest dilution. The maximum horizontal (X_m) and vertical (Z_m) spreads for inclined jets varying linearly with $|Fr_o|^{\frac{1}{2}}$ as was suggested by previous workers, has been verified by present study as well. It is proposed that a curvature correction factor might be pursued to see if it affects the predictions. Like vertical jet case, density stratification in the ambient does not seem to have significant effect on the dilution and the spread of the inclined dense jets.

6. CONCLUSIONS

The principal conclusions of the present investigation are:

1 The finite-difference prediction method which is based on an axisymmetric flow model offers the potential of significant savings in computation time over fully three-dimensional prediction methods for flows of the type considered in this study. The numerical scheme is potentially very useful for application to the discharge design process.

2 The introduction of buoyancy correction factor and intermittency function appear to improve predictions but the overall agreement between predictions and experiments is not very good. However, the experimental data is very limited and additional relevant data is needed before any conclusive remarks can be made. Significant disparities among the available experimental data are seen to exist.

3 The present axisymmetric model is flexible enough to solve either or both energy and concentration equations along with momentum and continuity equations. It can, therefore, be applied to power plant discharge design,

sewage diffuser design or the design of desalination plant discharge system if the theoretical results are confirmed by experiments.

4 The model is well adaptable to handle variable boundary conditions such as ambient stratification which allows T_∞ and C_∞ to be functions of altitude. Ambient stratification results in less dilution but the effect of stratification which normally occurs in oceans is nominal on jet trajectories and centerline decay values of temperature and velocity.

5 No general model has been successful to date for dense jet predictions, and the present investigation is an attempt to fill this gap in the literature.

7. SUGGESTIONS FOR FURTHER STUDY

Several recommendations concerning the extension of this work can be suggested.

The present approach needs further verification by experiment and any discrepancy analysed as to where the origin of discrepancy lies and improvements made.

Attention could be directed to analysis of jets discharged to flowing ambients. Surface effects could be included in the analysis for submerged, shallow water discharges and more complex turbulence models could be studied using the present calculation scheme.

Other related problems that can be attempted using extensions of the same general method are:

1 Discharge of effluent from large multiport diffusers. The present round jet analysis can be used until the jets begin to interact. Once the jets merge, the analysis would shift to that of a slot jet.

2 The entire analysis could be extended to solve for jets and plume with three-dimensional trajectories. This would involve two angles to be determined in tracing the jet trajectory; one in the horizontal plane, and the other in the plane perpendicular to the horizontal.

3 For large density differences, assumption of a Boussinesq fluid may not be valid. In such a case physical

properties should be allowed to vary with temperature and/or concentration.

4 More experimental data for horizontal, inclined, and vertical dense jets are needed to compare the predicted jet growth, trajectory, and the associated profiles. Experimental data for flows with three-dimensional trajectories seem to be non-existent. Intermittency measurements over the jet or plume cross-section are also needed, as they would be helpful in providing a physical basis for improving the turbulence models used to analyze the flow.

5 The prediction method could be extended to include surface and bottom effects. For this, the boundary layer approximation would need to be removed, and partial differential equations in elliptic form would have to be solved. The applicability of simple turbulence models would also need to be evaluated for this configuration.

REFERENCES

1. Howe, E.D., 'Fundamentals of Water Desalination', Marcel Dekker, Inc., New York, (1974).

2. Zeitoun, M.A., W.F.McIlhenny, and R.O.Reid, 'Disposal of Effluents from Desalination Plants', Chem. Engng. Prog. Symp. Series, No.97, Vol.65, (1969).

3. Abraham, G., 'Horizontal Jets in Stagnant Fluid of Other Density', ASCE Journal of Hydraulic Division,91, HY4, (1965), 139-153.

4. Abraham, G., 'Jets with Negative Buoyancy in Homogeneous Fluid', Journal of Hydraulic Research, 5 (1967), No.4, 235-248.

5. Morton, B.R., 'Forced Plumes', Journal of Fluid Mechanics, 5, (1959), 151-163.

6. Morton, B.R., G.I.Taylor, and J.S.Turner, 'Turbulent Gravitational Convection from Maintained and Instantaneous Sources', Proceedings of the Royal Society of London, A234, (1956), 1-23.

7. Fan, L.N., and N.H.Brooks, 'Numerical Solutions of Turbulent Buoyant Jet Problems', W.M.Keck Lab of Hydraulics and Water Resources, California Institute of Technology, Report # KH-R-15, (1967).

8. Hirst, E.A., 'Analysis of Round Turbulent Buoyant Jets Discharged to Flowing Stratified Ambients', Report # ORNL-4585, Oak Ridge National Laboratory, (1971).

9. Riester, J.B., R.A.Bajura, and S.H.Schwartz, 'Water Temperature Effects on Horizontal Buoyant Submerged Jets', September 1977, West Virginia University Thermal Hydraulics Lab, NTIS # PB-297 293.

10. Trent, D.S., and J.R. Welty, J.R., 'Computers and Fluids', Vol.1, (1973), 331-357.

11. Crew, H., and R.O.Reid, ASCE Journal of Engineering Mech. Division, Vol.102, February 1976, 77-87.

12. Madni, I.K., 'A Finite Difference Analysis of Turbulent, Axisymmetric Buoyant Jets and Plumes', Ph.D.Thesis, Mechanical Engineering, Iowa State University, (1975).

13. Madni, I.K., and R.H.Pletcher, 'Prediction of Jets in Coflowing and Quiescent Ambients', J. Fluids Engineering, Trans. ASME, Vol.97, (1975), 558-567.

14. Madni, I.K., and R.H.Pletcher, 'Prediction of Turbulent Forced Plumes Issuing Vertically into Stratified or Uniform Ambients', J. Heat Transfer, Series C, Vol.99, (1977).

15 Madni, I.K., and R.H.Pletcher, 'Buoyant Jets Discharging Nonvertically into a Uniform Quiscent Ambients - A Finite Difference Analysis and Turbulence Modeling', J. Heat Transfer, Vol.99, (1977), 201.

16. Madni, I.K., and R.H.Pletcher, 'A Finite-Difference Analysis for Turbulent Axisymmetric Jets', NSF Report, Engg. Research Institute, Iowa, Ames, (1977).

17. Chan, D.T.L., and J.P.Kennedy, 'Submerged Buoyant Jets in Quiescent Fluids', Proc. ASCE, J. Hyd. Div., 101, HY6 (June 1975), 733-47.

18. Anwar, H.O., 'Behavior of Buoyant Jet in Calm Fluid', Proc. ASCE, J. Hyd. Div., ASCE, 95, HY4 (July 1969), 1289-1303.

19. Hirst, F., 'Buoyant Jets with Three-Dimensional Trajectories', Proc. ASCE, J. Hyd. Division, Vol.98, HY11, (Nov. 1972), 1999-2013.

20. Bosanquet, C.H., G.Horn, and M.W.Thring, 'The Effect of Density Differences on the Path of Jets', Proc. Roy. Soc. London, A263 (1961), 340-52.

21. Turner, J.S., 'Jets and Plumes with Negative or Reversing Buoyancy', J. Fluid Mech. Vol.26, Part 4, (1966), 779-792.

22. Abraham, G., 'Jets with Negative Buoyancy in Homogeneous Fluid', J. Hydraulic Research, 5, No.4, (1967), 235-248.

23. Priestley, C.H.B., and F.K.Ball, 'Continuous Convection from an Isolated Source of Heat', Quart. J. Roy. Met. Soc., 81, No.348, (1955), 144-157.

24. Zeitoun, M.A., W.F.McIlhenny, and R.O.Reid, 'Conceptual Designs of Outfall System for Desalting Plants', Office of Saline Water Research and Development Progress Report # 550, United States Department of the Interior, NTIS # PB 201 033.

25. Holly, F.M., and J.L.Grace,'Model Study of Dense Jet in Flowing Fluid', Proc. ASCE, J. Hyd. Div., Vol.98, No.HY11, (Nov. 1972).

26. Jain, S.C., and J.M.Pena, 'Numerical Analysis of Warm, Turbulent Sinking Jets Discharged into Quiescent Water at Low Temperature', Iowa Institute of Hydraulic Research Report # 154, University of Iowa, NTIS # PB 254 858 (Feb. 1974).

27. Pena, J.M., and S.C.Jain, 'Turbulent Jets with Reversible Buoyancy', J. Hyd. Division, Proc. ASCE, Vol.101, # HY9, (Sept 1975), 1221-1233.

28. Csanady, G.T., 'The Buoyant Motion Within a Hot Gas Plume in a Horizontal Wind', J. Fluid Mech., Vol.22, # 2, (1965), 225-239.

29. Riester, J.B., R.A.Bajura, and Schwartz, 'Effects of Water Temperature and Salt Concentration on the Characteristics of Horizontal Buoyant Submerged Jets', J. Heat Transfer, Vol. 102, (Aug. 1980), 557-562.

30. LeGros, P.G., et al., 'A Study of the Disposal of the Effluent from a Large Desalination Plant', Research and Development Progress Report, No.316, Office of Saline Water, U.S.Dept. Interior, (Jan. 1968), 491.

31. Hinze, J.O., Turbulence, McGraw-Hill, New York, (1959), 376-439.

32. Hwang, S.S., and R.H.Pletcher, 'Prediction of Turbulent Jets and Plumes in Flowing Ambients', Affiliate Research Program in Electrical Power, HTL-15, ISU-ERI-AMES-79003, Iowa State University,Ames,(1978).

33. Spalding, D.B., "Turbulence Models for Heat Transfer", Vol.6, Sixth Int. Heat Transfer Conference, Toronto, Hemisphere Publishing Corporation, Washington, D.C. (1978).

34. Keffer, J.F., and W.D.Baines, 'The Round Turbulent Jet in a Cross-Wind', J. Fluid Mech., 15, No.4 (1963), 481-497.

35. Marble, R.W., and R.F.Robidean, 'Thermal Field Resulting from an Offshore-Submerged Nuclear Electric Power Generating Station', Paper # 71-WA/NE-3, presented at the ASME Winter Annual Meeting, Washington, D.C., (1971).

36. DuFort, E.C., and S.P.Frankel, 'Stability Conditions in the Numerical Treatment of Parabolic Differential Equations', Mathematical Tables Aid Computation 7 (1953), 135-152.

37. Langley Working Conference on Free Turbulant Shear Flows, Proc. NASA, SP-321, Vol.1, (1972).

38. Pletcher, R.H., 'Survey of Finite Difference Strategy for Predicting Heat Transfer in Turbulent Channel Flows,' Turbulent Forced Convection in Channels and Bundles, McGraw-Hill Book Company, (1979).

39. Pletcher, R.H., 'Finite Difference Methods for Predicting Channel Flows, Turbulence Models and Some Comparisons with Experimental Data', Turbulent Forced Convection in Channels and Bundles, McGraw-Hill Book Company (1979).

40. Patankar, S.V., and D.B.Spalding, Heat and Mass Transfer in Boundary Layers, 2nd Edition, London: Intertext Books, (1970).

41. Richtmyer, R.D., and K.W.Morton, Difference Methods for Initial Value Problems, 2nd Edition, New York: Wiley (Interscience), (1967).

42. Oosthuizen, P.H., 'Low Velocity Heated Air Jets', Presented at the Fourth Western Canadian Heat Transfer Conference, Winnipeg, Manitoba, (1972).

43. Richardson, L.F., 'The Supply of Energy From and to Atmospheric Eddies', Proc. Royal Soc. (London), A97, (1920), 354-373.

44. Ellison, T.H., and J.S.Turner, J. Fluid Mech., Vol.8 (1960), 514-544.

45. Webster, C.A.G., 'An Experimental Study of Turbulence in a Desnity-Stratified Shear Flow', J. Fluid Mech., Vol.19, (1964), 221-245.

46. Mizushina, T., F.Ogino, H.Ueda, and S.Komori, 'Buoyancy Effect on Eddy Diffusivities in Thermally Stratified Flows in an Open Channel', Paper MC16, Sixth Int. Heat Transfer Conference, Toronto, (August 1978), published by Hemisphere Publishing Corporation, Washington, D.C.

47. Hart, W.E., 'Jet Discharge into a Fluid with a Densitv Gradient'. ASCE. J.Hyd. Division. 87. HY6 (1961). 171-200.

48. Pryputniewicz, R.J., and W.W.Bowley, 'An Experimental Study of Vertical Buoyant Jets Discharged into Water of Finite Depth', ASME, J. Heat Transfer, (May 1975), 274-281.

49. Hwang, S.S., and R.H.Pletcher, 'Prediction of Buoyant Turbulent Jets and Plumes in a Cross Flow', Paper MC-19, Sixth Int. Heat Transfer Conference, Toronto,(August 7-11, 1979), Hemisphere Publishing Corporation.

50. Launder, B.E., and D.B.Spalding, Mathematical Models of Turbulence, Academic Press, New York. (1972).

51. Bradshaw, P., 'The Analogy Between Streamline Curvature and Buoyancy in Turbulent Shear Flows', J. Fluid Mech., 36, Part 1, (1969), 177-191.

52. Ahmad, S.Z., and I.K.Madni, 'On the Effects of Buoyancy in Turbulence Modeling of Shear Flows', Paper presented at the 16th Southeastern Seminar on Thermal Science, University of Miami, Miami Beach, Florida, (April 19-21, 1982).

53. Axcel, B.P., and W.B.Hall, 'Mixed Convection to Air in a Vertical Pipe', Paper MC-7, Sixth Int. Heat Transfer Conference, Toronto, (1978).

54. Taylor, G.I., 'Effect of Variation in Density on the Stability of Superposed Streams of Fluid', Proc. Roy. Soc. A.132, 499-523. (1931).

55. Hossain, M.S., and W.Rodi, 'Influence of Buoyancy on the Turbulence Intensities in Horizontal and Vertical Jets', Proc. Int. Seminar on Turbulent Buoyant Convection, Debrovnik, Yugoslavia, Hemisphere Publishing Corporation, Washington, D.C., (1976).

56. Giles, J.A., A.P.Hays, and R.A.Sawyer, 'Turbulent Wall Jets on Logarithmic Spiral Surfaces', The Aeronautical Quarterly, Vol.XVII, (August 1966).

57. Nelson, R.M., and R.H.Pletcher, 'An Explicit Scheme for the Calculation of Confined Turbulnet Flows with Heat Transfer', Proc. 1974 Heat Transfer and Fluid Mech. Institute, Stanford University Press, Palo Alto, California, (1974), 154-170.

58. Bacliĉ, B.S., 'On the Nonlinear Temperature Wave Propagation into the Depth of Ocean', Heat Transfer and Turbulent Buoyant Convection, Vol. 1, Hemisphere Publishing Corporation (1977). Eds. D.B.Spalding and N. Afgan.

59. Viscanta, R., and R.G.Hills, 'Temperature Modeling in Rivers with Thermal Discharges', Heat Transfer and Turbulent Buoyant Convection, Vol.1, Hemisphere Publishing Corporation (1977). Eds. D.B.Spalding and N. Afgan.

60. Schlichting, H., Boundary Layer Theory, 6th Edition, McGraw-Hill Book Company. (1968).

61. Kays, W.M., and M.E.Crawford, Convective Heat and Mass Transfer, 2nd Edition, McGraw-Hill Book Company. (1980).

62. Ricou, F.P., and D.B.Spalding, 'Measurements of Entrainment by Axisymmetrical Turbulent Jets', J. Fluid Mech., 11, pp.21-33, (1961).